INFORMATION TO USERS

This manuscript has been reproduced from the microfilm master. UMI films the text directly from the original or copy submitted. Thus, some thesis and dissertation copies are in typewriter face, while others may be from any type of computer printer.

The quality of this reproduction is dependent upon the quality of the copy submitted. Broken or indistinct print, colored or poor quality illustrations and photographs, print bleedthrough, substandard margins, and improper alignment can adversely affect reproduction.

In the unlikely event that the author did not send UMI a complete manuscript and there are missing pages, these will be noted. Also, if unauthorized copyright material had to be removed, a note will indicate the deletion.

Oversize materials (e.g., maps, drawings, charts) are reproduced by sectioning the original, beginning at the upper left-hand corner and continuing from left to right in equal sections with small overlaps. Each original is also photographed in one exposure and is included in reduced form at the back of the book.

Photographs included in the original manuscript have been reproduced xerographically in this copy. Higher quality 6" x 9" black and white photographic prints are available for any photographs or illustrations appearing in this copy for an additional charge. Contact UMI directly to order.

U·M·I

University Microfilms International
A Bell & Howell Information Company
300 North Zeeb Road, Ann Arbor, MI 48106-1346 USA
313/761-4700 800/521-0600

Order Number 9405516

Time-resolved light scattering and fluorescence spectroscopy in biomedical and model random media

Das, Bidyut Baran, Ph.D.

City University of New York, 1993

U·M·I
300 N. Zeeb Rd.
Ann Arbor, MI 48106

TIME-RESOLVED LIGHT SCATTERING AND FLUORESCENCE SPECTROSCOPY IN BIOMEDICAL AND MODEL RANDOM MEDIA

by

BIDYUT BARAN DAS

A dissertation submitted to the Graduate Faculty in Physics in partial fulfilment of the requirements for the degree of Doctor of Philosophy, The City University of New York.

1993

This manuscript has been read and accepted for the Graduate Faculty in Physics in satisfaction of the dissertation requirement for the degree of Doctor of Philosophy

Date 9/27/93

Prof. Robert R. Alfano
Chairman of Examining Committee

Date 9/30/93

Executive officer

Prof. K. M. Yoo

Prof. J. Gersten

Prof. P. P. Ho

Prof. R. Dorsinville

Prof. R. Barbour

Supervisory Committee

The City University of New York

Abstract

TIME-RESOLVED LIGHT SCATTERING AND FLUORESCENCE SPECTROSCOPY IN BIOMEDICAL AND MODEL RANDOM MEDIA

by

Bidyut Baran Das

Advisor: Prof R. R. Alfano

Optical spectroscopy, light scattering and ultrafast time-gated imaging have been shown to offer novel approaches to study the optical characteristics of various biomedical and other random media.

Fluorescence spectra from human malignant and nonmalignant breast tissues were measured at 300 nm excitation and a significant spectral difference was found between the two tissue types by using the ratio of fluorescence intensities at 340 and 440 nm.

Optical density measurements on thin breast tissues show that the scattering cross-sections of breast tissues are relatively constant over the visible and the uv region.

Transport mean free paths and the absorption lengths for various tissues and model random media were measured using time-resolved transmission. The scattering coefficients for human breast and chicken tissues were found to remain relatively constant in 570 - 630 nm wavelength region while they change significantly at 1064 nm. Chicken breast and fat tissues were found to be good models for human breast tissues as the values of the optical parameters of both the tissues are about the same. The less scattering

observed at 1064 nm makes tissues more transparent in the IR region making it easier to image in thick tissues.

Time-resolved backscattering measurements show that the scattering and the absorption parameters of a random medium can be obtained accurately in a two-fiber configuration as long as the radial distance is more than about seven times the transport mean free path of the sample. The single point source-detection configuration provides a tool to diagnose breast malignancy though it fails to give accurate values of the optical parameters of tissues. This failure is attributed to the invalidity of the diffusion approximation in this experimental configuration.

A 2.5 mm thin chicken fat strip was imaged inside a 40 mm thick chicken breast tissue using snake photons at 625 nm with ultrafast time-gated detection.

A simple model to describe the effect of small objects embedded inside a highly scattering medium on the attenuation of snake photons is developed.

asato mA sadgamaya !
tamaso mA jyotirgamaya !
mrtyor mA amrtamgamaya !!

(I. iii. 28)
brhadAraNyaka upaniShad

Lead me from untruth to Truth !
Lead me from darkness to Light !
Lead me from mortality to Immortality !!

ACKNOWLEDGEMENTS

It is a great pleasure to acknowledge my thesis advisor Robert. R. Alfano, Distinguished Professor of Science and Engineering, for his patient guidance, deep involvement, creative ideas and intuitive insight during this research work. I gratefully acknowledge his encouragement, trust and understanding during this period. I am particularly grateful to Prof. K. M. Yoo, my co-thesis Advisor, for his bright ideas and immense help. I gratefully acknowledge Prof. Feng Liu for his help and for providing some data for this work.

It is a pleasure to thank Dr. E. Celmer, Dr. J. Cleary, Dr. R. Prudente, and Dr. A. Caron for providing tissue samples for this project and for their valuable advice in medicine. My sincere thanks to G. C. Tang, Dr. Antonios Seas, Prof. Vladimir Petricevic, Ms. Megan Gibbs and Ms. Joan Brijlall for their help and advice.

I would like to thank Prof. Joel Gersten, Prof. P. P. Ho, Prof. R. Dorsinville and Prof. R. Barbour for serving on my Doctoral Committee.

I would take this opportunity to thank all my friends at IUSL, and Masood Siddiq in particular, for their help during this research. My special thanks and appreciation go to Dr. Asima Pradhan for her immense help and valuable discussions. It is a pleasure to acknowledge Mr. T. K. Ramkumar and Dr. Chandra Balachandra for providing the quotation from the Brhadaranyaka Upanishad at a very short notice.

This work was possible with the financial support from SDI-ONR Free Electron Medical Program, Mediscience Technology Corp., the Physics Department and the Organized Research at the IUSL.

TABLE OF CONTENTS

	Page
CHAPTER 1: INTRODUCTION	
1.1 Background	1
1.2 Thesis Statement	6
1.3 Thesis Organization	7
1.4 References	9
CHAPTER 2: FLUORESCENCE SPECTROSCOPIC STUDIES OF HUMAN TISSUES AND MODEL FLUOROPHORES	
2.1 Introduction	12
2.2 Human Tissue and Pathology	15
2.3 Experimental Methods	19
2.3.1 Visible Fluorescence Spectroscopy	19
2.3.2 UV Fluorescence Spectroscopy	21
2.4 Results	24
2.5 A Comparison of Various Breast Diagnostic Procedures	27
2.6 Potential Fluorophores	30
2.7 Effect of Absorption and Scattering on Tissue Fluorescence	33
2.8 References	37
CHAPTER 3: SPECTRAL OPTICAL DENSITY MEASUREMENTS ON SMALL PARTICLES AND BREAST TISSUES	
3.1 Introduction	41

3.2 Experimental Method 47

3.3 Results 47

3.4 References 54

CHAPTER 4: DIFFUSION OF LIGHT IN TURBID MEDIA

4.1 Introduction 56

4.2 Transport Theory 58

4.3 Diffusion Approximation 58

4.4 Forward Scattering Through a Slab of Turbid Medium 61

4.5 Experimental Setup 64

4.6 Results 65

4.7 References 72

CHAPTER 5: TIME-RESOLVED BACKSCATTERING OF LIGHT IN BIOMEDICAL AND RANDOM MEDIA

5.1 Introduction 75

5.2 Theory 77

5.2.1 Single Point Source-Detection 77

5.2.2 Two-Fiber Input Output Configuration 79

5.3 Experimental Methods 81

5.4 Results 83

5.4.1 Single Point Source-Detection 83

5.4.2 Two-Fiber Input Output Configuration 86

5.5 A Comparison of Time-Resolved Back and Forward Scattering 88

5.6 Conclusion 91

5.7 References 93

CHAPTER 6: ULTRAFAST TIME-GATED IMAGING IN THICK TISSUES

6.1 Introduction 95

6.2 Experimental Methods 98

6.3 Results 100

6.4 An Empirical Model for Snake Photon Attenuation 106

6.5 Conclusion 110

6.6 References 112

CHAPTER 7: SUMMARY 114

CHAPTER 8: FUTURE EXPERIMENTS 117

Appendix I

Computer program to calculate σ_s and g 119

Appendix II

Computer program to calculate l_t and l_a 129

BIBLIOGRAPHY 134

LIST OF TABLES

CHAPTER 2

Table 2.1 The statistics of 87 human breast tissue samples showing the accuracy of the uv-fluorescence technique 26

CHAPTER 4

Table 4.1 The transport mean free paths and the absorption lengths for various random media at 620 nm measured using time-resolved transmission and diffusion approximation. 67

Table 4.2 Transport mean free paths and absorption lengths at 620 nm wavelength for milk at two different concentrations. 69

Table 4.3 The l_t s and l_a s at various wavelengths for a chicken breast tissue and a fatty human breast tissue. 70

CHAPTER 5

Table 5.1 Transport mean free paths and absorption lengths at 625 nm wavelength for 25% whole milk (Delwood) measured using two- fiber configuration 88

Table 5.2 Transport mean free paths and absorption lengths measured using back and forward scattering of light. 90

LIST OF FIGURES

CHAPTER 1

Fig. 1.1. Simplified energy level diagram of a polyatomic organic molecule. 2

CHAPTER 2

Fig. 2.1. The experimental setup for fluorescence measurement in the visible region. 19

Fig. 2.2. Average emission spectra from benign and malignant samples with 488 nm excitation. 21

Fig. 2.3. A schematic diagram of the Perkin Elmer LS 50 Fluorescence Spectrometer. S: Source, B.S. : Beam Splitter 22

Fig. 2.4. Fluorescence spectra from normal, cancer and benign breast tissues excited at 300 nm wavelength. 24

Fig. 2.5. A histogram of fluorescence intensity ratio at 340 to 440 nm, excited at 300 nm for normal, malignant, benign tissue and benign tumor samples. 25

Fig. 2.6. Ratio of fluorescence intensity at 340 nm to that at 440 nm plotted against different excitation wavelengths for malignant and benign tissue samples. 27

Fig. 2.7. Excitation spectra from benign and malignant tissue samples at 340 nm emission. 31

Fig. 2.8. Excitation spectra from benign and malignant tissue samples at 460 nm emission. 31

Fig. 2.9a. Emission spectra of tyrosine, tryptophan and NADPH excited at 300 nm wavelength. 32

Fig. 2.9b. Emission spectra of collagen, elastin and trypsine excited at 300 nm. 32

CHAPTER 3

Fig. 3.1. The dependence of g on particle diameter at 0.625 μm. 45

Fig. 3.2. The mean cosine of the scattering angle (g) at different wavelengths for 0.4 μm diameter intralipid scatterer in water, index = 1.4. 45

Fig. 3.3. The dependence of scattering cross-section of Latex beads in water on bead diameter at 625 nm. 46

Fig. 3.4. Optical density spectra measured for latex beads suspension in water for different bead diameters 49

Fig. 3.5. Optical density curves for various thin tissue samples 50

Fig. 3.6. Scattering coefficient spectra for different latex bead suspensions in water computed using Mie theory. 51

CHAPTER 4

Fig. 4.1 Scattering of light incident on the volume dl in the direction $\hat{n}'$ into the direction $\hat{n}$. 59

Fig. 4.2 Simulated transmission profiles for different transport mean free paths (0.5, 4 and 25 mm). 62

Fig. 4.3 A plot of peak time versus transport mean free path obtained from various simulated transmission curves. 63

Fig.4.4 The experimental setup for the time-resolved transmission measurements through a random medium. 64

Fig. 4.5 The experimental transmission profile through a 21 mm human benign breast tissue with its theoretical fit. 65

Fig. 4.6 The temporal profile of a transmitted pulse (solid line) through a milk solution is shown with its best fit (open circle) 66

Fig. 4.7 Temporal profile of a transmitted signal through a 5.7 cm thick chicken tissue at 1064 nm. 70

Fig. 4.8 The transport mean free path for a chicken breast sample is plotted against the wavelength. 71

CHAPTER 5

Fig. 5.1. Backscattered light where the points of incidence and collection are the same. 77

Fig. 5.2(a) Temporal Profiles of backscattered pulses computed from eqn. (5.1) with convolution of 8ps Impulse response function 78

Fig. 5.2(b) Temporal Profiles of backscattered pulses computed from eqn.(5.1) with convolution of 8ps Impulse response function. 79.

Fig. 5.3. Backscattered light with different input-output positions. 79

Fig. 5.4(a). Temporal profiles of two backscattered pulses with transport mean free paths of 0.5 mm (solid) and 2.0 mm, and an absorption length of 250 mm at a radial distance of 7.5mm. 80

Fig. 5.4(b). Temporal profiles of two backscattered pulses with absorption lengths of 100 mm (solid) and 250 mm, and a transport mean free path of 0.5 mm at a radial distance of 7.5mm. 81

Fig. 5.5. The experimental setup for the time-resolved back-scattering measurements using 100 fs laser pulses. 82

Fig. 5.6. Time-resolved backscattered intensity curves from human malignant and benign breast tissues at 625 nm. 84

Fig. 5.7. Temporal profiles of back scattered pulses from a malignant breast tissue sample at different wavelengths 86

Fig. 5.8 Time-resolved back scattered pulse profiles for various radial distances between the two fibers. 87

Fig. 5.9 The temporal profile of a transmitted signal through a 3 cm thick human fatty breast tissue with its best fit curve giving $l_t = 0.7\ mm$ and $l_a = 208\ mm$ at 620nm. 89

Fig 5. 10 Backscattered pulse with the two fiber configuration from a human fatty breast tissue at 620 nm fitted (open circles) according to the eqn. 5.3 with $l_t = 0.7\ mm$ and $l_a = 242\ mm$. 89

Fig 5. 11 Backscattered pulse with the single point source-detection configuration from a human fatty breast tissue at 620 nm fitted according to the eqn. 5.1 with $l_t = 6.0\ mm$ and $l_a = 80\ mm$. 90

CHAPTER 6

Fig. 6.1. An ultrashort pulse spreads into a ballistic and a diffuse component after propagating through a highly scattering medium. 96

Fig. 6.2. Experimental setup for the detection of snake photons to image translucent objects hidden in scattering random media. 98

Fig. 6.3. A cross-section of the chicken breast tissue sample in the plane of the scanning with a thin fat strip embedded in it. 99

Fig. 6.4.a. Temporal profiles of two transmitted pulses through the 2.6 cm thick sample: the dotted curve is for incidence through the center of the fat strip, while the solid curve is at a 5 mm distance away from the center. 101

Fig. 6.4.b. Snake photons diagram 102

Fig. 6.5. Time integrated intensity from the transmitted signal through the 2.6 cm thick sample at different time gates versus different beam incidence positions. (a) 220-820ps, (b) 120-967ps, (c) 120-170ps, and (d) 120 -130ps. 103

Fig. 6.6. Time integrated intensity from the transmitted signal through the 4 cm thick sample with a 2.5 mm thick fat strip within a 20 ps window (308-328 ps) versus different beam incidence positions 104.

Fig. 6.7. Time integrated intensity curve of first 100 ps versus beam positions for a 15 mm wide fat strip embedded inside a 6 cm thick chicken breast tissue at 1064 nm. 105

Fig. 6.8 Two temporal profiles simulated using eqn. 6.5 108

Fig. 6.9 Two transmitted pulse profiles with (a) $w'/w = 0.01$ and (b) 0.05. 110

Fig. 6.10 The difference in the integrated intensity for a 12 ps time gate is plotted against the fat-breast thickness ratio (w'/w). 111

CHAPTER 1

Introduction

1.1 Background

Optical physics offers various ways to probe at a fundamental level the physical and chemical processes occurring in the microscopic world. Fundamental information obtained using optical methods can be broadly categorized as structural, dynamic, and analytical. Fluorescence spectroscopy and light scattering are two major approaches in optical physics.

Fluorescence is the emission of radiation that occurs when a molecule in an excited electronic state returns to the ground state emitting light. Figure 1.1 shows the various processes involved leading to the fluorescence emission. Absorption of radiation is a very rapid (10^{-15} sec) process that populates a number of vibrational levels of the excited electronic states. The excited molecule very quickly (10^{-13} sec) loses a part of the excitation energy to populate the lowest vibrational level of the excited electronic state and this process is known as *vibrational deactivation.* The molecule can then de-excite itself to the ground level by emission of radiation (fluorescence) or through several nonradiative processes called *internal conversion* without any emission of radiation. This alternative mechanism of de-excitation through nonradiative processes results in a diminution of the fluorescence intensity known as *quenching.* Under certain circumstances a molecule can cross over from a singlet state to a triplet state in a process called *inter-system crossing.* The life time of a singlet state is in the order of 10^{-9} sec to 10^{-7} sec while that of a triplet state is between 10^{-6} to 10^{2} sec. This long life time of a

triplet state due to the forbidden transition between the triplet and the ground singlet state gives rise to delayed emission known as *phosphorescence.*

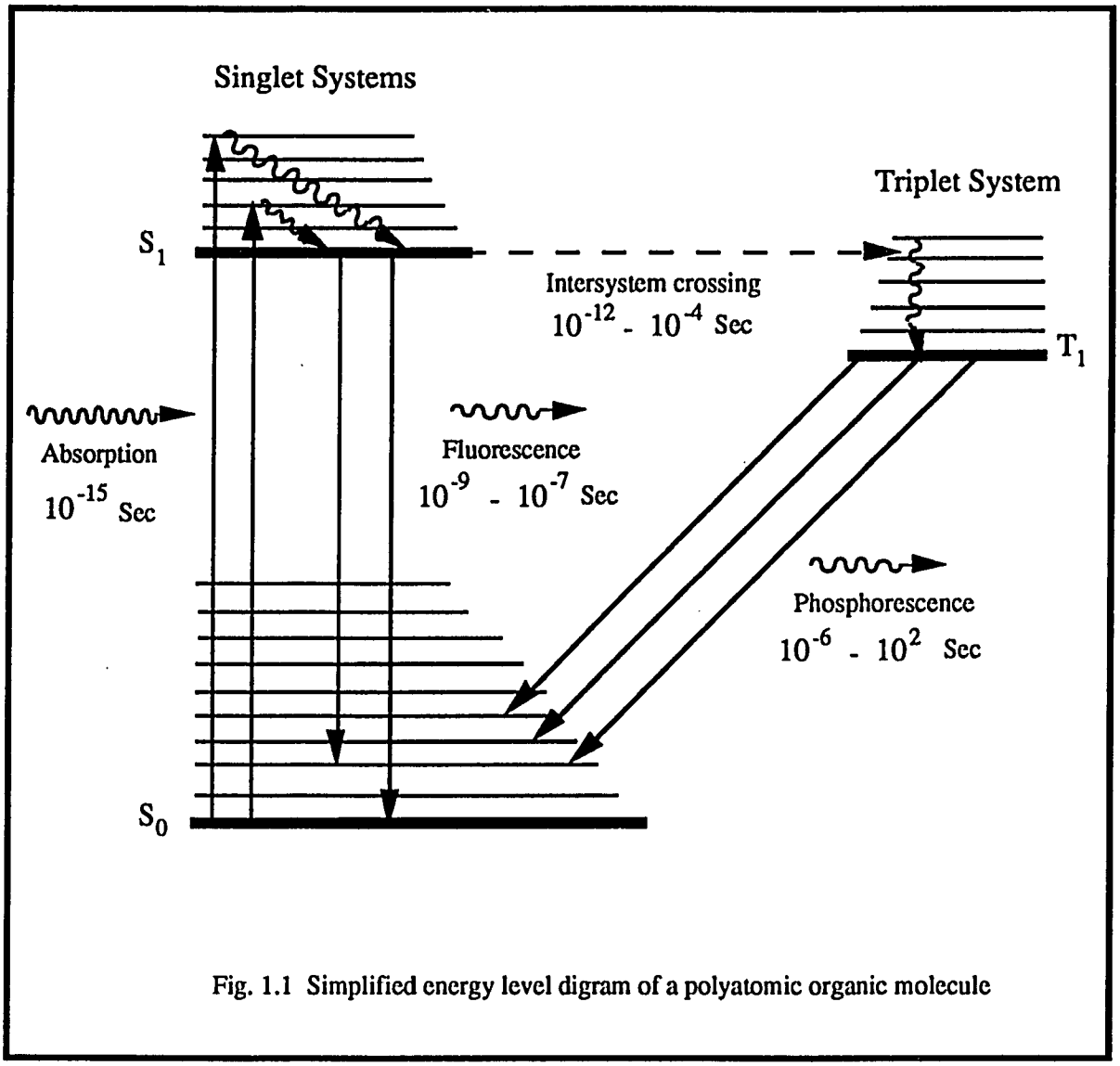

Fig. 1.1 Simplified energy level digram of a polyatomic organic molecule

In general, fluorescence spectroscopy is used in two ways: steady-state and time-resolved. Steady-state fluorescence uses continuous wave (cw) light to study the characteristic *excitation* and *emission* spectra of a material to gain information on its internal processes. Time-resolved methods use pulse light excitation sources to study

the kinetics of relaxation from the excited to the ground state.

The key parameters that are used in the study of fluorescence emission are: λ_{max} - the *position of maximum emission, bandwidth, spectral profiles,* Φ_f - the *quantum yield* (the fraction of molecules that get de-excited through emission of radiation), and τ_f - the fluorescence *relaxation time*[1,2]. These parameters are very sensitive to environmental changes and can be affected in a variety of ways. For example, an increase in the polarity of the environment around the fluorophore can result in more non-radiative losses, yielding a red shift in the emission spectrum. This will also result in a decrease in the quantum yield and a change in the decay time. While the analysis of various fluorescence quenching processes can provide information on the dynamics of collision between the fluorophore and the surrounding ions present in the medium, the study of the relaxation time can provide information on the heterogeneous nature of fluorescence. Fluorescence emitted by a heterogeneous material such as a tissue by external irradiation is intrinsically dependent on its constituent fluorophores. The response of native fluorophores in different environments varies significantly resulting in fluorescence spectral differences. The high sensitivity of these key fluorescence parameters (λ_{max}, Φ_f and τ_f) to such environmental changes make optical spectroscopy a viable method for applications in medicine. The presence of intrinsic fluorophores such as *tryptophan, collagen, elastin, NADH,* and *flavins* in animal and human tissues[1,3] offers exciting possibilities to develop novel diagnostic and therapeutic approaches using fluorescence spectroscopy as a sensitive index of the morphological changes occurring in tissues.

The study of light transport in a scattering medium provides a novel way to obtain information about the optical properties of various random media. It depends on the physical structure and the chemical composition of the medium, and is highly sensitive to physiological and chemical changes occurring in it. A fundamental

understanding of light scattering and photon migration in biomedical and other model media is crucial to tap the potential uses of light in medicine and in solid state physics. When light enters an inhomogeneous medium, such as a tissue, it will be multiply scattered because of continuous fluctuation in the refractive index in the medium. Light scattering in a random medium depends on the optical properties of the medium which can be characterized by a few key optical parameters[4, 5]. These key parameters are the *scattering mean free path* (l_s), the *absorption length* (l_a), the *transport mean free path* (l_t) and the *mean cosine of the angle of scattering* (g). The absorption length (l_a) is the mean distance a photon travels in the medium before it is absorbed. This length depends on the chemical composition of the medium, i.e. the absorption cross-section and the concentration of the absorbers present in the medium. The scattering mean free path (l_s) is the mean distance between scattering. In the independent scatterer approximation, $l_s = 1/n\sigma_s$, where n is the scatterer number density and σ_s is the scattering cross-section of the scattering particle. This scattering cross-section depends on its shape, its size compared to the wavelength of light, and its refractive index with respect to that of the surrounding medium. The scattering cross-section σ_s is related to the differential scattering cross-section $\sigma_d(\theta,\phi)$ by the expression

$$\sigma_s = \int \sigma_d(\theta,\phi) \sin\theta d\theta d\phi \quad . \qquad (1.1)$$

The differential scattering cross-section $\sigma_d(\theta,\phi)$ is the probability of light being scattered in the direction (θ, ϕ) by a scatterer. For a particle of size much smaller than the wavelength (Rayleigh scattering) the light is scattered almost uniformly in all directions (isotropic scattering). For a large particle, light is scattered mostly in the forward direction (anisotropic scattering) within an angle of $1.2\lambda/d$, where λ is the wavelength of light and d is the diameter of the particle. For intermediate size particles

$\sigma(\theta,\phi)$ depends strongly on the scattering angle θ.

The transport mean free path (l_t) describing the random walk of photons is given as: $l_t = 1/n\sigma_m$, where σ_m is the momentum exchange scattering cross-section of the scatterer, and $l_t = l_s/(1-g)$, where g - the mean cosine of the scattering angle - measures the anisotropy of the scattering. These relations are valid only when the scatterers are far apart and uncorrelated. The σ_m and g are given by the following expressions

$$\sigma_m = \int \sigma_d(\theta,\phi)(1-\cos\theta)\sin\theta d\theta d\phi \qquad (1.2)$$

and

$$g = \int \sigma_d(\theta,\phi)\cos\theta\sin\theta d\theta d\phi / \int \sigma_d(\theta,\phi)\sin\theta d\theta d\phi \quad . \qquad (1.3)$$

These parameters depend on the particle size compared to the wavelength of light and the refractive index of the particle. A change in the chemical composition of the medium will result in a change of l_a, while physical changes such as changes in number density, cell size, cell-cell correlation, aggregation of several cells into a larger particle will result in a change of l_t. Observing such changes can be very useful in detecting abnormalities that might have developed in tissues.

Light propagation in a scattering medium can be described analytically using Maxwell equations[4,5]. Because of the mathematical complexities involved in solving these equations in such complex systems various approximate theories and models such as *transport theory, diffusion approximation*, and *Kubelka-Munk theory* have been developed to predict the propagation of light in a random medium[4-9]. The optical parameters of various biomedical media can be obtained from the predictions of these theories and the experimental measurements. One of the common methods to obtain the optical parameters of tissues has been to measure the attenuation of cw light transmission as a function of tissue thickness[10-21]. This technique, generally, measures

the coherent part of the transmitted light. It is difficult to measure the optical parameters for thick samples this way as the coherent transmission decreases exponentially with the sample thickness. With the advent of pulsed lasers and ultrafast detection systems, one can obtain the optical parameters using time-resolved scattering techniques[5,22-33].

1.2 Thesis Statement

The focus of this thesis is to study biomedical and other model random media using fluorescence spectroscopy and ultrafast time-resolved elastic light scattering. The goal is to study the optical properties of these random media that are sensitive to the morphological changes occurring therein by measuring fluorescence and photon transport.

The main objectives of the work described in this thesis are:

* to investigate *native fluorescence* in tissues at various excitation wavelengths that are sensitive to benign and cancer environment;

* to study the effect of *self absorption* and *scattering* on the fluorescence yield in the uv and visible region;

* to study *photon migration* in biomedical and other random media using ultrashort laser pulses to determine the key optical parameters such as the transport mean free path and the absorption length;

* to study various geometries for forward and backscattering of ultrashort laser pulses using diffusion approximation; and

* to study the viability of using snake photons to image a translucent object hidden inside a random medium with ultrafast time-gated detection.

1.3 Thesis Organization

In Chapter 2, a spectroscopic study of native fluorescence from normal, benign and malignant human breast tissues in visible and ultra violet region is presented. First, visible excitation is used to study benign and malignant breast tissues *in vitro*. A lack of spectral difference in this region leads to a study of uv excitation in order to involve various other native fluorophores such as tryptophan, collagen, elastin, and NADH. A further study of excitation spectra from various benign and malignant tissues suggests the suitability of uv excitation around 300 nm region for detection of breast malignancy.

Chapter 3 presents spectral optical density measurements of small particles and thin breast tissues. This qualitative study shows a relative independence of scattering cross-sections of breast tissues from the wavelength of light in the visible and uv region. Optical density measurements through various random media of small latex bead suspensions in water agree qualitatively with the theoretical predictions based on Mie theory.

Chapter 4 describes photon migration in a random scattering medium. Forward light scattering using *diffusion approximation* is used to determine the optical parameters l_t and l_a for various tissues and model random media by fitting the measured temporal profiles. Experimental methods based on time-resolved detection techniques to measure the transmission of ultra short laser pulses through thick tissues and other model random media are described.

Chapter 5 describes backscattering of light from various random media. First it shows how a qualitative study of temporal profiles of back scattered pulses from malignant and non-malignant samples can provide a diagnostic tool that can complement

other breast diagnostic methods such as the fluorescence ratio technique described in chapter 2. Backscattered pulses are further studied to determine the optical parameters for various tissues and model random media. Two different experimental setups are used with single-point source-detection and two-fiber input-output configuration to measure the temporal profiles of the backscattered pulses. These temporal intensity profiles are fitted to appropriate equations based on the diffusion approximation to obtain the transport mean free paths and the absorption lengths. A comparison of the optical parameters obtained from these backscattering measurements with those obtained from time-resolved pulse transmission is made to complete the chapter.

Chapter 6 describes ultrafast time-gated detection methods for imaging one type of tissue inside another. The work is done in both visible and infrared wavelength region.

In Chapter 7 I summarize my work. Finally, in Chapter 8, I describe some related experiments in optical spectroscopy and light scattering that can be conducted for further investigation.

1.4 References

1. W. Demtroder, *"Laser Spectroscopy"*, 2nd Ed., Springer Verlag, 1973

2. I. D. Campbell and R. A. Dwek, *Biological Spectroscopy*, The Benjamin/ Cummins Publishing Co., Inc. California (1984)

3. S. Udenfriend, *"Fluorescence Assay in Biology and Medicine"*, New York: Academic, Vol. 1, 1962, Vol. 2, 1969

4. A. Ishimaru,"Diffusion of light in turbid material," *Appl. Opt.*, 28, p2210-2215, 1989

5. A. Ishimaru, *Wave propagation and scattering random media*, New York: Academic, 1978

6. A. E. Profio,"Light transport in tissue," *Appl. Opt.*, 28, p2216-2222, 1989

7. R. Graaff, J. G. Arnoudse, F. F. M. de Mul and H. W. Jentink,"Light Propagation for anisotropically scattering scattering media based on a rigorous solution of the transport equation," Appl. Opt., 28, p2273-2279, 1989

8. A. E. Profio and D. R. Doiron,"Dosimetry considerations in phototherapy," Med. Phys., 8,p 190-196, 1981

9. A. J. Welch, G. Yoon, and M. J. C. van Gemert,"Practical models for light distribution in laser irradiated tissue," Lasers in Surgery and Medicine, 6, p488-493, 1987

10. B. C. Wilson, W. P. Jeeves and D. M. Lowe, In vivo and post-mortem measurements of the attenuation spectra of light in mammalian tissue," Photochem. and Photobiol., 42, p153-162

11 B. C. Wilson, M. S. Patterson and S. T. Flock,"Indirect versus direct techniques for the measurement of the optical properties of tissues," Photochem. and Photobiol. 46, p601-608, 1987

12. R. Marchesini, A. Bertoni, S. Andreola, E. Melloni and A. E. Sichirollo, "Extinction and absorption coefficients and scattering phase functions of human tissues in vitro," Appl. opt., 28, p2318-2324, 1989

13. J. L. Karagiannes, J. Zhang, B. Grossweiner and L. I. Grossweiner," Application of the 1-D diffusion aaproximation to the optics of tissues and tissue phantoms," Appl. Opt., 28, p2311-2317, 1989

14. S. Nakamura, Y. Nishiwaki, S. Sujuki, S. Sakaguchi, Y. Yamashita and K. Ohta," Light attenuation in human liver and hepatic tumors after surgical resection," Lasers in Surgery and Medicine, 10, p12-15, 1990

15. S. L. Jacques, C. A. Alter, and S. A. Prahl, "Angular dependence of HeNe laser light scattering by human dermis," Lasers in the Life science 1, p309-333, 1987

16. R. Marchesini, A. Bertoni, S. Andreola, E. Melloni and A. E. Sichirollo, "Extinction and Absorption Coefficients and Scattering Phase Functions of Human Tissues *in vitro*,,"*Appl. Opt.*, 28, p2318-2324, 1989

17. P. Parsa, S. L. Jacques and N. S. Nishioka, "Optical Properties of Rat Liver between 350 and 2200 nm," Appl. Opt., 28, p2325-2330, 1989

18. L. O. Svaasand and R. Ellingsen, "Optical Properties of Human Brain," Photochem. Photobiol., 38, p73-76, 1983

19. L. O. Svaasand and R. Ellingsen, "Optical Penatration in Human Intracranal Tumors," Photochem. Photobiol., 41, p73-76, 1985

20. M. Motamedi, S. Rastegar, G. LeCarpentier and A. J. Welch, "Light and Temperature Distribution in Laser Irradiated Tissue: The Influence of Anisotropic Scattering and Refractive Index," Appl. Opt., 28, p2230-2237, 1989

21. G. A. Navarro and A. E. Profio, "Contrast in Diaphanography of the Breast," Med. Phys., 15, p181-187, 1988

22. K. M. Yoo, Y. Takiguchi and R. R. Alfano, "Dynamic Effect of Weak Localization on the Light Scattering from Random Media Using Ultrafast Laser Technology," Appl. Opt., 28, p2343-2349, 1989

23. M. S. Patterson, B. Chance and B. C. Wilson, "Time Resolved Reflectance and Transmittance for the Noninvasive Measurement of Tissue Optical Properties," Appl. Opt., 28, p2331-2336, 1989

24. S. L. Jacques, "Time Resolved Propagation of Ultrashort Laser Pulses within Turbid Tissues," Appl. Opt., 28, p2223-2229, 1989

25. K. M. Yoo, F. Liu and R. R. Alfano, "Angle-and Time-Resolved Studies of Backscattering of Light from Biological Tissues," Proceedings of SPIE: Time-Resolved Laser Spectroscopy in Biochemistry II Convention-1990

26. K. M. Yoo and R. R. Alfano, "Time-Resolved Depolarization of Light Scattering in Random Media," Phys. Lett. A, 142, p531, 1989

27. K. M. Yoo and R. R. Alfano, "Determination of Attennuation Lengths Arising from Scattering and Absorption from the Temporal Profile of the Backscattered Pulse," Opt. Lett., 15, p276, 1990

28. K. M. Yoo, F. Liu and R. R. Alfano, "Biological Materials Probed by the Temporal and Angular Profiles of the Backscattered Ultrafast Laser Pulses," J. Opt. Soc. Am. B, 7, p1685-1693, 1990

29. K. M. Yoo, K. Arya, G. C. Tang, J. L. Birman and R. R. Alfano, "Coherent Backscattering of a Picosecond Pulse from a Disordered Medium : Analysis of Pulse Shape in the Time Domain," Phys. Rev. A, 39, p3728-3731, 1989

30. R. A. Ahmed, K. M. Yoo, R. M. Klapper and R. R. Alfano, "Time Resolved

Backscattering of Pulse to Monitor Different Stages of Eye Cataract," Appl. Opt., 29, p896, 1990

31. R. Vreeker, M. P. Van Albada, R. Sprik and A. Lagendijk, "Femtosecond Time-Resolved Measurement of Weak Localization of Light," Phys. Lett., 132, p516-519, 1988

32. K. Shimizu, A. Ishimaru, L. Reynolds and A. P. Bruckner, "Backscattering of a Picosecond Pulse from Densely Distributed Scatterers," Appl. Opt., 18, p3484, 1979

33. Y. Kuga and A. Ishimaru, "Retroreflectance from a Dense Distribution of Spherical Particles," J. Opt. Soc. Am. , A8, p831-845, 1984

CHAPTER 2

Fluorescence Spectroscopic Studies of Human Tissues and Model Fluorophores

2.1 Introduction

Fluorescence spectroscopy has been extensively used for over 50 years by the medical and biological community using fluorescent probes. In the past, there has been a search for novel diagnostic approaches to differentiate diseased and normal tissues using optical spectroscopy[1-5]. The harmful effects of x-rays and nuclear radiation have prompted researchers to look for various other diagnostic and imaging techniques without the disadvantages of the ionizing radiation. For example, during the past three decades various procedures such as thermography, ultrasonography, cytology of breast secretions, immune diagnosis, computed tomography, and magnetic resonance imaging have been developed with the goal of achieving the same or better accuracy than mammography[6-10]. Fluorescence spectroscopy and time-resolved optical imaging are recent additions to these methods though they are still at a very early stage of development.

The fluorescence of extrinsic dyes such as hematoporphyrin derivative (HPD) is currently being investigated for cancer detection[11]. HPD is injected into the body where it spreads to different tissues. Malignant tumors retain this extrinsic fluorophore longer than their surrounding normal tissues. Consequently, with external light excitation at an appropriate wavelength and at a later time, the malignant tumor with a higher concentration of HPD yields greater fluorescence than its surrounding normal tissue, enabling the tumor to be detected. However such extrinsic markers interact and interfere with the native cellular environment.

Recent efforts have been made to investigate the use of the intrinsic fluorophores present in tissues to characterize their physiological state. The use of such intrinsic (native) fluorophores enables us to gain information about the tissue micro structure and the changes therein without interfering with the native cellular environment. Tissues are made up of proteins, nucleic acids, lipids, and other components with many fluorescing and non-fluorescing chromophores[4,11]. There are a number of natural fluorophores in cells and tissues fluorescing in the ultraviolet and visible regions such as flavins, tryptophan, tyrosine, nicotinamide adenine dinucleotide (NADH), collagen and elastin to name a few key ones.

Over the past several years, significant progress has been made in using native fluorescence spectroscopy to detect tooth decay, cancer and atherosclerosis[11-31]. In 1981, Alfano and Yao used native fluorescence as a diagnostic tool for the first time in the detection of carious teeth. In the early 1980s, Alfano and co-workers[13-14] clearly established that differences exist in fluorescence spectra from malignant and normal rat tissues and later extended the work to normal and malignant tissues of human breast and lungs, and found differences in the spectral profiles[15,18]. This work was done at 457 nm, 488 nm, and 514 nm excitation wavelengths using a cw argon laser.

Buccal carcinoma has been studied by a Chinese group[17] with optical fibers coupled to a spectrometer excited by a xenon-ion laser operating at 365 nm. Premalignancy studies have also been pursued using this technique. Alfano and group found differences in the fluorescence spectra of normal and malignant breast tissues[18] photoexcited by the second and the third harmonics of an Nd-glass laser. Spectral profiles from buccal carcinoma and other breast malignancies were found to display different spectroscopic signatures.

Normal and diseased bladder wall and gastrointestinal tracts have also been studied by Feld's group[21,22]. Fluorescence spectra of adenoma and normal mucosa

have been found to be different using a nitrogen-pumped dye laser. Fluorescence contour mapping of tissues where a measurement of fluorescence emission as a function of the excitation wavelength has also been performed along with a study of chromophores and proteins to establish the molecular details of the physiological properties of tissues by Feld and his group[23]. Fluorescence contour mapping has also been performed on human colon. Kapadia et al. tested the hypothesis that adenomatous transformation of colonis mucosa results in an alteration of laser induced fluorescence spectra that enables differentiation from normal or hyperplastic tissue[24].

Another study of colonic polyps by Schomacker et al using uv laser fluorescence has reported an 86% sensitivity of this modality[25]. Since the heterogeneous nature of polyps means significant differences in histological interpretation, the group compared the analysis of the polyps by two senior pathologists and found an 86% concordance with the pathology report issued by the clinical pathology department for polyps ultimately classified as adenomatous and an 89% concordance for hyperplastic polyps. So in their view, "if the assessment by senior pathologists is taken as the gold standard, the predictive value positive of 86% achieved by laser induced fluorescence (in their study) suggests that the technique might have the potential of achieving high accuracy comparable with clinical pathology."

Diseased artery as compared to normal artery have also been studied using native fluorescence. Kittrel et al. made the first attempt to distinguish between normal and fibrous arterial atherosclerosis[16] in 1985 by comparing the fluorescence intensity ratio at 600 nm relative to 580 nm obtained after irradiation at 480 nm with a Perkin-Elmer spectrofluorometer. Sartori et al.[26] were able to correlate the intimal thickness with the ratio of fluorescence intensities at 530/550 nm. Ratio of fluorescence intensities at 448 nm to 514 nm, and 538 nm to 524 nm measured by Deckelbaum were capable of discriminating normal and atherosclerotic aorta[19]. In 1987 Anderson et al.[20] also used a

nitrogen laser and found differences between the normal artery wall and atherosclerotic lesions, both for large arteries such as aorta, arteria femoralis and pulmonaris, as well as for coronary arteries. Differences in fluorescence from plaque and normal artery wall excited at 476 nm from an argon ion laser have also been observed by Feld and coworkers[27]. However different types of plaque have not been distinguished from normal artery. Deckelbaum et al. failed to distinguish calcified atherosclerotic plaque from normal artery using the steady state technique. To solve this problem it became necessary to probe other techniques such as time-resolved fluorescence.

In developing a diagnostic method for cancer detection it is essential to separate malignant tumors not only from normal tissues but also from benign tissues and tumors. This necessity to include the benign tumors led to our work on normal, benign and malignant tissues and tumors from human breast and lungs using both visible and uv fluorescence spectroscopy which is detailed in this chapter.

We have demonstrated[28-30] that it is possible to separate malignant tumors from benign and normal samples using uv fluorescence spectroscopy - a major breakthrough. This work clearly shows the potential of fluorescence spectroscopy to be used as a new modality in breast cancer diagnosis.

2.2 Human Tissue and Pathology

Human tissues are broadly classified into four main categories: epithelial, muscular, nervous and connective according to its cell type.

(a) Epithilial tissue: Epithilial cells serve as protective covering. They are arranged in a series of layers or strata to form the outer part of the skin. They also line digestive, respiratory, and urinary tracts. The various external secretory glands (digestive, mammary, sweat, etc.) are composed of epithelial cells. Thus breast tissues are composed of epthelial cells. The various types of epithelial cells are: *columnar,*

cuboidal and *squamous*. The shapes of the columnar and cuboidal cells are evident from their names. Squamous cells are scale-like or plate-like. Glands composed of epithelial cells form *glandular tissue.* The simplest type of these secreting cells form a single tube and is called simple tubular. In other glands, the cells surround a central spherical cavity into which the glandular secretion is received. The channel or duct from the cavity leads to the surface. Breast tissue contains such ducts. Several lobules are formed in breast tissues by means of separation of the connective tissue.

(b) Muscular tissue: Muscular tissue form the muscles. The two types of muscular tissues are *striated* and *unstriated.* Skeletal or voluntary muscle are striated while involuntary muscle of the internal organs except the heart, are unstriated.

(c) Connective tissue: Connective tissue serves as a strengthening, connecting, and supporting material. It binds together masses of different types of cells and forms a supporting framework for various organs. It also serves to fill in spaces between neighboring organs and parts and replaces tissue destroyed by injury or disease. Connective tissue consists of slender fibers embedded in a homogeneous jelly like matrix or ground substance. The ground substance dominates and cells are relatively few. The fibers in some cases possess elastic properties and contain the protein *elastin*. In other parts, they are bundles of strong fibers with no elastic properties. These contain a protein known as *collagen*. Adipose or fatty tissue is a modified connective tissue.

(d) Intercellular substances: Between the cells forming a solid tissue there is a semifluid viscous and structureless material resembling a soft jelly. In most tissues this acts as a glue to hold cells together and to permit water, dissolved substances and certain other materials to pass between cells. In some other tissues such as connective tissue, this intercellular substance is more abundant and forms a matrix in which cells and fibers are embedded. Tissues are made up of cells in between which are

connective tissue which contains the tissue fluid and ground substance. The tissue fluid contains various large proteins, ions, gases, amino acids, sugars, vitamins, lipids and hormones, which are exchanged between cells. The body contains 55% water, 19% proteins, 19% fats, 1% carbohydrates and 7% inorganic materials. This implies that the tissue fluid contains more amounts of proteins and lipids than other substances.

Human breast tissue contains main ducts which branch out into several smaller ducts that lead into lobules. Approximately 15 lobules serve each duct. The lining of the ducts and the lobules are epithelial tissue. The space in between lobules is filled with fat and connective tissue in varying proportions.

(i) *Normal* breast tissue are generally glandular and lipomatous in nature.

(ii) *Benign tissue* includes fibrocystic mastopathy. These benign tissues are the fibrous tissue of the breast which appear white in color.

(iii) A *neoplastic tumor* is an abnormal mass of tissue, the growth of which exceeds and is uncoordinated with that of the normal tissue.

Benign tumor includes neoplasms that do not usually recur after excision. Chances of transformation to malignancy is also less. The cells in a benign tumor are well-differentiated, that is, they closely resemble the parent tissue. There are some cases of *cystosarcoma phylloides*, though, which may already be cancerous. Benign tumors of the surface epithelia are called *papillomata* and those of the solid epithelia are *adenomata.* In the connective tissues, the benign tumors are named after the tissue of origin, e.g. *fibroma* and *osteoma.* The benign tumors that are of concern in these studies are generally *fibroadenomas* and some are *adenofibromas.*

A malignant tumor always invades the surrounding tissue. It eventually enters channels like the lymphatic and blood vessels, and groups of cells are carried to other parts, where they set up secondary growths, or metastases. Microscopically, they show less accurate reproduction of the parent tissue than do benign tumors. Malignant

epithelial tumors are all *carcinomata.* The cancers originating from mesoepithelial tissue (which include the tiny muscles and the connective tissue) are known as *sarcomas.* Most breast cancers originate from the cells which line the ducts (*ductal carcinoma*). Breast malignancy can generally be categorized as *invasive* or *non-invasive.* Invasive cancer penetrates the basement membrane extending through the duct wall into the surrounding fibrous supporting tissue. These cancers are more commonly seen. The noninvasive cancers have cells that have not penetrated the limiting basement membrane and remain confined within the walls of the ducts. Breast cancers originate from the *epithelia* and *mesoepithelial* tissue. Again the tumor may arise from the lobules or the ducts of the breast. These are called *lobular* and *ductal*, respectively. The malignancy usually originates from the cells which line the ducts. Ductal carcinomas arise either in the main ducts or the smaller ducts, more often deep in the smaller branches.

Breast tissue, like any other tissue of the human body, contains *elastin* and *collagen* as the structural proteins and other fluorophores such as *NADH* (nicotinamide adenine dinucleotide-reduced form), *NADPH* (nicotinamide adenine dinucleotide phosphate-reduced form), NAD^+ (nicotinamide adenine dinucleotide-oxydised form), *tryptophan, tyrosine, flavins* (FAD - flavin adenine dinucleotide and FMN - flavin mononucleotide), porphyrins and other biomolecules. The framework of tissues is given by the structural proteins collagen and elastin. Breast malignancies are known to induce productive fibrosis[32-33] or produce collagen directly[34]. Studies have also shown that there is increase in elastic tissue in infiltrating ductal carcinomas[35-36]. Studies with rat kidney fibroblasts[37] have shown a 2-3 fold decrease in the absolute concentrations of NAD^+ and *NADH* following murine sarcoma virus transformation. Recent medical studies have found that lung and breast malignancies show higher plasma free tryptophan levels[38]. Free tryptophan should show higher fluorescence yield because of less non-radiative decays.

2.3 Experimental Methods

Here we describe the various experimental set-ups used in our spectroscopic measurements. The visible fluorescence measurements were done using an argon laser while the uv fluorescence work was done using a spectrophotometer.

2.3.1 Visible fluorescence spectroscopy

The experimental set up used to measure the fluorescence spectra with visible excitation from various biological samples is displayed in Fig. 2.1. A cw argon ion laser is used to excite the sample. The laser wavelengths used to excite the sample is selected from 457.9 nm, 488 nm, and 514.5 nm. Depending on the fluorescence yield from the sample the laser power can be changed from 1 to 100 mW. For most biological samples, a power of about 10 mW is strong enough.

The laser beam is focused onto the front of the sample to a spot size of about

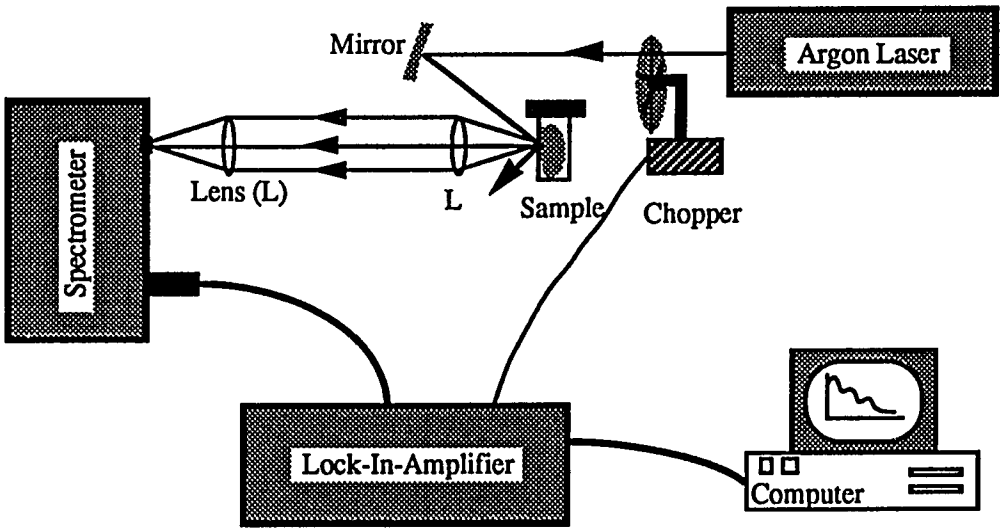

Fig. 2.1. The experimental setup for fluorescence measurement in the visible region.

200 μm. To avoid the influence of the weak emission lines surrounding the strong laser

line used to excite the sample, a corresponding narrow band filter of 458 nm, 488 nm, or 514.5 nm is inserted in the laser path to eliminate the spectral lines from the laser. The laser is chopped at about 200 Hz. The laser reflection from the cuvette surface is strong so that one should be careful and avoid directing the reflection into the collection optics.

The fluorescence from the sample's surface is collected and focused into the entrance slit of a double 1/2 m grating spectrometer (Spex Industries) blazed at 500 nm. A photomultiplier tube (Model RCA 7265, S-20) is located at the exit of the spectrometer to measure the fluorescence intensities at different wavelengths. The spectral resolution of the spectrometer is 2 nm. The output of the photomultiplier tube is connected to a lock-in-amplifier (EG&G Princeton Applied Research), and then to a X-Y recorder and a personal computer to display the spectrum.

As was mentioned earlier, 488 nm excitation was found to be important to distinguish malignant tumors from normal breast tissues. In order to check the diagnostic capability of this method, a need to study benign breast tissues and tumors was felt.

Seven cases of benign tumors (fibroadinoma) and benign tissues (with fibrosystic disease) were studied along with 5 cases of malignant tumors (ductal carcinoma) from human breast. They were excited at 488 nm and the emission spectra were recorded from 500 nm to 700 nm. Figure 2.2 displays two average spectral profiles of the benign and the malignant samples along with their difference. Both of these spectral profiles are smooth curves without the signature of absorbance of blood.

This makes the 488 nm excitation of flavin molecules untenable as a complete diagnostic method as it fails to differentiate between malignant and benign tumors. This led us to probe other native fluorophores in order to distinguish malignant tumors not only from normal tissues but from benign tissues and tumors as well. The abundance

of native fluorophores in the uv region made it a viable proposition to investigate tissue fluorescence at this wavelength range.

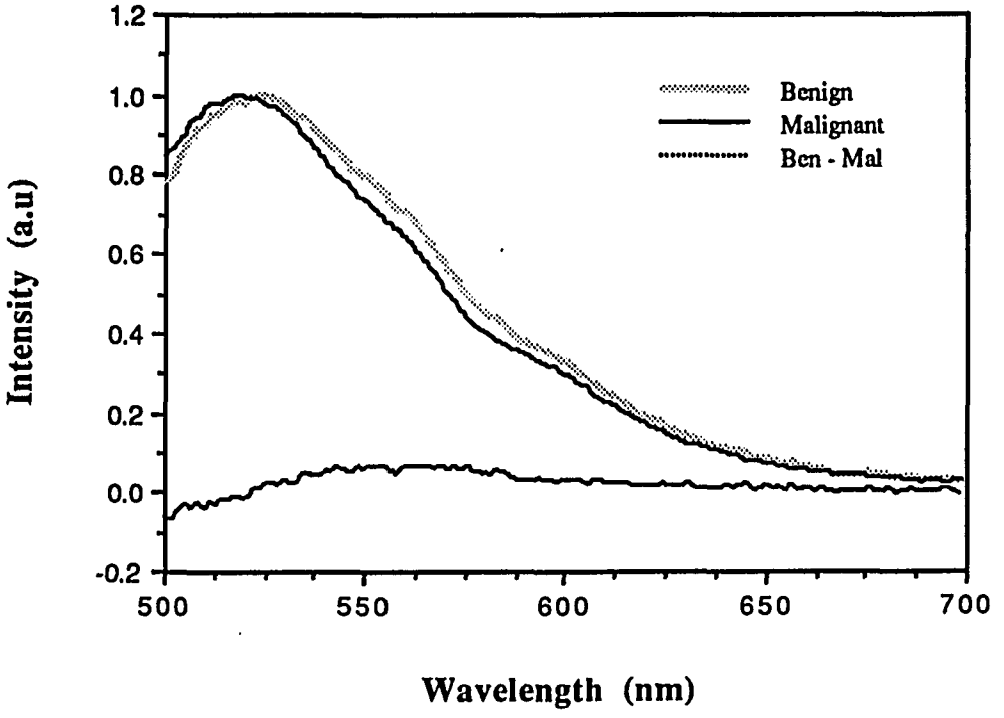

Fig. 2.2. Average emission spectra from benign and malignant samples with 488 nm excitation. The bottom curve is the difference between the two.

2.3.2 UV Fluorescence Spectroscopy

The apparatus used in this experiment is a lamp based Mediscience CD Scan spectrofluorometer based on *Perkin-Elmer LS-50 Fluorescence Spectrometer* shown in Figure 2.3. The excitation source in this spectrometer is a special xenon flash tube which produces an intense, short duration pulses of radiation over the spectral range of the instrument. A small lamp close to the excitation source maintains an even triggering of the xenon flash tube at line frequency. Energy from the source is focused by the ellipsoidal mirror and reflected by a toroidal mirror onto the entrance slit of the excitation

monochrommator. The monochromator consists of the entrance slit, with the central wavelength being determined by the setting of the grating, the angle of which is controlled by a stepper motor. The majority of the excitation beam is transmitted to the sample area via the focusing toroidal mirror, a small proportion is reflected by a beam splitter onto the reference photomultiplier.

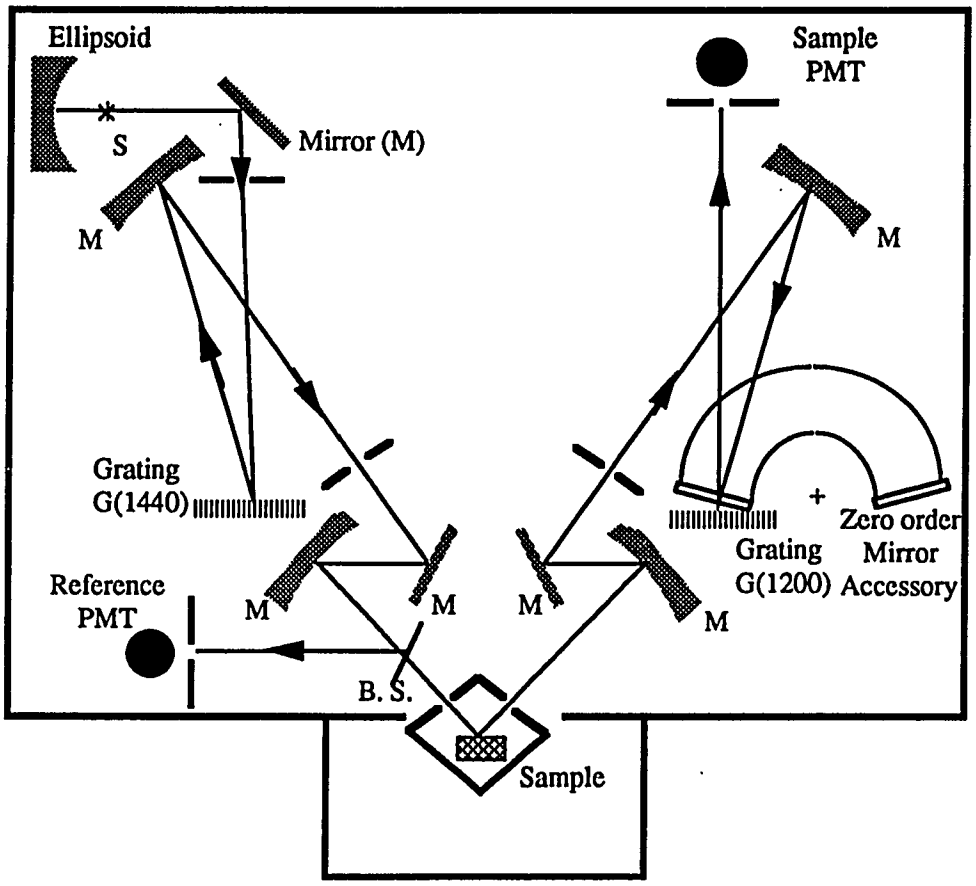

Fig. 2.3 A schematic diagram of the Fluorescence spectrometer. S: Source, B. S. - Beam Splitter

Energy emitted by the sample is focused by the toroidal mirror onto the entrance slit of the emission monochromator. The monochromator consists of the entrance slit, a spherical mirror, a 1200 lines per millimeter grating and the exit slit. A narrow

wavelength band emerges from the exit slit, with the central wavelength being determined by the setting of the grating, the angle of which is controlled by a stepper motor. The excitation and emission monochromators can be scanned over their ranges independently, synchronously or driven to selected points in their ranges. Synchronous scanning can be either a fixed wavelength difference or a fixed difference between the excitation and emission monochromators. The spectral ranges of the monochromators are about 230 nm to 800 nm for excitation and about 230 nm to 900 nm emission. The excitation and emission spectra are stored by a personal computer.

This lamp based spectrometer was used for our uv fluorescence spectral measurements on human breast tissues. Frontal excitation was used to pump the tissue samples placed in quartz cells. The samples were excited at 300 nm wavelength and the resulting emission spectra were recorded from 320 to 580 nm. Excitation spectra at 340 nm and 440 nm emission were recorded for exciting wavelengths from 250 to 325 nm. The full width at half maximum (FWHM) of the exciting beam was about 5 nm. Some 25 malignant (ductal carcinoma), 13 benign tissues and 12 benign tumors (fibroadenoma), 6 normal samples from human breast were tested. Also one malignant and one normal lung sample were tested. Except for some samples which were later used in a blind study, histopathologic study was done on all others and the histology was known before the fluorescence experiment was performed. The samples were collected fresh within an hour of surgery without fixing them with formalin. The ratio of intensities at 340 nm to 440 nm were calculated for each sample and compared for differences. This pair of wavelengths (340 and 440 nm) was selected to eliminate the effect of absorption on the fluorescence by the blood present in the tissues, which is important in developing a diagnostic modality for *in vivo* studies.

To have a better insight into what could cause the fluorescence spectra profiles from the tissues, a number of potential fluorophores such as proteins - collagen, elastin

and trypsin ; amino acids - tryptophan, tyrosine; and NADPH - a nucleotide were tested for fluorescence. Except trypsin which was tested as a 25 % solution with EDTA all other compounds were tested after solution in water.

2.4 Results

The fluorescence spectra from 320 nm to 580 nm fromnormal, benign and malignant breast tumors under 300 nm excitation are displayed in Figure 2.4. The difference in spectral profile shown in the figure permits separation of cancerous from other tissue types. The ratio of intensities at 340 nm to 440 nm was calculated for each sample and compared for differences.

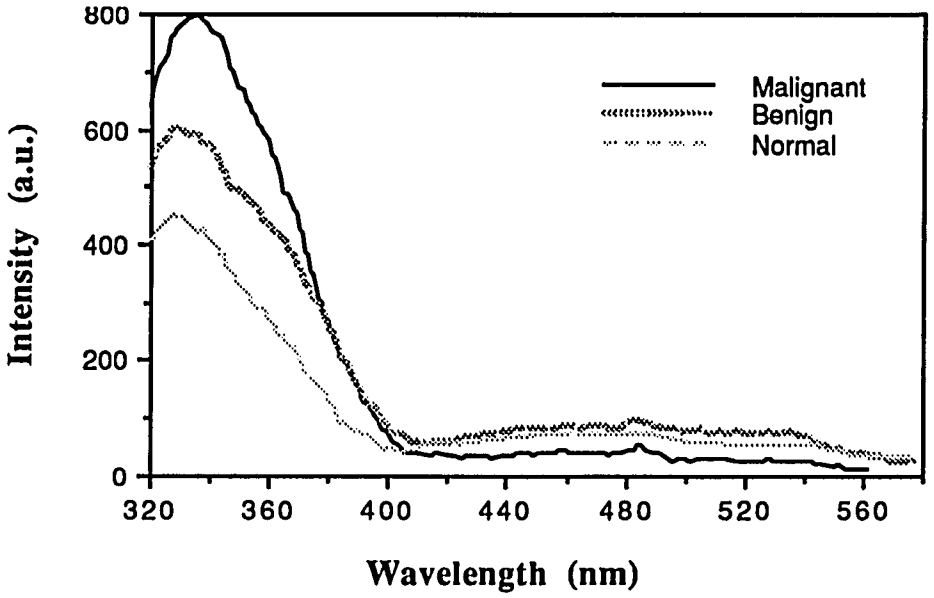

Fig. 2.4 Fluorescence emission spectra from normal, benign and malignant human breast tissues excited at 300 nm.

This pair of wavelengths (340, 440 nm) was selected to eliminate the effect of absorption on the fluorescence by the blood present in the tissues. This is possible because the blood absorbances at these two wavelengths are the same[27]. The relative

difference between the intensities at 340 nm and 440 nm is prominent in malignant tissues compared to benign and normal samples. The ratios of intensities at 340 nm and 440 nm wavelengths were calculated, and all cancer ratios were found to lie above 10, while benign and normal ratios lie below 9. A histogram of ratios for cancer, benign and normal tissues are displayed in Figure 2.5. The average number for malignant tissue is 14.9 and for benign tissues and tumors is 4.9 while the single normal sample gave a ratio of 4.85. The ratio range for malignant tissue extends from 9 to 20 while that for benign samples is from 2 to 9.

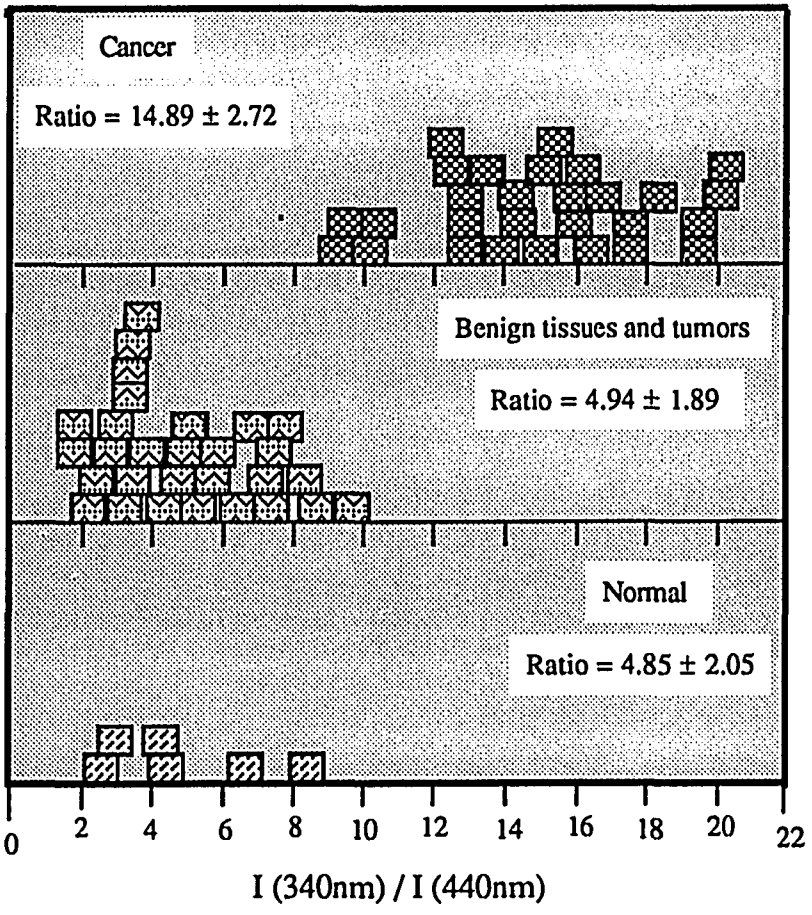

Fig. 2.5. A histogram of fluorescence intensity ratio at 340 to 440 nm, excited at 300 nm for normal, malignant and benign tissue samples. Each box represents one sample. Center of each box matches with the ratio I(340) / I(440) of the corresponding sample.

The histogram shown in Figure 2.5 clearly demonstrates that malignant tissue samples can be distinctly distinguished from normal and benign breast samples using the 300 nm excitation. To check the accuracy of this diagnostic approach, a blind study was done on several samples without prior knowledge of their morphology. The result was later found to be consistent with the histological assessment of the of those samples. Further studies have been conducted by the IUSL group[39-40]. The statistics of a larger number of samples are given in Table 2.1. The accuracy is determined in comparison with the histological assessment of the tissue samples by a senior pathologist.

Although our experiment was done mainly on human breast samples, one malignant and one normal lung sample were also tested, and the ratios of intensities in these two cases agree well with the histogram for breast samples displayed in Figure 2.5.

Cancer	Number of Samples	40
	Sensitivity	92.5%
	False Negative	7.5%
Benign and Normal	Number of Samples	47
	Specificity	98%
	False Positive	2%

Table 2.1 The statistics of 87 human breast tissue samples showing the accuracy of the uv-fluorescence technique[39-40].

Four malignant and three benign samples were run for excitation spectra from 250 to 325 nm at emission wavelengths 340 nm and 440 nm. The ratio of these two excitation spectra was calculated for each sample and compared to determine what

excitation wavelength yields maximum possible ratio difference between malignant and benign samples. The ratio of intensities at 340 to 440 nm for different excitation wavelengths is shown in Figure 2.6. The wavelength of 300 nm appears to be the most appropriate excitation wavelength for breast, but wavelengths from 250 to 315 nm can also be used to detect the difference.

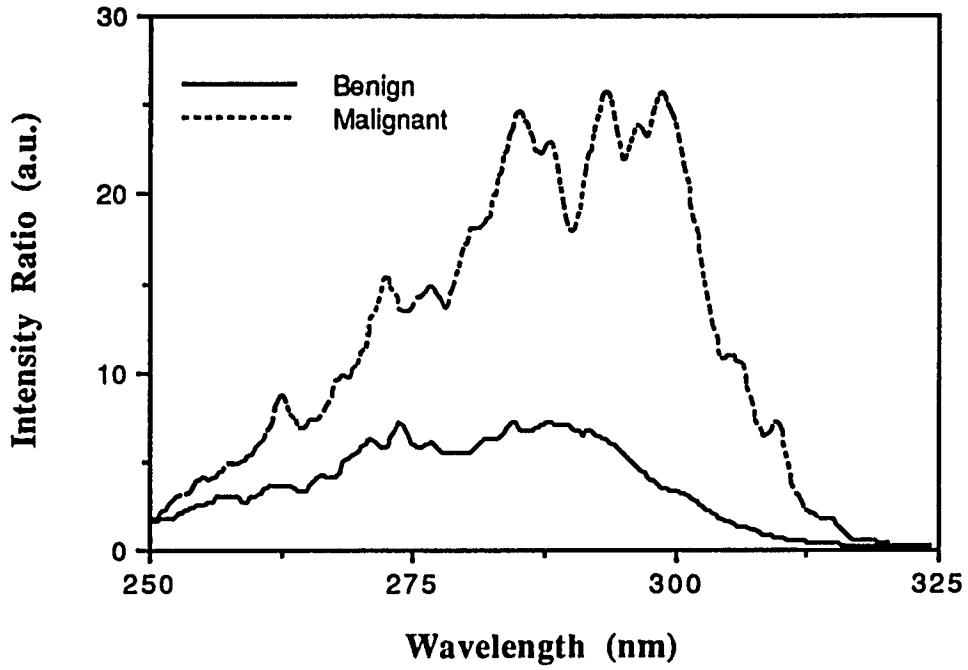

Fig. 2.6 Ratio of fluorescence emission intensity at 340 nm to 440 nm versus excitation wavelengths for malignant and benign tissues.

2.5 A Comparison of Various Breast Diagnostic Procedures

In general, a breast diagnostic process starts with a clinical examination and ends with a histological assessment of the suspected lesion after a surgical biopsy. X-ray mammography has been a routine complement to clinical examination before a biopsy is done. During the past three decades various other procedures such as xeroradiography, thermography, ultrasonography, cytology of breast secretions, immune diagnosis,

computed tomography, and magnetic resonance imaging (MRI) have been developed to further improve the breast diagnostic procedure[6-10]. To these methods fluorescence spectroscopy and time-resolved optical imaging are recent additions though they are still at a very early stage of development. Out of these various techniques mammography and ultrasonography (cyst vs solid mass) are presently accepted, computational tomography is at an acceptable stage, and the acceptability of thermography, MRI, fluorescence spectroscopy and optical imaging are to be determined[10].

The accuracy of these methods are determined in general by comparing them with the results of the histological assessment (using the paraffin section) which is taken as the golden standard. Histological assessment of a suspected lesion is done by a pathologist using frozen section and permanent section diagnosis[41-42]. After a surgical biopsy is conducted the tissue specimen is frozen at -20° C. Then approximately 4 μm frozen sections are prepared on glass slides using a michrotome at -20° C, and fixed with formalin and ethanol. This tissue fixation stops the cell processes. Then these fixed sections are stained with hematoxylin and eosin, and cover slips (thin glass plates) are put on them. The pathologist makes his diagnosis in about 15 minutes after the surgery by looking at the types of cells and their arrangement under a microscope with the knowledge of the source of the tissue. The remaining tissue is processed for permanent section by putting it in a tissue processor overnight. The machine subjects the tissue after fixing it to various concentrations of ethanol to remove water from the tissue. Then it subjects it to paraffin to remove water further from the cells and keep them from crushing. Next morning it is removed from the processor and mounted on a paraffin block. then the block is cooled and 4 μm sections are prepared. These sections are baked in order to stick to the slide and melt off the excess paraffin. Then the sections are stained and cover slips are put on them. These are called the permanent sections. The final diagnosis is made after looking at these permanent sections. In a

study of 2743 cases using frozen section diagnosis, an accuracy of more than 99% was obtained with only one false positive and 8 false negative cases[43]. Conventional film mammogram and xeroradiogram use x-ray radiation while ultrasonography uses ultrasonic waves to detect microcalcifications and large tumors with varying degree of accuracy. Thermography is another technique for breast examination. It registers the heat pattern of the breast via a monitor sensitive to infrared radiation. The increased metabolic rate of tumors causes increased heat production resulting in an abnormal thermal pattern. A comparison of clinical examination, mammography and thermography in 306 histologically confirmed breast cancers shows the detection sensitivity of these modalities at 82%, 85% and 72%, respectively[7,44]. When clinical examination was combined with mammography, the accuracy increased to 92%. Ultrasonography has been reported to show an accuracy of 90% though with only 82% correct diagnosis for lesions less than 2 cm in size[45]. The cytologic examination has been credited as a complementary technique with an accuracy of 50-80%[46]. Immune diagnosis of breast cancer based on various antigen and antibody assays have provided limited success[46]. For example, leukocyte-migration-inhibition test has shown positive results in 47% benign and 53% malignant cases[47]. Another study[9] has done a comparison of these various techniques reported by several groups over the years. It puts the sensitivity of mammography in patients with palpable breast lumps between 73% to 87% for various age groups. The sensitivity of ultrasound is found to be between 83-93%.

In comparison, the uv fluorescence method described above shows good accuracy with more than 90% sensitivity in the diagnosis of breast malignancy (Table 2.1). Another study of colonic polyps by Schomacker et al using uv laser fluorescence has reported an 86% sensitivity of this modality[25]. In their view, "if the assessment by senior pathologists is taken as the gold standard, the predictive value positive of 86%

achieved by laser induced fluorescence (in their study) suggests that the technique might have the potential of achieving high accuracy comparable with clinical pathology."

2.6 Potential Fluorophores

As the histogram in Fig. 2.5 suggests the comparison of two fluorescence intensity peaks at around 340 nm and 460 nm can separate malignant from normal and benign tissues and benign tumors. Since the ratio of the two intensities at 340 nm and 440 nm varies greatly by changing the excitation wavelength around 300 nm (shown in Fig. 2.6), it suggests that the two peaks could not be due to only one fluorophore[48]. Though the determination of the exact fluorophores giving rise to the fluorescence peaks requires extensive study one can make reasonable assignments to potential fluorophores by studying the excitation and emission spectra from tissues and model flurophores.

In order to have an insight into the group of potential fluorophores responsible for the tissue fluorescence, excitation spectra measurements were performed on several tissue samples (four malignant and three benign) with emissions at the two peaks of 340 and 460 nm. In addition, fluorescence spectra from several potential fluorophores were recorded. Figure 2.7 and 2.8 display the excitation spectral curves from benign and malignant samples at 340 and 460 nm emission wavelengths. The fluorescence spectra from collagen and elastin are shown in Fig. 2.9(a), while that from tryptophan and NAD(P)H are displayed in Fig. 2.9(b). The fluorescence maxima of tryptophan and NADPH are at 360 nm and 460 nm respectively, while both collagen and elastin give broadband fluorescence.

The two excitation spectra from both the tissues at 340 nm emission show peaks around 280-290 nm region (Fig. 2.7), while the spectrum at 460 nm emission from the benign tissue shows a composite structure (Fig. 2.8). These peaks in Fig. 2.7 may be

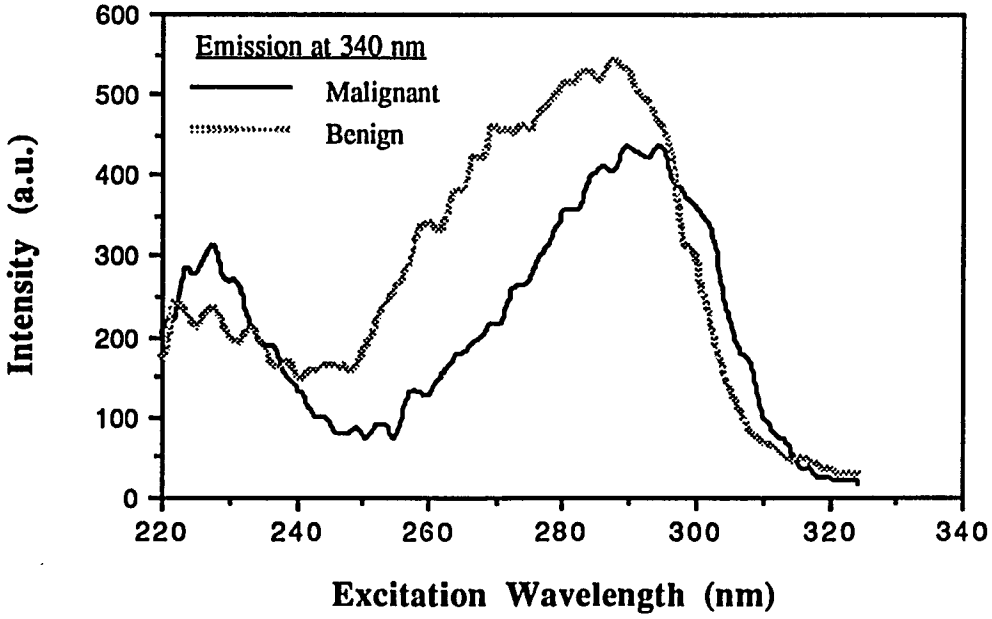

Fig. 2.7 Excitation spectra from benign and malignant tissue samples at 340 nm emission

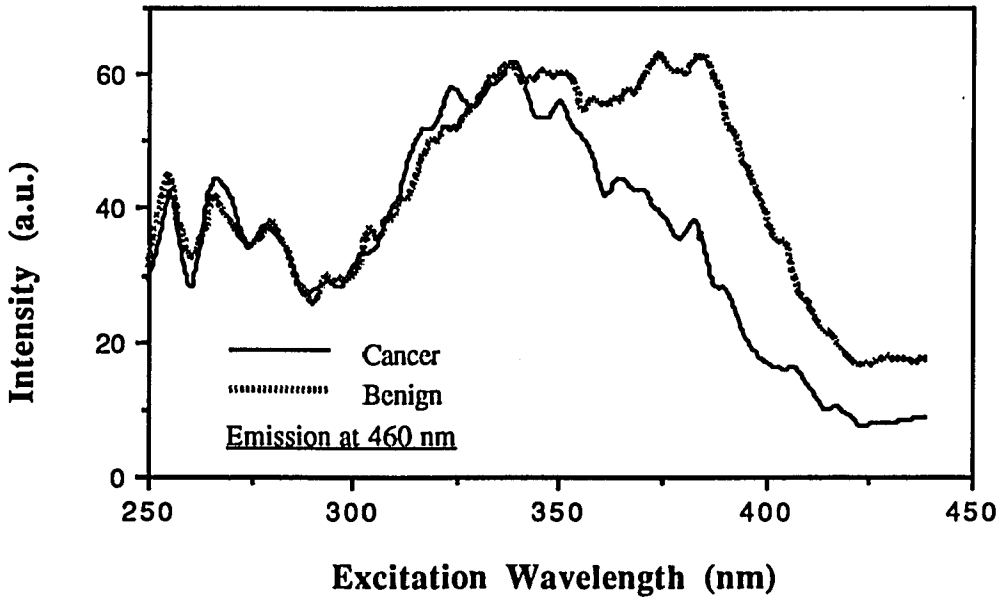

Fig. 2.8 Excitation spectra from benign and malignant tissue samples at 460 nm emission.

attributed to a potential native fluorophore tryptophan which has a strong excitation peak around 280 nm[49] and shows a strong emission peak at 360 nm as displayed in Fig. 2.9 (a). The fact that this emission peak from tryptophan has also been observed to

show spectral shift to 340 nm in human serum albumin[49] suggests that the 340 nm emission peak in tissue fluorescence is due to this abundant native fluorophore. Our assumption is also consistent with work done by other groups[38,50]. Recent medical studies have found that lung and breast malignancies show higher plasma free tryptophan levels[38].

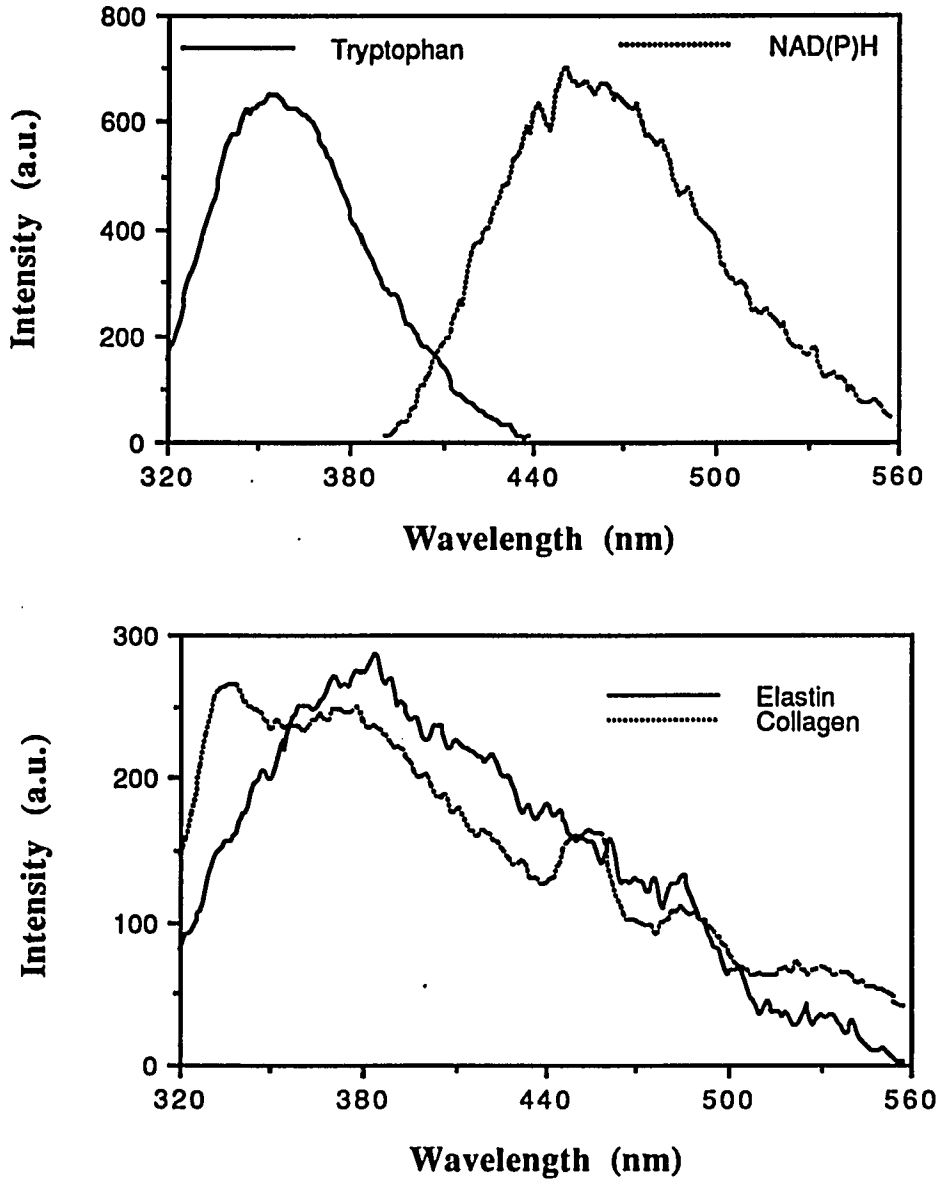

Fig. 2.9 Emission spectra of (a) Tryptophan and NAD(P)H and tryptophan, and (b) collagen and elastin at 300 nm excitation.

Free tryptophan should show higher fluorescence yield because of less non-radiative decays. A study[50] of time-resolved fluorescence from human normal and malignant breast tissues at our institute using femtosecond pulse lasers at 310 nm finds that the temporal profiles of the fluorescence at 340 nm show a double exponential decay. The study finds that the ratio of the fast decay component to the slower one is lower for malignant tissues compared to the non-malignant ones, and that points to more fluorescence yield at 340 nm in malignant tissues.

Similarly, the second fluorescence maximum from the tissues around 460 nm could be due to the nucleotide NAD(P)H, collagen or elastin, or due to a combination of all of these. Collagen, elastin and NADH show excitation peaks at 340, 390 and 340 nm regions[4, 34, 49]. This matches well with the composite excitation spectra from tissues at 460 nm emission shown in Fig. 2.8. Studies with rat kidney fibroblasts[37] have shown a 2-3 fold decrease in the absolute concentrations of NAD^+ and NADH following murine sarcoma virus transformation. Such a decrease in concentration will result in less fluorescence yield at 460 nm region for malignant tissues and that is consistent with our findings.

More studies will have to be conducted to have any definitive answer. Similar studies on cells, tissue fluids and other components are necessary and are being carried out by other members of the IUSL group[49].

2.7 Effect of Absorption and Scattering on Tissue Fluorescence

As we mentioned earlier tissue fluorescence can be greatly affected by self absorption in tissue itself. This was analytically shown by Pradhan[51]. A simple model was developed by them following Foerster's theory[52] to show the effect of absorption due to blood on the fluorescence spectra from breast tissues. But it ignored the effect of

scattering in tissues which is more dominant than absorption at different wavelength regions. The model can be modified further to take into account the effect of scattering on the incident beam and on the resulting fluorescence. Here we will ignore the fluorescence resulting from diffuse light which will be negligible in comparison to the fluorescence yield from the coherent beam.

We start with a monochromatic beam of light of intensity I_0 and wavelength λ_0 incident on a tissue sample of thickness d. The incident beam decays exponentially as per the Beer-Lambert Law[53]:

$$I_x(\lambda_0) = I_0(\lambda_0)e^{-\sigma_{T0}(\lambda_0)x} \tag{2.1}$$

where x is the distance propagated, $\sigma_{T0}(\lambda_0)$ is the sum of absorption and scattering cross-sections ($\sigma_T = \sigma_a + \sigma_s$) of the medium. The amount of absorption within a thickness dx will be

$$dI_x = I_0(\lambda_0)e^{-\sigma_{T0}(\lambda_0)x}\sigma_a dx \tag{2.2}$$

where $\sigma_a = \sigma_{ch} + \sigma_{fl}$ is the absorption by fluorophores and chromophores.

The equation 2 then reduces to

$$\begin{aligned} dI_x &= I_0(\lambda_0)e^{-\sigma_{T0}(\lambda_0)x}\sigma_{ch}dx + I_0(\lambda_0)e^{-\sigma_{T0}(\lambda_0)x}\sigma_{fl}dx \\ &= dIch + dI_{fl} \end{aligned} \tag{2.3}$$

The fluorescence emitted from dx at a distance x from the surface is proportional to *only* dI_{fl}. So the emission collected at λ_f with a bandwidth $d\lambda_f$ is given by

$$d^2 I_{\lambda_f}(\lambda_f, x) = \frac{F_R \Omega}{4\pi n^2} I_0 L(\lambda_f) \phi \sigma_{fl} e^{-(\sigma_{T0}+\sigma_{Tf})x} dx d\lambda_f \qquad (2.4)$$

where F_R is the reflection loss, $\Omega/4\pi$ is the solid angle, ϕ is the quantum efficiency, n is the refractive index, σ_{Tf} is the sum of absorption and scattering cross-sections at λ_f, and $L(\lambda_f)$ is the spectral distribution which is independent of the exciting wavelength.
By integrating the equation from 0 to d, where d is the thickness of the sample we get

$$dI(\lambda_f) = \frac{F_R \Omega}{4\pi n^2} I_0 L(\lambda_f) \phi \frac{\sigma_{fl}}{\sigma_{T0} + \sigma_{Tf}} (1 - e^{-(\sigma_{T0}+\sigma_{Tf})d}) d\lambda_f \qquad (2.5)$$

The spectral distribution $Li(\lambda_f)$ for various fluorophore components is given by the Lorenzian line-shape function for the i^{th} fluorophore as

$$L_i(\lambda_f) = \frac{1}{2\pi} \frac{d\lambda_{f,i} / \lambda_f^2}{(\frac{d\lambda_{f,i}}{2\lambda_f^2}) + (\frac{1}{\lambda_f} - \frac{1}{\lambda_{m,i}})^2} \qquad (2.6)$$

where $\lambda_{m,i}$ is the center wavelength of the i^{th} peak. So the fluorescence intensity for several fluorophore components will be given by the sum:

$$dI(\lambda_f) = \Sigma_i \frac{F_R \Omega}{4\pi n^2} I_0 L_i(\lambda_f) \phi \frac{\sigma_{fl}}{\sigma_{T0} + \sigma_{Tf}} (1 - e^{-(\sigma_{T0}+\sigma_{Tf})d}) d\lambda_f \qquad (2.7)$$

We see from this simple model that the fluorescence collection is strongly dependent on the scattering and absorption in the tissue. Now coming back to our uv-fluorescence experiment we find that by choosing the ratio of fluorescence intensities at 340 to 440 nm we can overcome the absorption due to blood. But what about the effect of scattering at these two wavelengths? Human tissue is a highly scattering medium. So

this must be taken into consideration. We will see in the next chapter that the scattering cross-section for breast tissues is relatively independent of wavelength in the visible and uv region. That means the ratio method will remain valid in this wavelength region or at any two wavelengths where both the absorption and scattering cross-sections are the same.

2.8 References

1. J. Yguerabide,"Nanosecond fluorescence spectroscopy of biological macromolecules and membranes," in *Fluorescence Techniques in Cell Biology*, Edited by A. A. Thaer and M. Sernetz, Springer Verlag, Berlin, p 311-31, 1973.

2. P. Pringsheim, *Fluorescence and Phosphorescence*, Interscience, New York, 1949.

3. J. B. Birks, *Photophysics of Aromatic Molecules*, Wiely, New York, 1970

4. S. Udenfriend, *Fluorescence Assay in Biology and Medicine*, New York: Academic, Vol. 1, 1962, Vol. 2, 1969

5. D. A. Long, *Raman Spectroscopy*. McGraw Hill, New York, 1977

6. *Early Detection of Breast Caner*, eds. S. Brunner, B. Langfeldt, and P. E. Anderson, Springer Verlag, New York, 1984

7. *Breast Cancer Diagnosis*, eds. G. S. Johnson, and A. E. Jones, Plenum Medical Bokk Co. New York, 1980

8. H. Vorherr, *Breast Cancer*, Urban & Schwarzenberg, Baltimore-London, 1980

9. I. S. Fentiman, *Detection and Treatment of Early Breast Cancer*, J. B. Lippincott Company, Philadelphia, p. 39-57, 1990

10. R. T. Girolamo,"Imaging systems other than mammography," in *Breast Cancer : Diagnosis and Treatment*, eds. I. M. Ariel and J. B. Cleary, McGraw-Hill Book Company, 1987

11. A. E. Profio, and O. Balchum,"Fluorescence diagnosis of cancer," in *Methods in Porphyrin Photosensitization*, Ed. D. Kessel, Plenum, New York, p 843, 1985

12. R. R. Alfano and S. S. Yao, "Human teeth with and without caries studied by visible luminiscent spectroscopy," *J. Dent. Res.*, 60, p120-122, 1981

13. R. R. Alfano, D. Tata, J. Cordero, P. Tomashefsky, F. Longo and M. A. Alfano,"Laser induced fluorescence spectroscopy from native cancerous and normal tissues," IEEE *J. Quantum Electron*, QE-20, p1507-1511, 1984

14. R. R. Alfano, and M. A. Alfano,"Medical diagnostics: a new optical frontier," *Photon Spectra* 19:55-60, 1985.

15. R. R. Alfano, G. C. Tang, A. Pradhan, W. Lam, D. C. Choy and E. Opher,"Fluorescence spectra from cancerous and normal human breast and lung tissues," IEEE *J. Quantum Electron*, QE-23, p1806, 1987

16. C. Kittrel, R. L. Willet, C. de Los Santos Pacheo, N. B. Ratcliff, J. R. Kramer, E. G. Malk and M. S. Feld, "Diagnosis of fibrous arterial artherosclerosis using fluorescence," Appl. Opt., 24, p2280-2281, 1985

17. Y. Yuanlong, Y. Yanming, L. Fuming, L. Yufen and M. Paozhong, "Characteristic autofluorescence for cancer diagnosis and its origin," *Lasers Surg. Med.*, 7, p528, 1987

18. G. C. Tang, A. Pradhan, W. L. Sha, J. Chen, C. H. Liu, S. J. Wahl and R. R. Alfano, "Pulsed and cw laser fluorscence spectra from cancerous normal and chemically treated normal human breast and lung tissue," *Appl. Opt.*, 28, p2337-2342, 1989

19. L. I. Deckelbaum, J. K. Lam, H. S. Cabin, K. S. Clubb and M. B. Long, "Discrimination of normal and artherosclerotic aorta by laser induced fluorscence," *Lasers surg. Med.*, 7, p330-335, 1987

20. P. S. Anderson, A. Gustafson, U. Stenram, K. Svanberg and S. Svanberg, "Diagnosis of arterial artherosclerosis using laser induced fluorescence," *Lasers Med. Sci.*, 2, p261-266, 1987

21. R. E. Petras, R. R. Kortrum, L. Tong, M. Fitzmaurice, M. feld and M. Sivak, "Fluorescence spectroscopy of colonic adenomas: Implications for an endoscopic laser diagnostic system," *Gastrointest. Endosc.*, 35, p181-182, (abstract), 1989

22. R. R. Kortum, L. Tong, R. Rava et al.," Spectral studies of GI tissues: Optimizing excitation and emission wavelengths for discrimination of normal and adenomatous tissues," *Lasers in Srg. and Med.* 9, p. 21 (abstract) 1989

23. R. R. Kortum, R. Rava, R. E. Petras, M. Fitzmaurice, M. SivaK and M. S. Feld," Clinical applications of fluorescence excitation and emission matrices: diagnosis of colonic adeoma," Manuscript in preparation.

24. C. R. Kapadia, F. W. Cutruzzola, K. M. O'Brein, M. L. Stetz, R. Enriquetz, and L. I. Deckelbaum,"Detection of adenomatous transformation of colonic mucosa by fiberoptic laser-induced fluorescence spectroscopy," *Gastroenterology*, 94, 216A, 1988.

25. K. T. Schomacker et al,"Ultraviolet Laser Induced Fluorescence of Colonic Polyps," *Gastroenterology*, 0411, p 4-5, 1992

26. M. Sartori, P. D. Henry, R. Roberts, R. P. Chin, and M. J. Berry," Estimation of arterial wall thickness and detection of atherosclerosis by laser induced fluorescence," *J. Am. Coll. Cardiol.*, 7: 207A (abstract) 1986

27. R. Richards-Kartum, Masters Thesis, Dept. of Physics, M.I.T., (1987)

28. R. R. Alfano, B. B. Das, J. Cleary, R. Prudente, E. Celmer, "Light sheds light on cancer - distinguishing malignant tumors from benign tissues and tumors, "Bulletin of the New York Academy of Medicine, 67, p143-150, 1991

29. B. B. Das, W. Sha Glassman, R. R. Alfano, J. Cleary, R. Prudente, E. Celmer and S. Lubicz, "UV fluorescence spectroscopic technique in the diagnosis of breast, ovarian, uterus and cervix cancer," SPIE Proceedings, 427, Laser-Tissue Interaction II, p368-373, 1991

30. W. Sha Glassman, C. H. Liu, G. C. Tang, S. Lubicz and R. R. Alfano, "Ultra

Violet fluorescence spectra from non-malignant and malignant tissues of the gynecological tract," *Lasers in the Life Sciences*, 4(1), p1-9, 1991

31. C. R. Kapadia, F. W. Cutruzzola, K. M. O'Brein, M. L. Stetz, R. Enriquetz, and L. I. Deckelbaum,"Laser induced fluorescence spectroscopy of human colonic mucosa," *Gastroenterology*, 99, p150-157, 1990

32. J.L. Bennington," Major problems in pathology," in *Problems in Breast Pathology*, Vol. II in the series, W. B. Saunders Co Ltd., London, p393 (1979)

33. H. S. Gallager,"Corrent concepts in breast cancer and tumor immunology," in *Newer Understanding of Pathology of Breast Cancer*, p27, New York: Medical Examinatoin (1974)

34. J.L. Bennington," Major problems in pathology," in *Problems in Breast Pathology,* Vol. II in the series, W. B. Saunders Co Ltd., London, p 383-385 (1979)

35. M. S. Al-Adnani, J. A. Kirrane, J. O'D McGee," Inappropriate production of collagen and prolyl hydroxylase by human breast cancer cells in vivo, *British Journal of Cancer*, 31, 653-660 (1975)

36. G. Tremblay, "Elastosis in tubular carcinoma of the breast," *Archives of Pathology*, 98, 302-307 (1974)

37. J. P. Schwartz, J. V. Possoneau, G. S. Johnson, I. Pastan," The effect of growth conditions on NADH+:NADH ratio in normal and transformed fibroblasts, *J. Bilo. Chem.*, 249, 4138 (1974)

38. A. Cascino, C. Cangiano, F. Cefi, T. Mineot, M. Mulieri, M. Muscaritoti and F. R. Fanelli, Increased plasma free tryptophan levels in human cancer: a tumor relsted effect?" *Anticancer Res*, 11(3) : 1313, 1991,

39. C. -H, Liu, B. B. Das, W. L. Sha-Glassman, G. C. Tang, K. M. Yoo, H. R. Zhu, D. L. Akins, S. S. Lubicz, J. Cleary, R. Prudente, E. Celmer, A. Caron, and R. R. Alfano,"Raman, fluorescence and time-resolved light scattering as optical diagnostic techniques to separate diseases and normal biomedical media," *J. Photochem. Photobiol., B. Biol.*, 16, p. 187-209, 1992

40. C. -H, Liu, B. B. Das, W. L. Sha-Glassman, G. C. Tang, H. R. Zhu, D. L. Akins, S. S. Lubicz, J. Cleary, R. Prudente, E. Celmer, A. Caron, and R. R. Alfano,"NIR Raman and fluorescence spectroscopies Diagnose cancer!" *SPIE* Vol. 1887, p.188

41. Dezna C. Sheehan and Barbara Hrapchak, *Theory and Practice of Histotechnology*, C. V. Mosby Co., London, 1980

42. C. M. Balch, S. E. Singletary and K. I. Bland, "Clinical decision making in early breast cancer," in *Annals of Surgery*, vol. 217, No. 3, p.207-225, J. B. Lippincott Co., 1993

43. N. J. Agnantis, N Apostolikas, I. Christodoulou, C. Petrakis, and J. Garas in *Early Detection of Breast Caner*, eds. S. Brunner, B. Langfeldt, and P. E. Anderson,

Springer Verlag, New York, p. 205, 1984

44. H. Isard, W. Becker, R. Scilo, and B. Ostrum," Breast thermography after 4 years and 10,000 studies." *Amer. J. Roentgenol* 115: 811, 1972

45. T. Kobayashi et al, "The sensitivity graded method of ultrasonotomography and clinical evaluation of its diagnostic accuracy." *Cancer* 33: 940, 1974

46. H. Vorherr, *Breast Cancer*, Urban & Schwarzenberg, Baltimore-London, p.343, 1980

47. G. B. Canon et al,"Immunologic relationship between breast carcinoma and benign breast disease as detected by the Leukocyte Migration Inhibition Assay," *J Natl Cancer Inst* 61, p 1181-1186, 1978

48. G. Weber, "Enunciation of components in complex systems by fluorescence spectro-photometry," *Nature* 190, 27, 1961

49. W. Sha-Glassman, Doctoral Thesis, The City Univ. of New york, 1993

50. A. Pradhan, B. B. Das, K. M. Yoo and R. R. Alfano, "Time-resolved uv photoexcited fluorescence kinetics from malignant and non-malignant Human breast tissues," Lasers in Life Sciences, p 225-234, 4(4), 1992

51. A. Pradhan, Ph. D. thesis, The City Univ. of New York, 1991

52. T. Foerster,"Fluorenz Organischer Verbindungen," Goettingen: Vandenhoek & Ruprecht, p.35-42, 273 (1951)

53. I. D. Campbell and R. A. Dwek, *Biological Spectroscopy,* The Benjamin/ Cummins Publishing Co., Inc. California, p.98, (1984)

CHAPTER 3

Spectral Optical Density Measurements on Small Particles and Breast Tissues

3.1 Introduction

The understanding of light transport in tissues is an active and important area because of its potential applications in medical diagnostics, therapeutic and surgical procedures[1-4]. As we have seen in the previous chapter the fluorescence yield in a tissue can be greatly affected by the scattering and the absorption in the medium. One can overcome the problem of absorption in a tissue to a large extent by using the ratio of fluorescence intensities at two wavelengths where the blood absorbance are the same. But the effect of scattering still remains. We plan to address this issue here. In this chapter we describe our work on optical density measurements on thin breast tissues to investigate the spectral dependence of tissue scattering cross-sections. To ensure the accuracy of the results, measurements were performed on latex bead suspensions in water with various bead sizes, and the results were compared with the theoretical predictions based on Mie theory.

As introduced in Chapter 1, light transport in tissues can be quantitatively characterized by a few key optical parameters[5,6] : the *scattering cross-section* ($\Sigma_s = n\sigma_s$), the *absorption cross-section* ($\Sigma_a = n'\sigma_a$), the *total extinction coefficient* (Σ_{total}), and the *mean cosine of the scattering angle* (g), where n, n' σ_s, and σ_a are the *scatterer density, absorber density, single particle scattering cross-section and absorption cross-section* respectively. The total extinction coefficient is given by the sum of the scattering and the absorption cross-sections ($\Sigma_T = \Sigma_s + \Sigma_a$). The *transport mean free path* (l_t) is

given as: $l_t = 1/n\sigma_m$, where σ_m is the *momentum exchange scattering cross-section* of the scatterer given in eqn. (1.2), and $l_t = l_s/(1-g)$.

These scattering cross-sections are defined in terms of the *scattering amplitude* $f(\hat{n},\hat{n}')$ that represents the amplitude, the phase and the polarization of the scattered wave at a large distance from the particle in the direction $\hat{n}$ when the particle is illuminated by a plane wave in the $\hat{n}'$ direction. The *differential scattering cross section* $\sigma_d(\hat{n},\hat{n}')$, and the *phase function* $p(\hat{n},\hat{n}')$ are related as

$$\sigma_d(\hat{n},\hat{n}') \equiv |f(\hat{n},\hat{n}')|^2 \equiv \frac{\sigma_T}{4\pi} p(\hat{n},\hat{n}') \quad , \tag{3.1}$$

where

$$\sigma_T = \sigma_s + \sigma_a \quad ,$$

$$\sigma_s = \int_{4\pi} \sigma_d d\omega \quad , \tag{3.2}$$

$$g = \frac{\int \sigma_d(\theta,\phi)\cos\theta \sin\theta d\theta d\phi}{\int \sigma_d(\theta,\phi)\sin\theta d\theta d\phi} \quad . \tag{3.3}$$

These scattering parameters depend on the spatial size of the scatterers, refractive index contrast between the scatterer and the host medium, and the spatial dimension of the scatterers relative to the wavelength of light. For particles much larger than the wavelength of light, the scattering cross-section is approximately equal to the geometric cross-section of the particle, and light is scattered mainly in the forward direction restricted within an angle $\theta \approx 1.2\lambda / d$, where d is the diameter of the particle. For particles with sizes much smaller than the wavelength Σ_s can be approximated in the

Rayleigh scattering limit, and light is scattered in all directions. For particles with sizes comparable to the wavelength, the scattering cross-sections can be computed using Mie theory.

The problem of arbitrary size particles has been solved for simple cases like scattering of a plane wave by a homogeneous sphere using the Maxwell equations. If u and v are the two scattered wave solutions of the scalar wave equations then they can be expanded as[6]:

$$u = e^{iwt}\cos\varphi \sum_{n=1}^{\infty} -a_n(-i)^n \frac{2n+1}{n(n+1)} P_n^1(\cos\theta) h_n^{(2)}(kr) \qquad (3.4)$$

$$v = e^{iwt}\sin\varphi \sum_{n=1}^{\infty} -b_n(-i)^n \frac{2n+1}{n(n+1)} P_n^1(\cos\theta) h_n^{(2)}(kr) \qquad (3.5)$$

For a sphere with a radius a and a refractive index m in vacuum (refractive index =1) the scattering cross section and g have been shown by Debye in terms of the constants a_n and b_n (the expansion coefficients in eqn. 3.4 & 3.5) as

$$\frac{\sigma_s}{\pi a^2} = \frac{2}{x^2} \sum_{n=1}^{\infty} (2n+1)\{|a_n|^2 + |b_n|^2\} \qquad (3.6)$$

with $x = ka = 2\pi a/\lambda$, and

$$g.\frac{\sigma_s}{\pi a^2} = \frac{4}{x^2} \sum_{n=1}^{\infty} \frac{n(n+2)}{n+1} Re(a_n a_{n+1}^* + b_n b_{n+1}^*) + \frac{4}{x^2} \sum_{n=1}^{\infty} \frac{2n+1}{n(n+1)} Re(a_n b_n^*) \qquad (3.7)$$

These constants have been determined in terms of the *Riccati-Bessel* functions $\psi_n(x), \zeta_n(x)$ as:

$$a_n = \frac{\psi_n'(y)\psi_n(x) - m\psi_n(y)\psi_n'(x)}{\psi_n'(y)\zeta_n(x) - m\psi_n(y)\zeta_n'(x)}$$

$$b_n = \frac{m\psi_n'(y)\psi_n(x) - \psi_n(y)\psi_n'(x)}{m\psi_n'(y)\zeta_n(x) - \psi_n(y)\zeta_n'(x)} \qquad (3.8)$$

Equations (3.6) - (3.8) enable one to calculate the scattering cross-sections and g values of spheres at different wavelengths if one knows the diameters and the refractive indices of the spheres. In practice the eqn.s (3.6) and (3.7) are summed for about a hundred terms to get sufficient accuracy. The computer program used to obtain the scattering cross-sections and the mean cosine of the scattering angle is given in the Appendix I.

Figure 3.1 displays a theoretical curve of g versus particle diameter a for latex beads in water at 625 nm. This curve shows a ripple structure with a decreasing amplitude as the particle size becomes larger. Figure 3.2 displays a theoretical curve of g versus wavelength (λ) for 0.4 μm diameter intralipid suspensions in water with an index of refraction equal to 1.4. Figure 3.3 shows the dependence of scattering cross-section on particle diameter at 625 nm. This also shows a ripple structure.

When a collimated beam of light is incident on a random medium it is attenuated as[5]

$$I = I_0 \exp -[(\Sigma_a + \Sigma_s)\, z] \qquad (3.9)$$

where I is the coherent intensity of the transmitted beam called the ballistic component, I_0 is the intensity of the incident beam, and z is the path traversed, respectively.

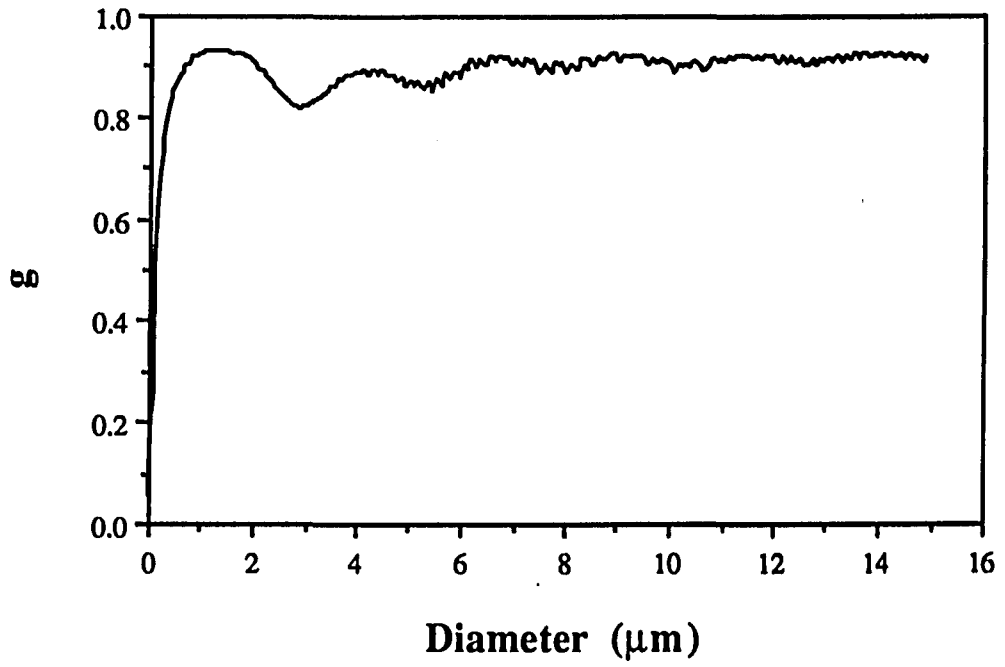

Fig. 3.1 The dependence of g on particle diameter at $\lambda = 0.625$ μm.

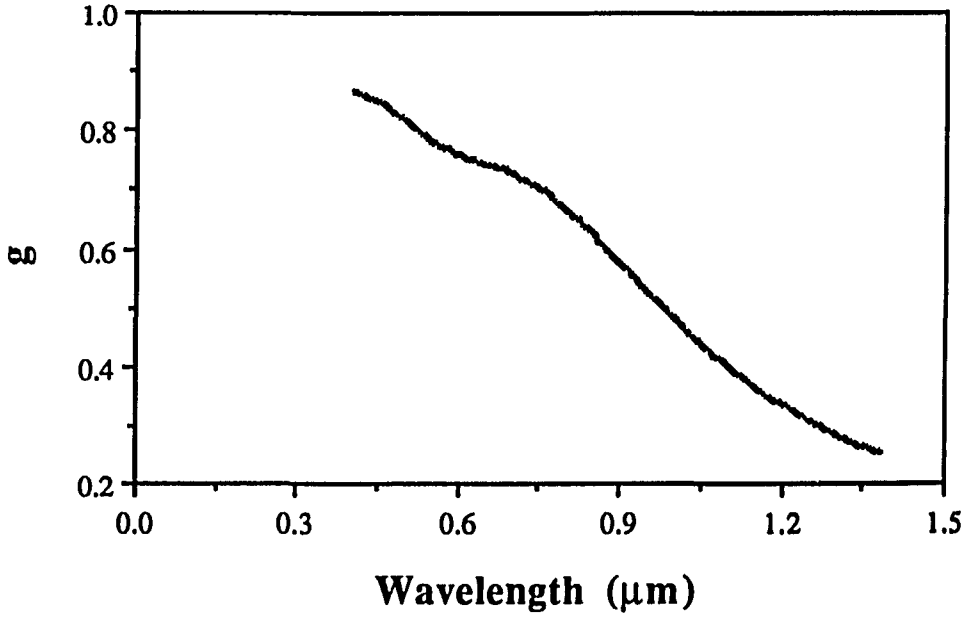

Fig. 3.2 The mean cosine of the scattering angle (g) at different wavelengths for 0.4 μm diameter intralipid scatterer in water, with index of refraction = 1.4.

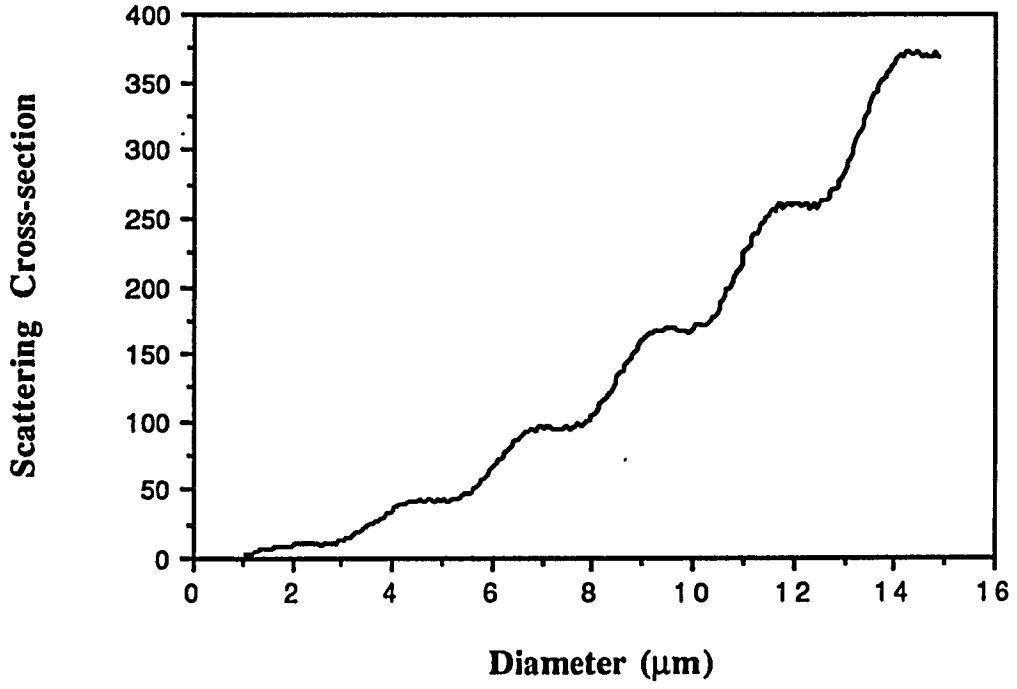

Fig. 3.3 The dependence of scattering cross-section (μm^2) of Latex beads in water on bead diameter at 625 nm.

These optical parameters can be related to effective optical density (OD) which is obtained directly from experiment using a spectrophotometer. The effective OD is defined as

$$OD = log\,(I_0 / I) \tag{3.10}$$

The optical cancer diagnostic technique that was discussed[3,4] earlier is based on measuring fluorescence intensity from tissues at two different wavelengths. The photons emitted in fluorescence undergo random scattering and travel various pathways inside the medium. Consequently the fluorescence intensity is reduced by both absorption and scattering. So it is crucial to know how the transport of light varies at these two wavelengths. The transport of light is determined by the optical parameters which can be obtained from the OD measurements using a spectrometer.

3.2 Experimental Method

Absorption measurements were performed on latex beads and thin breast tissues. Suspensions in water of latex beads of various sizes of 11 μm, 2.9 μm, 0.46 μm and 0.09 μm were prepared using de-ionized water. These solutions were placed in 10 mm thick quartz cells. Their optical densities over the wavelength range from 320 nm to 800 nm were measured using a Perkin-Elmer (Lambda 9) spectrophotometer.

Breast tissue samples for the experiment were prepared at the Beth Israel Hospital, North Division, New York. Thin frozen sections of one benign and three malignant breast tumors were prepared on quartz slides. One of the malignant samples contained some blood due to internal hemorrhage. The thickness of samples are about 250 ± 25 μm. These tissues were placed in a small box dipped in liquid nitrogen to protect it from dying and transported from the hospital to the experimental site. The samples were thawed for a few minutes before the experiment and their optical densities were measured. The OD of the malignant sample containing blood was measured twice. The fresh sample containing blood was measured first; then blood was extracted from the tissue and the OD was measured again. Blood was extracted from the tissue by placing the sample for about 15 minutes in ammonium chloride (NH_4Cl, the concentration was 0.8 mg/ml of water, with the original pH 7) solution.

3.3 Results

The extinction spectra for the four different latex bead random media are displayed in Figure 3.4 (a)-(d). The media with 11 μm bead diameter shows near constant optical density for the whole range of incident wavelength from 320 to 800 nm, while the case with 2.9 μm beads gives a ripple structure. For 0.46 μm bead medium, OD increases as the wavelength is changed from longer to shorter wavelength. The OD for 0.09 μm diameter bead medium increases more sharply. These results clearly

demonstrate that for scatterers with sizes much larger than the visible wavelength the OD or scattering cross sections remain relatively constant over the whole visible spectrum.

The salient features of the OD spectra for thin breast tissues with and without blood are displayed in Figure 3.5. The measurements for the tissue with blood, before and after blood extraction, are displayed in Figure 3.5 (curve 1 and 2). The tissue with blood (curve 1) shows a sharp peak of optical density at 410 nm and two small peaks 540 nm and 575 nm. This OD profile (curve 1) resembles the absorbance profile of blood[6] indicating that these OD peaks mainly arise from the absorption by blood, and not due to any change in the scattering cross-section. These absorbance peaks in curve 1 are substantially reduced after most of the blood was extracted from the tissue (Fig. 3.5-curve 2). The optical densities for the tissues without blood (curve 3-5) remain more or less constant over the visible and near infrared spectrum. The OD of one of the tissues shown in Fig. 3.5 (curve 3) also shows a small blood absorption peak at 410 nm. In general, the scattering from the tissues are relatively constant.

Scattering cross-sections, which are directly proportional to optical densities, are computed versus wavelength using equation (3.6) for 2.9, 0.46 and 0.09 μm latex beads and displayed in Figure 3.6 (a), (b) and (c) respectively. The scattering cross-section for 2.9 μm beads shows a ripple structure similar to our experimental result. The slight difference near the 320 nm range between the experimental result and the curve computed using the Mie theory is due to our computational limitations at this range. The scattering cross-section for the 0.09 μm latex bead medium increases more sharply as we go from longer to shorter wavelength as compared with the 0.46 μm balls. The computed scattering cross-sections agree qualitatively with the measured OD for these two latex bead media. The OD or the extinction coefficients of much larger beads as compared to the wavelength are constant, and depend on the geometrical cross-

section of the particles. The OD measurement for the 11 μm latex beads, displayed in Fig.3.4 (a), shows that the OD over the visible spectrum remain relatively constant.

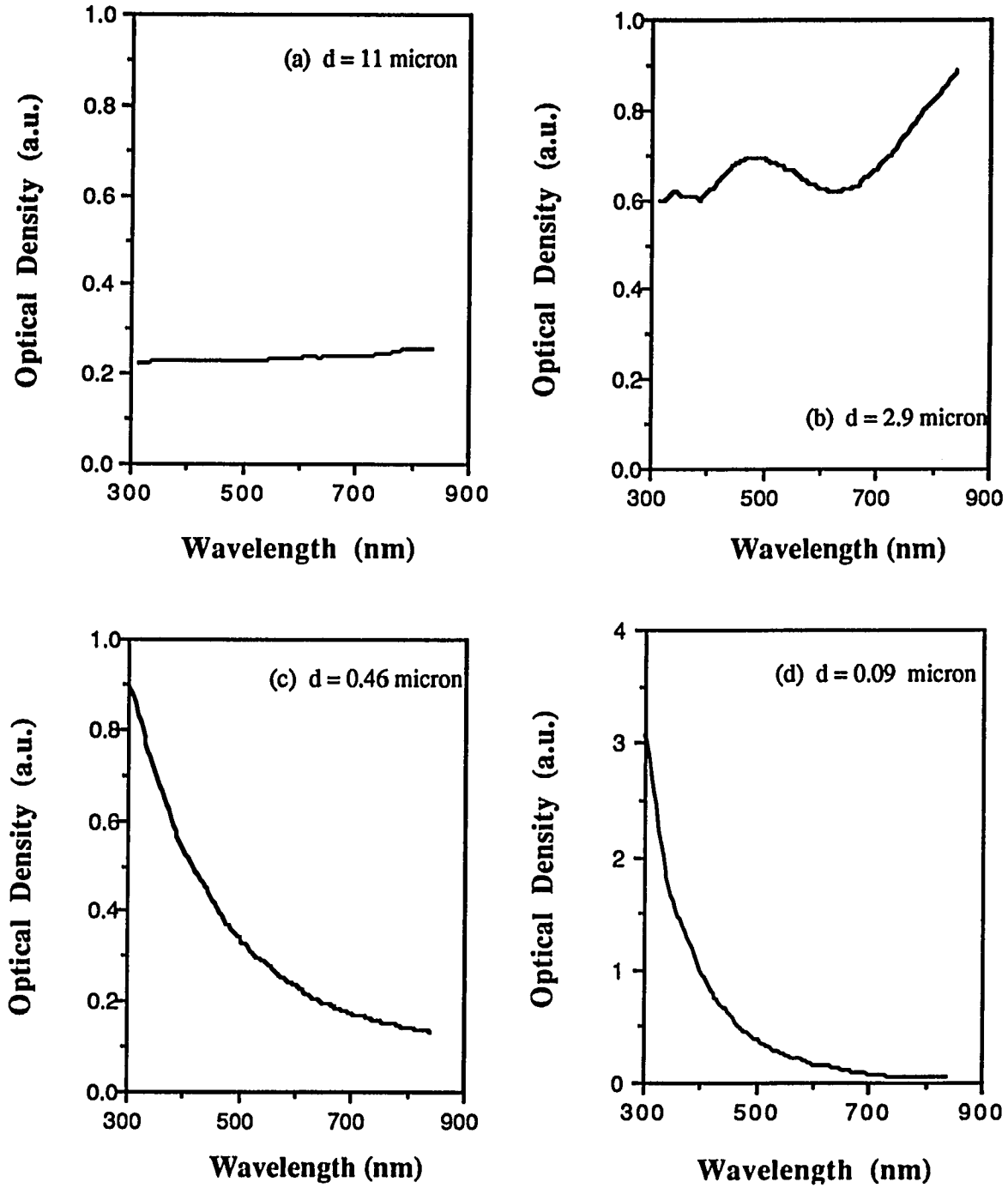

Fig. 3.4. Optical density spectra measured for latex beads suspension in water for different bead diameters : (a) 11μm, (b) 2.9μm, (c) 0.46μm and (d) 0.09μm.

The OD measurements on tissues also show a nearly constant optical density in the optical spectrum for the three tissues with little blood content. A signature of absorption due to blood was observed in case of the sample with significant blood content due to an internal hemorrhage. The constant OD over the visible spectrum for tissues with little blood content suggests that the scattering in the tissue arises from large particles. Typical human tissue cells measure between 10 to 20 microns[8]. The constant

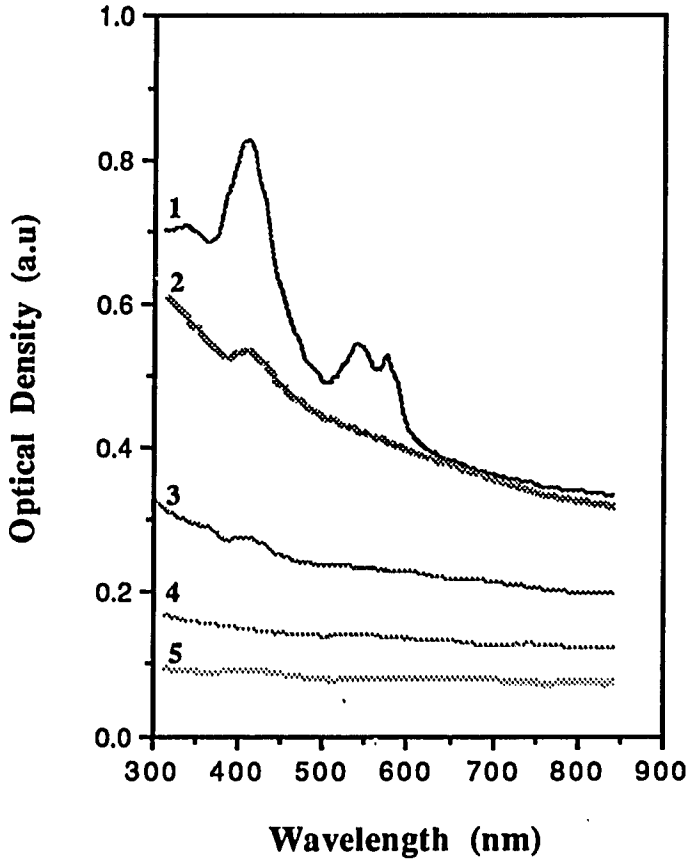

Fig. 3.5. Optical density curves for various thin tissue samples: a malignant breast tissue sample with some blood content due to internal hemorrhage before (curve 1) and after extracting the blood from the sample (curve 2). Curve 1 gives the absorption peaks for blood. Curves 3-5 give optical density spectra for three thin breast tissue sections with no blood: curves 3 and 4 for malignant samples and curve 5 for a benign sample.

OD means that the scattering cross-section over the optical spectrum in breast tissue remains the same and the scattering could be due to the cells in the tissues. The light

transport in tissues for different wavelengths remain the same in this optical spectrum in the absence of absorption due to blood.

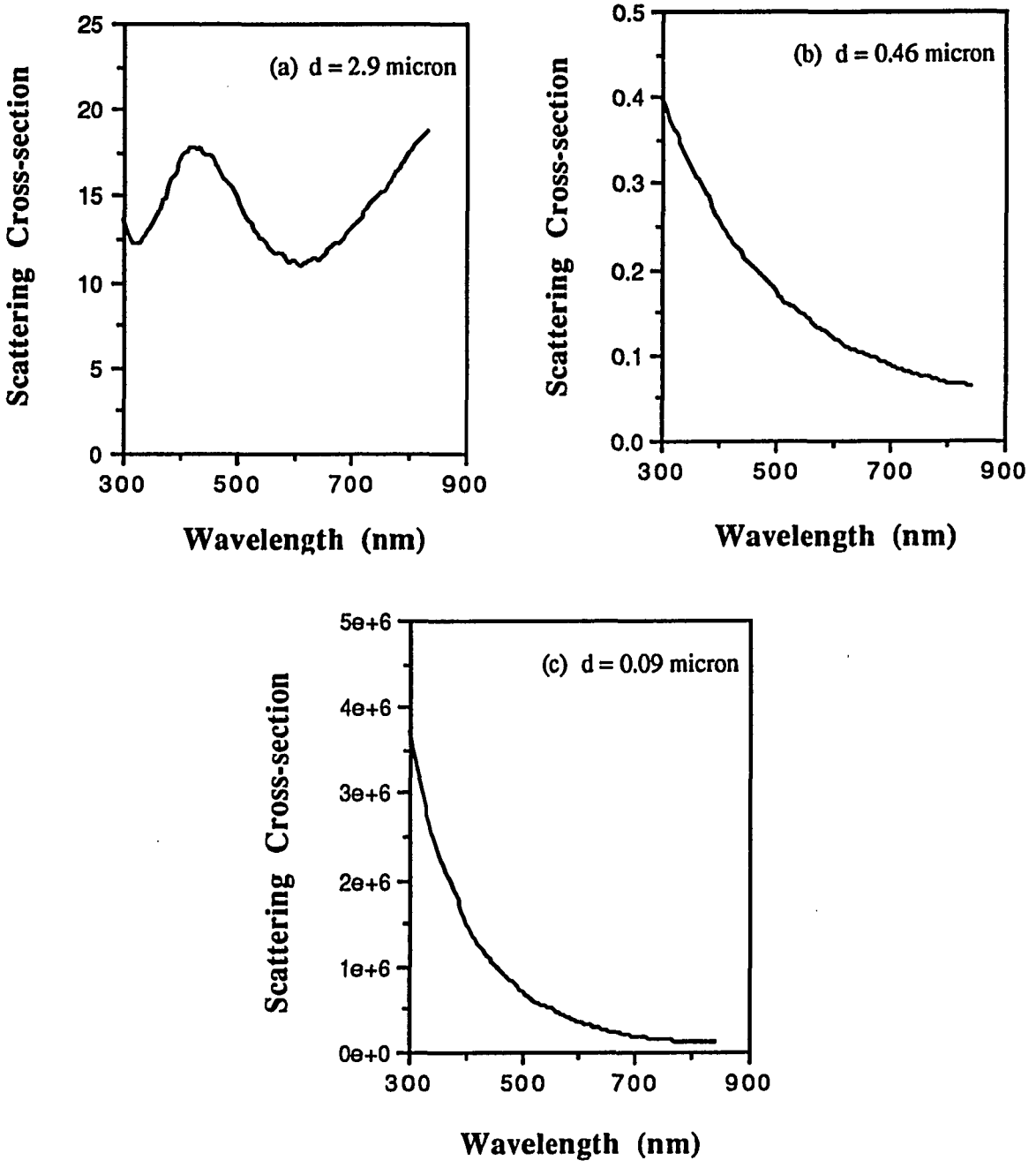

Fig. 3.6 Scattering coefficient for different latex bead suspensions in water computed using Mie theory. (a) bead diameter d = 2.9 μm, (b) d = 0.46 μm and (c) d = 0.09 μm.

Over the past several years, the use of fluorescence spectroscopy for medical diagnostics has become a major interest[3,4,9-16]. As discussed earlier the native fluorescence from breast tissues, excited at 300 nm (0.3 μm)was found to be useful for cancer diagnosis[3,4]. The ratio of fluorescence intensities at 340 nm to 440 nm from cancerous and non cancerous tissues excited at 300 nm shows a consistent difference. It is important to determine the cause of this difference. It can be due to absorption, scattering and intrinsic difference in fluorescence yield at these two wavelengths. The fluorescence light experiences multiple scattering and absorption in tissues. The effect of absorption in tissues on the ratio of the fluorescence intensities at two different wavelengths can be minimized by selecting two wavelengths with the same absorbance.

The constant optical density of breast tissues over the 320 - 800 nm wavelength range shows that the scattering cross-section in breast tissues is nearly constant at 340 and 440 nm. This measurement means that the average distance traveled by these two different colored photons remain the same. Thus, the reduction of fluorescence intensity at 340 and 440 nm due to multiple scattering is the same. The absorption near 340 and 440 nm are about equal. Thus, selecting the wavelength pair of 340 nm and 440 nm, the reduction of fluorescence intensity by both absorption and scattering remain about the same. The difference in intensity ratios at these two wavelengths arises from the different amount of fluorescence emitted from native fluorophores at these two wavelengths for different tissues. The scattering or absorption will not significantly affect the fluorescence intensity ratio. This ratio technique is independent of the structure of the tissue or the transport of light in the tissue.

In conclusion, the OD of thin breast tissues without blood are found to be relatively constant over the visible spectrum. This observation indicates that light is effectively scattered in breast tissues by scatterers of size much larger than the wavelength of light. These scatterers in the tissues are most likely the cells that have

sizes between 10 to 20 microns. The scattering cross section of a large cell or scatterer is not very sensitive to the variations of light wavelength if the size of the particle is much larger than the light wavelength. This conclusion is confirmed from independent experimental data using model discrete random media (latex beads) of various scatterer sizes. Scatterers of sizes comparable or smaller than the light wavelength show a large variation of OD as the wavelength is varied over the optical spectrum. No variation of OD is observed when the scatterer is much larger than the wavelength of light. This simple extinction measurement provides very useful information as to the scattering and absorption cross-sections of breast tissues.

We also come to the conclusion that the fluorescence intensity difference at 340 and 440 nm in the previously discussed cancer diagnostic method is not due to any loss by scattering but because of the difference in the intrinsic fluorescence yield in malignant and non-malignant samples.

3.4 References

1. A special issue on tissue optics, Applied Optics, v28, no.12, June 1989

2. L. M. Wang, P. P. Ho, C. Liu, G. Zhang and R. R. Alfano, " Ballistic 2-D imaging through scattering walls using ultrafast optical kerr gate" Science, v 253, 769-771, (1991)

3. R. R. Alfano, B. B. Das, J. Cleary, R. Prudente and E. Celmer, "Light Sheds Light on cancer - Distinguishing Malignant Tumors From Benign Tissues and Tumors", Bulletin of the New York Academy of Medicine, v 67, p.143-150, (1991)

4. B. B. Das, W. Sha Glassman, R. R. Alfano, J. Cleary, R. Prudente, E. Celmer and S. Lubicz, " UV fluorescence spectroscopic technique in the diagnosis of breast, ovarian, uterus, and cervix cancer", SPIE proceedings v 427 Laser-Tissue Interaction II, p 368-373 (1991)

5. A. Ishimaru, *Wave propagation and Scattering in Random Media*, v1&2 Academic Press, New York(1978)

6. H. C. van de Hulst, *Light Scattering by Small Particles*, Dover, New york, 1981

7. R. Richards-Kortrum, Masters Thesis, Dept. of Physics, M.I.T., (1987)

8. L. T. Threadgold,*The Ultrastructure of the Animal Cell*, 2nd edition, Pergamon Press. New York, (1976)

9. R. R. Alfano, S. S. Yao, "Human teeth with and without caries stydied by visible luminescent spectroscopy," J. Dent. Res. 60,120-122 (1981)

10. R. R. Alfano, D. Tata, J. Cordero, P. Tomashefsky, F. Longo and M. A. Alfano, " Laser induced fluorescence spectroscopy from native cancerous and normal tissues," IEEE J. Quantum Electron. QE-20, 1507-1511 (1984)

11. C. Kittrel, R. L. Willet, C. de Los Santos Pacheo, N. B. Ratcliff, J. R. Kramer, E. G. Malk and M. S. Feld, " Diagnosis of fibrous arterial artherosclerosis using fluorescence," Appl. Opt. 24,2280-2281 (1985)

12. Y. Yuanlong, Y. Yanming, L. Fuming, L. Yufen and M. Paozhong, "Characteristic autofluorescence for cancer diagnosis and its origin," Lasers Surg. Med. 7, 528 (1987).

13. G. C. Tang, A. Pradhan, W. L. Sha, J. Chen, C. H. Liu, S. J. Wahl and R. R. Alfano, " Pulsed and cw laser fluorescence spectra from cancerous, normal and chemically treated normal human breast and lung tissues," Appl. Opt., 28, 2337-2342 (1989).

14. R. E. Petras, R. R. Kortrum, L. Tong, M. Fitzmaurice, M. Feld and M. Sivak, "Fluorescence spectroscopyof colonic adenomas: Implications for an endoscopic laser diagnostic system," Gastrointest Endosc.,35 181-182 (abstract) (1989)

15. L. I. Deckelbaum, J. K. Lam, H. S. Cabin, K. S. Clubb and M. B. Long, "Discrimination of normal and atherosclerotic aorta by laser induced fluorescence," Lasers Surg. Med., 7, 330-335 (1987).

16. P. S. Anderson, A. Gustafson, U. Stenram, K. Svanberg and S. Svanberg,"Diagnosis of arterial atherosclerosis using laser induced fluorescence," Lasers Med. Sci., 2, 261-266 (1987).

CHAPTER 4

Diffusion Of Light In Turbid Media

4.1 Introduction

The problem of photon migration in a random medium has become increasingly important in recent years because of its potential for optical mammography. Its possible applications in the fields of solid state physics, remote sensing, medical diagnostics and imaging have drawn considerable attention. The increasing use of light in such diverse fields has created a need for better understanding and determination of the optical properties of various turbid media. An extensive study of the scattering of light has been done in the past[1]. Random media may be grouped into three different classes: random continua, random scatterers and rough surfaces. A random medium is characterized by random fluctuations of the index of refraction in space and time. These inhomogeneities in the medium scatter light randomly in all directions.

In principle propagation of light in any medium can be described analytically using the Maxwell equations[1-4]. However the mathematical complexities involved in the problem put sever limitations to its practical use in most of the cases. The common approach used today is known as the *transport theory*. It deals directly with the transport of energy through turbid media. This approach has proved to be very useful in solving several problems. Transport theory, or radiation transport theory as it is sometimes called, deals with the transport of intensities through random scatterers. The basic differential equation is similar to Boltzmann's equations in the kinetic theory of gases and in neutron transport theory. But analytical solutions to the transport equation have been obtained for only a few problems. The case of a semi-infinite, isotropically scattering, homogeneous medium with a large collimated beam has been solved by

Chandrasekhar[5], and the case of a similar medium with a narrow collimated beam by Rybicki[6]. However, various numerical techniques such as discrete ordinates (Duderstadt and Hamilton[7]), Monte Carlo method (Carter and Cashwell[8]), and approximate solutions such as diffusion theory[1], Kubelka-Munk approximation[9], multiple scattering theory have been formulated for diverse applications. The diffusion approximation is appropriate for dense distribution while the multiple scattering theory is for tenuous distribution. For thick tissues the diffusion theory is a good approximation. In recent years many of these approximations and numerical approaches have been used to obtain the various optical parameters of human and animal tissues and other model media[10-29]. While Wilksch et al.[10], Anderson et al.[11], van Germert et al[12], Wan et al[13], and Ertefai and Profio[14] have used the Kubelka-Munk method to obtain the optical parameters from reflectance and transmittance, Navarro and Profio[15] used discrete ordinate technique. Wilson et al[16] used thin samples in single scattering regime to measure total attenuation directly while Patterson et al[17] and Yoo et al[18-19] have used diffusion approximation to study time-resolved transmission and backscattering to obtain the absorption and transport coefficients. A comparative study by Wilson and Patterson[20] of four different methods (i) a discrete ordinate solution, (ii) a Monte Carlo solution, (iii) an analytical solution of diffusion equation, and (iv) a solution of two-flux (Kubelka-Munk) equation suggests that the discrete ordinate technique is less accurate in comparison to the Monte Carlo model. The diffusion approximation yields accurate results except near the sample surface and the two-flux method is the least successful. Yoo and Alfano[18-19] have shown that for thick samples (thicker than about 7 transport mean free paths) diffusion approximation is an excellent approach to determine the optical parameters of various turbid media.

In this chapter we describe our measurements of the optical parameters of various biological and model random media based on time-resolved transmission and

diffusion approximation. So we start with a brief description of the transport equation and the diffusion theory in the following sections.

4.2 Transport Theory

The diffusion theory that we are going to use to determine the optical properties of tissues and other model random media is only an approximation of the transport theory. The fundamental equation in the transport theory is the transport equation[1]

$$\frac{dI(\vec{r},\hat{n},t)}{dl} = -\Sigma_T I(\vec{r},\hat{n},t) + \frac{\Sigma_T}{4\pi}\int p(\hat{n},\hat{n}')I(\vec{r},\hat{n}',t)d\omega' + S(\vec{r},\hat{n},t) \qquad (4.1)$$

where $I(\vec{r},\hat{n},t)$ is known as the specific intensity in the radiative transport theory. To understand the transport equation, let us consider a specific intensity $I(\vec{r},\hat{n},t)$ incident on an elementary volume dl with a unit cross-section and with a particle density ρ. The loss of light due to the scattering and absorption by the particles are given by the first term in the right hand side of the equation (4.1)

The second term in the equation gives the contribution of light scattered into $\hat{n}$ direction from light incident in $\hat{n}'$ direction as illustrated in Figure 4.1.

The third term is the increase in light due to a source within the volume.

4.3 Diffusion Approximation

When light is incident on a turbid medium multiple scattering due to the random fluctuations in the refractive indices splits the incident beam into a coherent (ballistic) component I_c and a diffuse component I_d. The ballistic part consists of the photons that travel undeviated straight through, while the diffuse component consists of the multiple

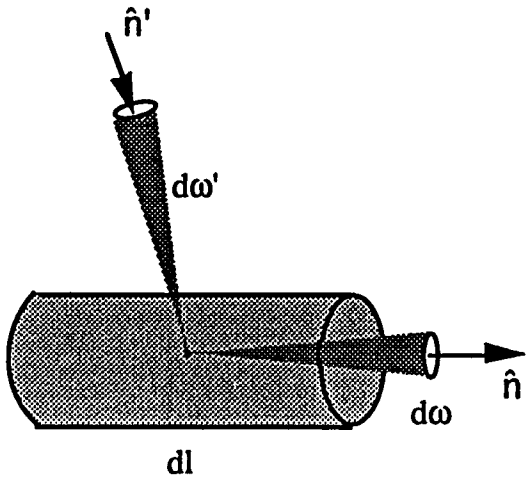

Figure 4.1 Scattering of light incident on the volume dl in the direction $\hat{n}'$ into the direction $\hat{n}$.

scattered photons. The ballistic component is attenuated with the distance of propagation d in the medium as

$$I = I_0 \exp -(\frac{1}{l_s} + \frac{1}{l_a})d$$

where I_0, l_s, and l_a are the incident intensity, the scattering length ($=1/\Sigma_s$) and the absorption length ($= 1/\Sigma_a$), respectively.

Using these two components in the transport equation (4.1) one finds that the diffuse component must satisfy the equation

$$\frac{dI_d(\vec{r},\hat{n},t)}{dl} = -\Sigma_T I_d(\vec{r},\hat{n},t) + \frac{\Sigma_T}{4\pi}\int p(\hat{n},\hat{n}')I_d(\vec{r},\hat{n}',t)d\omega' + S(\vec{r},\hat{n},t) + S_b(\vec{r},\hat{n},t) \qquad (4.2)$$

where $\Sigma_T = \Sigma_{total} = \Sigma_s + \Sigma_a$, $S_b(\vec{r},\hat{n},t)$ is another source term resulting from the ballistic component. Now if we expand the diffuse intensity in a series of spherical

harmonics and take *only* the first two terms as shown below, that will constitute the diffusion approximation

$$I_d(\vec{r},\hat{n},t) \approx \phi(\vec{r},t) + \frac{3}{4\pi}\vec{j}(\vec{r},t).\hat{n} \qquad (4.3)$$

where $\phi(\vec{r},t) = vn(\vec{r},t)$. And v and n are the velocity of light and the photon density in the medium respectively and $\vec{j}(\vec{r},t) = -D\hat{n}.\vec{\nabla}n(\vec{r},t)$ with the diffusion constant D given as

$$D = \frac{v}{3\{\Sigma_a + (1-g)\Sigma_s\}} \approx \frac{vl_t}{3} \text{ (with absorption being negligible).}$$

The temporal profile of the photon density has been obtained from the solution of the diffusion equation as[1, 30-31]

$$\frac{\partial n(\vec{r},t)}{\partial t} = D\nabla^2 n(\vec{r},t) - \frac{v}{l_a}n(\vec{r},t) + \delta(\vec{r})\delta(t) \qquad (4.4)$$

where the δ-function term represents the impulse photon source at time $t = 0$. In case of a large slab with a thickness w located between $z=z_0$ ($z_0 = 0.71l_t$ is the extrapolation length[1]) and $z = w+z_0$, with the boundary condition that the photon density vanishes at $z = 0$ and $z = w+2z_0$, the temporal profile of the photon density with the source at $x'=0$, $y'=0$ and z' can be obtained with the method of images as[30-31]

$$n(\vec{r},t) = \frac{e^{-R^2/4Dt}}{(4\pi Dt)^{3/2}} \sum_{m=-\infty}^{\infty} \{e^{-(2md+z'-z)^2/4Dt} - e^{-(2md-z'-z)^2/4Dt}\}$$
$$\times\ e^{-vt/l_a} \qquad (4.5)$$

where $R = x^2+y^2$ and $d = w+2z_0$.

For a very thick medium ($w \sim \infty$) the solution becomes

$$n(\vec{r},t) = \frac{1}{(4\pi Dt)^{3/2}} e^{-[R^2+(z-z')^2]/4Dt} e^{-vt/l_a} \qquad (4.6)$$

The equation (4.5) can also be written using the Poisson sum formula[32] as

$$n(\vec{r},t) = \frac{e^{-R^2/4Dt}}{(4\pi Dt)d} \sum_{m=-\infty}^{\infty} \left\{ \sin\frac{\pi m z'}{d} \sin\frac{\pi m z}{d} e^{-Dt(m\pi/d)^2} \right\}$$
$$\text{X } e^{-vt/l_a} \qquad (4.7)$$

In the above derivation the value of the extrapolation length was taken to be 0.71 l_t as suggested by Ishimaru[1] and this value is commonly used. This extrapolation length was derived for totally absorbing boundary conditions where no particles entered from outside. But Aronson[33] has recently shown that this value can be significantly different for photons in isotropic scattering because of interior reflection at the boundary when the mismatch in the index of refraction is larger than 1.4. In our experiments, the index of refraction mismatch is very small as our tissue samples are put in glass cells ($n_{glass}/n_{tissue} \approx 1.07$). But for air and tissue cases the mismatch could be significantly large (~ 1.4) and this aspect must be considered.

4.4 Forward Scattering Through a Slab of Turbid Medium

The photon density and the photon flux through a slab of turbid medium in the z direction can be obtained (with $z' = z_0$ and $z = w+z_0$) from the equation (4.7) as:

$$n_z(t) = \frac{e^{-R^2/4Dt}}{(4\pi Dt)d} \sum_{m=1}^{\infty} (-1)^m (1 - \cos\frac{2\pi m z_0}{d}) e^{-Dt(m\pi/d)^2} e^{-vt/l_a} \qquad (4.8)$$

and

$$j_z(t) = \frac{D.e^{-R^2/4Dt}}{(4\pi Dt)\pi\omega^2} \sum_{m=1}^{\infty} m(\frac{\pi\omega}{d})^2 \sin\frac{m\pi\omega}{d} e^{-Dt(m\pi/d)^2} e^{-vt/l_a} \qquad (4.9)$$

The temporal profile of a laser pulse at a point on the opposite side of a slab of thickness w can be obtained by integrating the equation (4.9) over the whole surface of the slab:

$$I_z(t) = \frac{D}{\pi w^2} \sum_{m=1}^{\infty} m(\pi w / d)^2 \sin(m\pi w / d) e^{-(Dt(m\pi/d)^2)} e^{-vt/l_a} \tag{4.10}$$

This equation can be used to fit the temporal profiles of the transmitted pulses to obtain the transport and the absorption lengths of a turbid medium (Appendix II gives a computer program to fit the equation). One can also use this equation to simulate various temporal profiles of transmitted pulses through various random media with different transport mean free paths, absorption lengths, sample thickness and index of refraction. Fig. 4.2

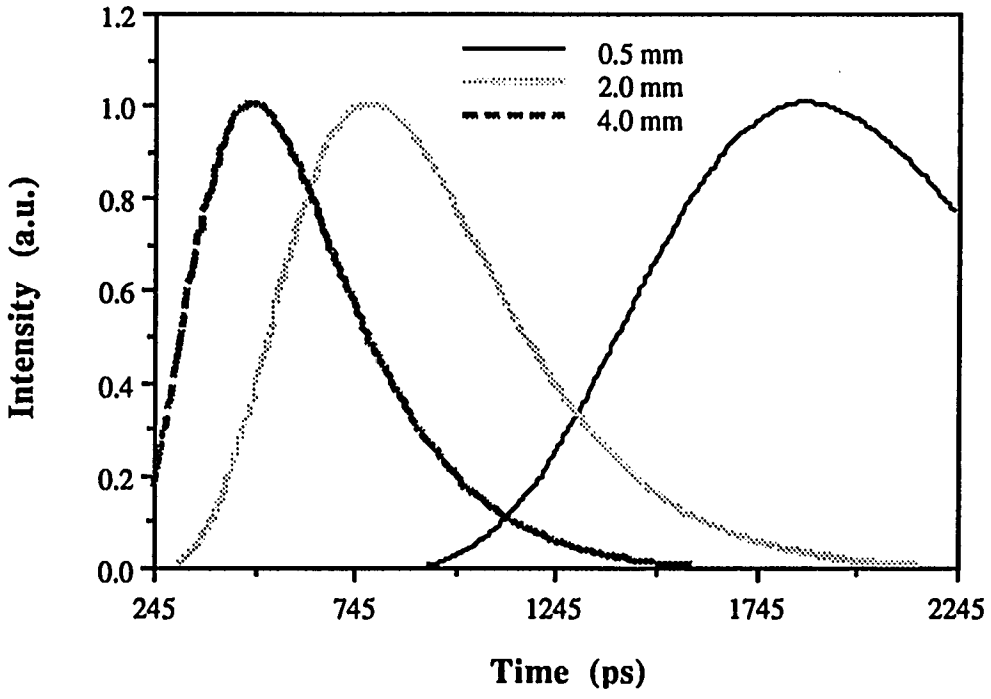

Fig. 4.2 Simulated transmission profiles for different transport mean free paths (0.5, 2 and 4 mm) with an absorption length of 60 mm and a sample thickness of 5 cm.

displays three simulated transmission profiles for a 5 cm thick, n = 1.4 sample with l_t = 0.5 , 2 and 4 mm and l_a = 60 mm. One finds significant broadening associated with a peak shift of the transmitted pulses as one goes from large to small transport mean free paths. This is because of higher degree of scattering resulting in the late arrival of photons. Fig. 4.3 shows a plot of the peak time versus transport mean free path. The absorption length was chosen as 60 mm for this case. The curve approaches zero and

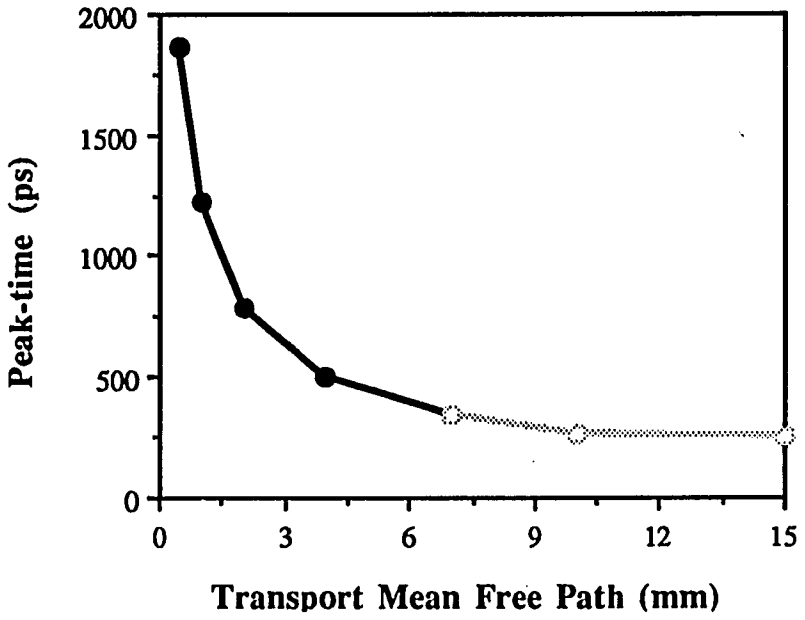

Fig. 4.3 A plot of peak time versus transport mean free path obtained from various simulated transmission curves. The lighter part shows the region where diffusion approximation is not strictly valid.

infinity asymptotically as l_t approaches infinity (no scattering) and zero (strong scattering), respectively. The lighter part of the curve shows the region where the diffusion approximation is not valid.

4.5 Experimental Setup

This section describes the experimental methods used to measure the optical parameters of various tissues and other model random media. Figure 4.4 displays our experimental setup to measure the time-resolved light transmission through a random medium.

For this experiment three different lasers - Colliding Pulse Mode-locked Dye laser (CPM), pulse compressed Nd-Yag laser and Synchronously pumped tunable dye laser - were used for 626 nm, 1064 nm and 570-630 nm wavelength range, respectively. In the first case, the CPM laser was used to produce ultrashort laser pulses of about 100 fsec at 620 nm. The pulse repetition rate and the power output of this CPM laser are 82 MHz and 10 mW, respectively.

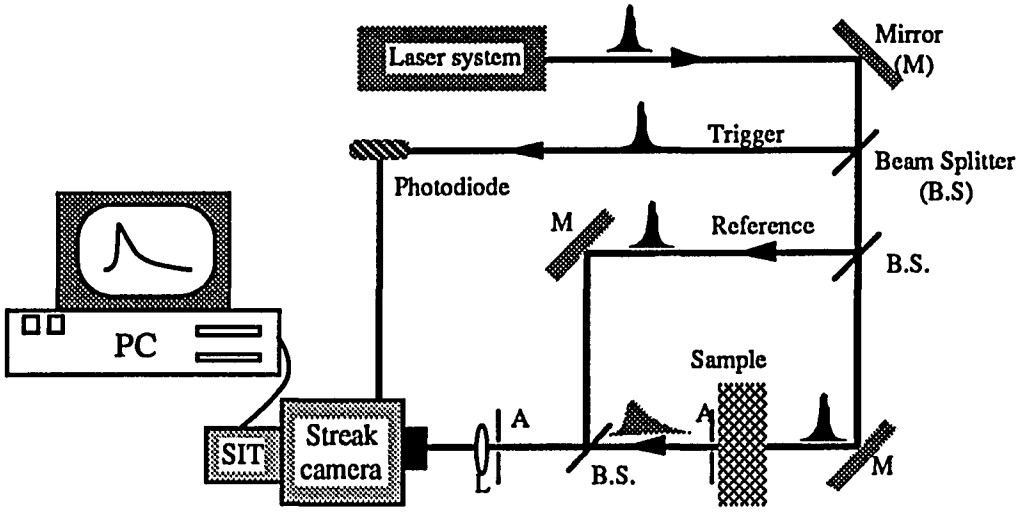

Fig. 4.4 The experimental setup for time-resolved transmission measurements through a scattering medium.

The pulse compressed Nd-Yag laser was used to provide 5 ps laser pulses at 1063 nm with a repetition rate of 82 MHz. The average power used was about 50 mW.

In the third case, a synchronously pumped tunable dye laser was used to provide laser pulses with wavelengths between 570 - 630 nm, ~ 200 mW power at a repetition rate of 82 MHz with a pulse duration of ~ 500 fs.

A part of the incident beam was used to trigger the streak camera using a photodiode. A reference pulse was used to obtain the zero time - the time when the pulses hit the sample. Various tissue samples were pressed between two parallel glass plates to keep them uniformly thick. The transmitted signal through the sample was detected by a Hamamatsu synchroscan streak camera. Small apertures were used to collect the transmitted photons scattered in the forward direction.

4.6 Results

Time-resolved transmission measurements were performed on several tissue samples from human breast (4 benign tissues and 4 fatty normal tissues from breast reduction), chicken, pork and on samples of milk and intralipid[34]. Figure 4.5 displays

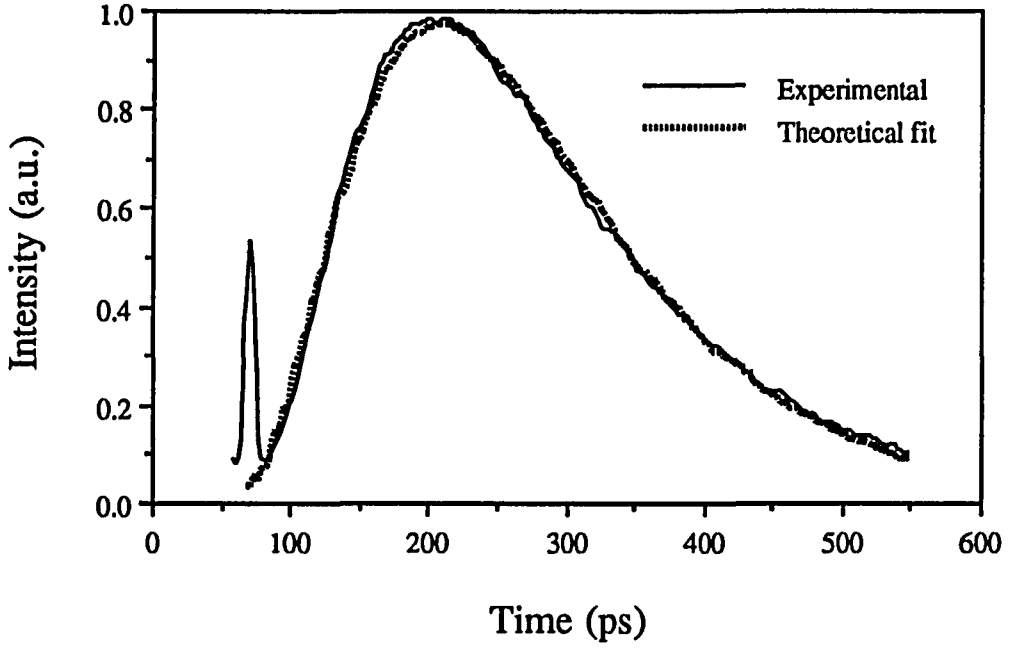

Fig. 4.5 The experimental transmission profile through a 21 mm human benign breast tissue with its theoretical fit. The l_t and la were found to be 2.2 mm and 34 mm respectively. The first peak is due to the reference pulse.

a typical temporal profile of a transmitted pulse at 620 nm for a human normal breast tissue. The first peak is due to the reference pulse. These temporal profiles were fitted with the equation (4.10) with a least square fitting program to obtain the transport mean free paths and the absorption lengths for these samples. It has been previously shown by Yoo et al.[18-19] that this least square fitting scheme using the eqn. (4.10) provides a

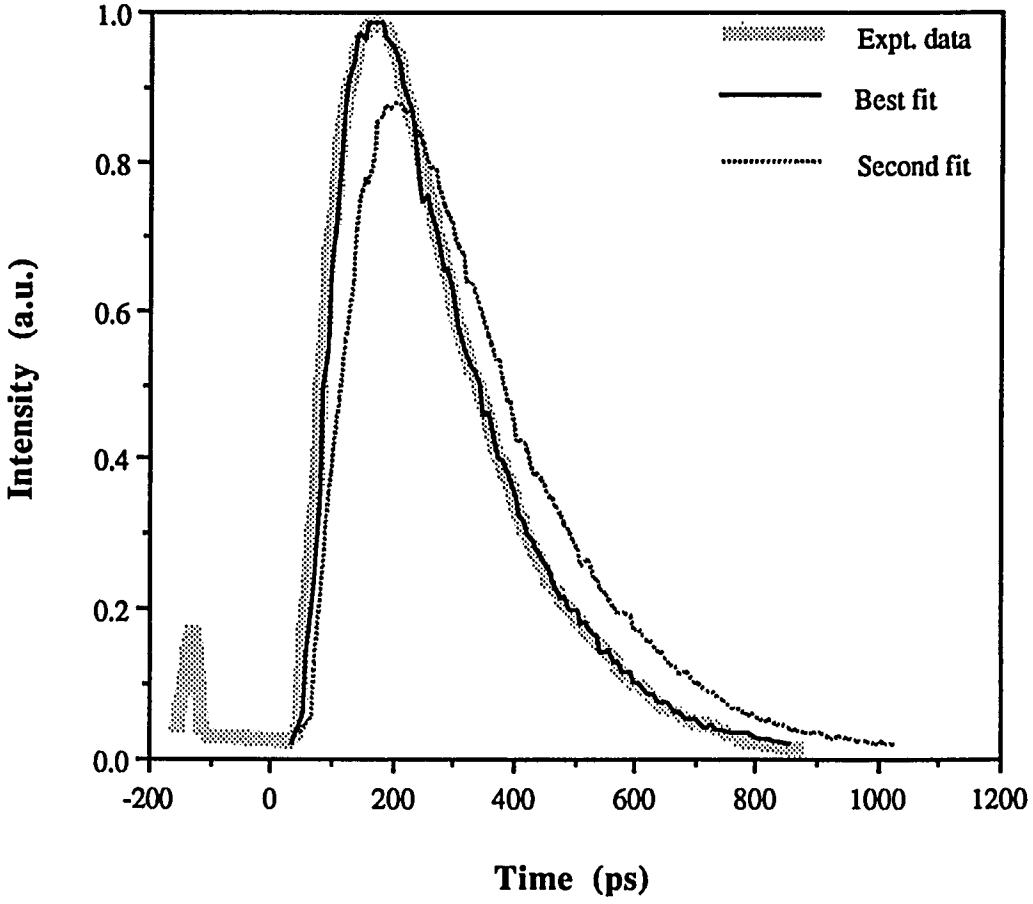

Fig. 4.6 The temporal profile of a transmitted pulse (the thick, hazy line) through a milk solution is shown with its best fit (solid curve) giving l_t = *1.0 mm*, l_a = *252 mm*. Another fit (the dotted line) giving l_t = *0.8 mm and* l_a = *202 mm* is displayed to give a feel for the accuracy of the best fit.

very accurate protocol to measure the transport mean free paths of various scattering media that are thicker than seven transport mean free paths.

Fig. 4.6 displays a temporal profile of a transmitted pulse (the thick, hazy line) through a milk solution with its best fit (the solid curve) at l_t = *1.0 mm*, l_a = *252 mm*. Another fit (the dotted line) with l_t = *0.8 mm* and l_a = *202 mm* is displayed to show the accuracy of the best fit.

Table 4.1 lists the transport mean free paths and the absorption lengths for these samples with the standard deviation. One finds from this table that chicken and human breast tissues have almost the same values for the scattering parameters while the absorption lengths are very close. It is also true for the fat tissues. Since light scattering is more dominant in tissues than absorption at this wavelength, chicken breast tissue and fat can serve as a very good substitutes for human breast tissues.

Random medium	Transport mean free path (l_t) *mm*	Absorption length (l_a) *mm*
Benign human breast	2.6 ± 0.2	30 ± 5
Fatty human breast	0.7 ± 0.1	155 ± 50
Chicken breast	2.5 ± 0.5	60 ± 30
Chicken fat	0.6	155
Pork breast	1.2 ± 0.2	70 ± 8
Pork fat	0.35 ± 0.05	300 ± 50
Whole milk (25%)	1.0 ± 0.1	253 ± 50
Intralipid (1%)	0.6 ± 0.1	195 ± 50

Table 4.1 The transport mean free paths and the absorption lengths with their standard deviations for various random media at 620 nm measured using time-resolved transmission and diffusion approximation.

Our measurements of the transport mean free paths and the absorption lengths compare well with the values reported by other groups. Using 1-D diffusion approximation Karagiannes et al.[35] have reported the value of the transport mean free path of cow muscle at 633 nm as 2.3 mm which is in close proximity with our measurements for chicken and human (benign) breast tissues. A value of 3.4 mm for normal human breast tissue at 695 nm reported by Navarro and Profio[15] using the discrete ordinate method is slightly higher than our measurements. But they have pointed out that some inaccuracy is expected in their measurements as this value was an extrapolated one. Wilson et al.[16] have indirectly calculated the transport mean free path for cow muscle to be 1.2 mm at 633 nm from their measurements of total attenuation through thin tissues using single scattering approximation. The problem with thin tissue measurements is that the thickness of the sample must be known with a great degree of accuracy. Besides, they had ground the tissue and frozen it while preparing their sample[36]. This alteration in the natural state might result in a change in the scattering parameters that one must be careful about. Thin tissues may also show properties characteristic of local inhomogeneities rather than that of the bulk tissue.

Similarly absorption lengths have been reported to be 25 mm and 33.3 mm for cow and chicken muscle respectively at 630 nm by Marynissen and Star[37], and 56.8 mm (at 760 nm) for human calf muscle by Patterson et al.[17] These measurements are close to the values obtained by our measurements.

Because of the unavailability of human tissue samples, several model random media are used to perform various scattering and imaging studies. Intralipid and milk are commonly used as such. So it is important to know the optical parameters of these samples. To check the dependence of the optical parameters on the sample concentration we did pulse transmission measurements on milk and our findings are listed in Table 4.2. As expected, the dilution with water simply changes the optical

parameters by the inverse proportion. This fact can save time as one does not have to measure the optical properties for each concentration.

Sample	(l_t) mm	(l_a) mm
Milk (25%)	1.0 ± 0.2	253 ± 50
Milk (12%)	2.2 ± 0.2	510 ± 50

Table 4.2 The transport mean free paths and the absorption lengths at 620 nm wavelength for milk at two different concentrations. The accuracy of the measurements were obtained from the fitting as shown in Fig. 4.6.

From a qualitative assessment of the scattering cross-sections from the optical density measurements on thin tissues we showed in the previous chapter that the scattering cross-section of human breast tissue is relatively wavelength independent in the visible and uv region. To investigate it more quantitatively we performed time-resolved transmission profile measurements on a chicken breast tissue and a human fatty breast tissue using a synchronously pumped dye laser in the wavelength region of 570 - 630 nm. The Nd:Yag laser was also used to measure the transmission in the infrared region at 1064 nm. The temporal profiles were fitted with the equation (4.10). Figure 4.7 displays a temporal profile of a transmitted signal through a 5.7 cm thick chicken tissue at 1064 nm. The dotted line is the theoretically fitted curve that gives $l_t = 5.1\ mm$ and $l_a = 70\ mm$.

These optical parameters at various wavelengths are listed in the Table 4.3.

We can see from this table and Figure 4.8 that the scattering cross sections are indeed relatively constant in the visible region while it is much larger at 1064 nm. This result means human and chicken breast tissues are much less scattering in the IR region than in the visible region. This low scattering is highly significant for thick tissue

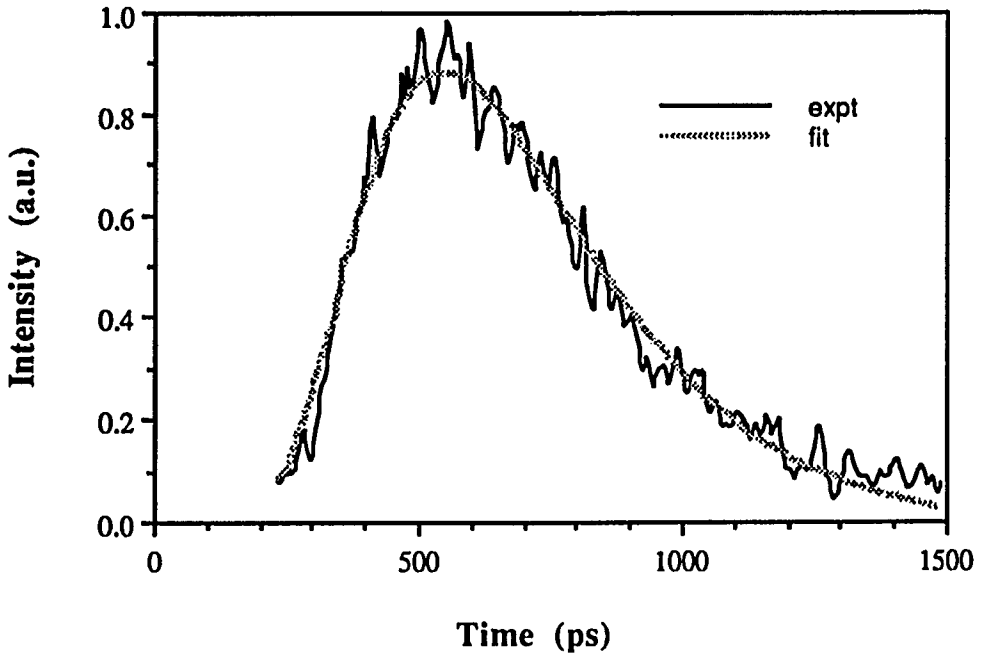

Fig. 4.7 Temporal profile of a transmitted signal through a 5.7 cm thick chicken tissue at 1064 nm. The dotted line is the theoretically fitted curve that gives lt = 5.1 mm and la=70 mm.

Wavelength (nm)	Chicken breast		Fatty human breast	
	(l_t) mm	(l_a) mm	(l_t) mm	(l_a) mm
570	2.7	19	0.7	30
580	2.3	16		
590	2.6	25		
600			0.7	55
610	3.0	58	0.6	47
620	2.5	52	0.7	55
630	3.3	87	0.7	58
1064	4.9	70		

Table 4.3 The transport mean free path and the absorption length at various wavelengths for a chicken breast tissue and a fatty human breast tissue.

imaging. However the absorption coefficients vary a great deal because of different chromophores involved, and this variation can help select suitable wavelengths for imaging small tumors in a breast.

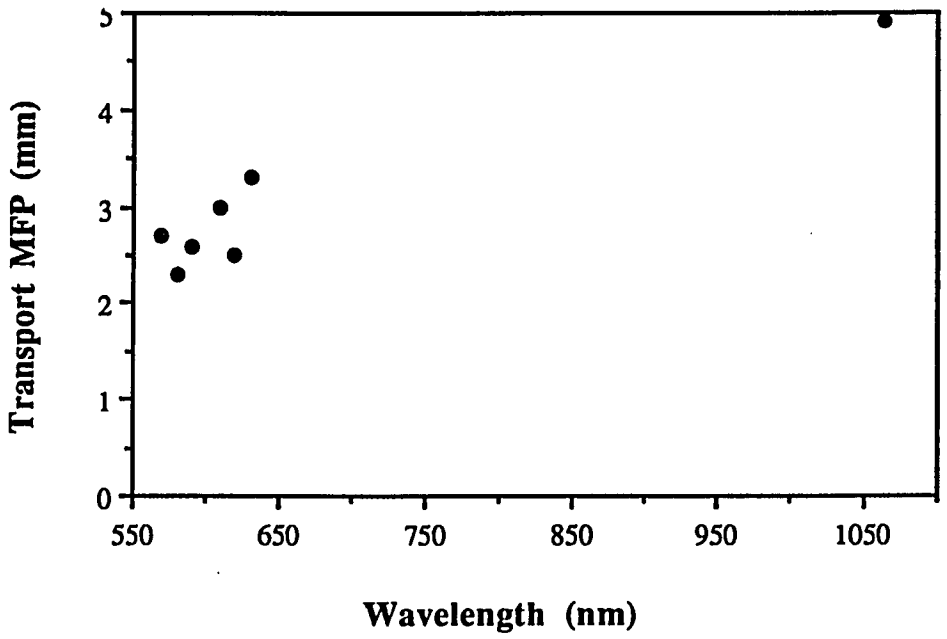

Fig. 4.8 The transport mean free path for a chicken breast sample is plotted against the wavelength.

In conclusion, we have measured the transport mean free paths and the absorption lengths for various tissues and model random media. We found that the scattering cross-section remains relatively constant in 570 - 630 nm wavelength region while it changes significantly for 1064 nm. The optical parameters for milk are found to be inversely proportional to the concentration in water. And chicken breast and fat tissues can be used as good models for human breast tissues as the optical parameters of the two tissue types are almost the same. The less scattering observed at 1064 nm makes tissues more transparent in the NIR region making it easier to image in thick tissues.

4.7 References

1. A. Ishimaru, *Wave propagation and scattering random media*, New York: Academic, 1978

2. J. A. Kong, *Electromagnetic Theory*, Wiely, New York, 1986

3. L. Tsang, J. A. Kong, and R. T. Shin, *Theory of Microwave Remote Sensing*, Wiely, New York, 1985

4. V. V. Varadan and V. K. Varadan, Eds., *Multiple Scattering of Waves in Random Rough Surfaces*, Penn State Univ., University Park, 1987

5. S. Chandrasekhar, *Radiative Transfer*, Oxford University Press, London, 1950

6. G. B. Rybicki, *J. Quant. Spectrosc. Radiat. Transfer*, **11**, p. 827-49

7. J. J. Duderstadt and L. J. Hamilton, *Nuclear Reactor Analysis*, Wiley, New York, 1976, p. 103-44

8. L. L. Carter and E. D. Cashwell, *Particle Transport Solution with the Monte Carlo Method* (Technical Information Center, Office of Public Affairs, US Energy Research and Development Administration) 1975

9. V. P. Kubelka and F. Munk, *Z. Tech. Phys.* **12**, 593-601

10. P. A. Wilksch, F. Jacha and A. J. Blake in *Porphyrin Localization and Tretment of Tumors*. D. R. Doiron and C. J. Gomer, eds. New York: Liss, p. 149, 1[illegible]4

11. R. R. Anderson, J. Hu and J. A. Parish, *Bioengineering and the skin*. R. Marks and P. A. Payne, eds. MTP Lancaster, p. 253, 1981

12. M. J. C. van Germert and H. J. P. Hulsbergen, *Arch. Dermatol. Res*, **270**, 429, 1981

13. S. Wan, R. R. Anderson and J. A. Parish, *Photochem. Photobiol.*, **34**, 493, 1981

14. S. Ertefai and A. E. Profio," Spectral Transmittance and Contrast in Breast Diaphanography," *Med. Phys.* **12**(4), 393, 1985

15. G. A. Navarro and A. E. Profio, "Contrast in Diaphanography of the Breast," *Med. Phys.*, 15, p181-187, 1988

16. B. C. Wilson, M.S. Patterson, S. T. Flock and J. D. Moulton, "The optical absorption and scattering properties of tissues in the visible and near-infrared wavelength range," in *Light in Biology and Medicine*, vol. 1, R. H. Douglas, J. Moan, and F. Dall'Acqua, eds. Plenum, New York, 1988, p.45

17. M. S. Patterson, B. Chance and B. C. Wilson, "Time Resolved Reflectance and Transmittance for the Noninvasive Measurement of Tissue Optical Properties," Appl. Opt., 28, p2331-2336, 1989

18. Yoo, K. M. ; Liu, F. ; and Alfano, R. R. ; *Phys. Rev. Lett.* **64**, 2647 (1990)

19. K. M. Yoo, Ph. D. Thesis, The City University of New York, 1990

20. B. C. Wilson and M. S. Patterson, "The physics of photodynamic therapy," *Phys. Med. and Biol.*, 31, p. 327-360

21. A. E. Profio,"Light transport in tissue," *Appl. Opt.*, 28, p2216-2222, 1989

22. R. Graaff, J. G. Arnoudse, F. F. M. de Mul and H. W. Jentink,"Light Propagation for anisotropically scattering scattering media based on a rigorous solution of the transport equation," *Appl. Opt.*, 28, p2273-2279, 1989

23. A. E. Profio and D. R. Doiron,"Dosimetry considerations in phototherapy," *Med. Phys.*, 8,p 190-196, 1981

24. A. J. Welch, G. Yoon, and M. J. C. van Gemert,"Practical models for light distribution in laser irradiated tissue," *Lasers in Surgery and Medicine,* 6, p488-493, 1987

25. B. C. Wilson, M. S. Patterson and S. T. Flock,"Indirect versus direct techniques for the measurement of the optical properties of tissues," *Photochem. and Photobiol.* 46, p601-608, 1987

26. R. Marchesini, A. Bertoni, S. Andreola, E. Melloni and A. E. Sichirollo, "Extinction and absorption coefficients and scattering phase functions of human tissues in vitro," *Appl. opt.*, 28, p2318-2324, 1989

27. S. Nakamura, Y. Nishiwaki, S. Sujuki, S. Sakaguchi, Y. Yamashita and K. Ohta," Light attenuation in human liver and hepatic tumors after surgical resection," *Lasers in Surgery and Medicine*, 10, p12-15, 1990

28. S. L. Jacques, C. A. Alter, and S. A. Prahl, "Angular dependence of HeNe laser light scattering by human dermis," *Lasers in the Life science* 1, p309-333, 1987

29. S. Andreola, A. Bertoni, R. Marchesini and E. Mellino,"Evaluation of optical characters of different human tissues in vitro," *Lasers Surg. Med.*, 8:142 (abstract), 1988

30. M. Lax, V. Nayaramamurti and R. C. Fulton in *Laser Optics of Condense Matters* edited by J. L. Birman, H. Z. Cummins, A. A. Kaplyanskii, Plenum, New York, 229, 1987

31. G. H. Watson, S. L. McCall, P. A. Fleury and K. B. Lyons, *Phys. Rev. B*, 41, 10947, 1990

32. M. Lax, *Symmetry Principles in Solid State and Molecular Physics*, p 198, Wiley, New York, 1974

33. R. Aronson,"Extrapolation distance for diffusion of light," SPIE Vol. 1888.

34. Feng Liu, Ph. D. Thesis, The City University of New York, 1993

35. J. L. Karagiannes, J. Zhang, B. Grossweiner and L. I. Grossweiner," Application of the 1-D diffusion aproximation to the optics of tissues and tissue phantoms," *Appl. Opt.*, 28, p2311-2317, 1989

36. S. T. Flock, B. C. Wilson and M. S. Patterson, "Total attenuation coefficients and scattering phase functions of tissues and phantom materials at 633 nm," *Med. Phys.* 14(5) 1987

37. J. P. A. Marynissen and W. M. Star in *Porphyrin Localization and Tretment of Tumors*. D. R. Doiron and C. J. Gomer, eds. New York: Liss, p. 133, 1984

CHAPTER 5

Time-Resolved Backscattering of Light In Biomedical and Random Media

5.1 Introduction

It has been discussed earlier that a fundamental understanding of light scattering and photon migration in various random media is crucial to tap the potential uses of light scattering in as diverse fields as solid state physics and medicine. In the last decade and a half there has been a spurt in efforts to use various steady-state and time-resolved techniques to study the back-scattering of light in tissues and various random media[1-24]. While diffuse reflectance has been studied mainly to determine the optical characteristics of various random media[1-5, 9-17,22], time-resolved measurements have been used for imaging hidden objects in bulk media[6,8]. Theoretical studies of photon transport and the diffusion approximation in turbid media have been done by Ishimaru[20] and Furutshu[21]. Egan and Hilgeman[1] have shown how to determine the absorption and scattering characteristics of turbid materials from reflection and transmission measurements on thin slabs. In 1979, Shimizu et al.[2] suggested the use of time-resolved reflectance to obtain the optical properties of random media such as tissue. Groenhuis et al.[3] used the diffusion approximation and Monte Carlo method in 1983 to determine the scattering and the absorption characteristics of dental enamel from steady-state reflection measurements. Parsa et al.[4] have used integrating sphere measurements of reflectance from thin specimens of rat liver to determine its optical properties. Barbour et al.[5] have devised various algorithms and analysis schemes, using simulated data, for the determination of the macroscopic optical properties of multilayer random media by remote sensing. The integrating sphere measurements on thin specimens put

certain limitations as the accuracy in measuring the absolute backscattered intensity, the thickness of the specimen becomes critical. Thin tissues may also show properties characteristic of local inhomogeneities rather than that of a bulk tissue. The shortcomings of the Kubelka-Monk method which is widely used besides the diffusion approximation has been discussed by Wilson and Patterson[9]. Alfano and his group have used both angle and time-resolved backscattered pulse measurements to obtain the optical characteristics of various biomedical and model random media[12-16]. The measurement of the temporal profiles of the backscattered pulses and the diffusion approximation provide an excellent approach for the determination of the macroscopic optical properties of bulk media. These temporal measurements have been performed using two-fiber and single point source-detection configurations that we will discuss in this chapter. Patterson et al.[10] have used *in vivo* picosecond pulse measurements with the two-fiber configuration to determine the optical parameters of human calf muscle. Alfano and his coworkers have used time-resolved backscattering of ultra short laser pulses to monitor different stages of eye cataract[16]. In this chapter, our study of time-resolved backscattering to determine the optical characteristics of various random media and its potential as a diagnostic tool is discussed.

As introduced before, these optical properties of various biological media can be characterized by their transport mean free paths l_t and the absorption lengths l_a. These scattering and absorption parameters determine the degree of photon migration in such media. For example, the absorption length depends on the chemical composition of the medium, i.e. the absorption cross-section and the concentration of the absorbing molecules present in the medium. Thus, a change in the absorption length may indicate a change in the chemical composition of the biomedical medium. A change in the physical condition of the tissue, such as dehydration, would change the number density and give different values for l_t. Observing such changes in the optical parameters can be

useful in distinguishing normal from abnormal tissues. This chapter describes our work on back scattering of ultrashort laser pulses for probing the optical properties of various random media.

5.2 Theory

In a highly scattering medium such as a human tissue the transport of light can be approximated by the diffusion theory. We will describe two different theoretical models for two different experimental configurations.

5.2.1 Single Point Source-detection

First we consider the case where the point of light incidence is same as the point of collection as shown in Fig. 5.1.

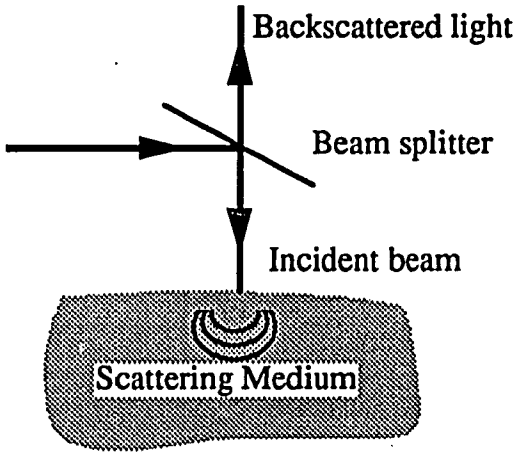

Fig. 5.1 Backscattered light where the points of incidence and collection are the same.

The temporal profile of a backscattered pulse for this case, as described by Yoo et al[15], is given by:

$$I(\hat{s},t) = \int_0^\infty dt' R(\hat{s},t')[1+e^{-D_0 q^2 t'}]e^{-\gamma_a t'} I_0(t-t') \qquad (5.1)$$

where $I_0(t-t')$ is the incident pulse, $D_0 \approx vl_t/3$ is the diffusion coefficient, $\gamma_a = v/l_a$ and $R(\hat{s},t')$ is the the response function of the random medium. In the diffusion approximation, one can write

$$R(\hat{s},t') = \frac{\alpha}{(2\pi)^{1/2}} e^{D_0 t'/2l_t^2} D_{-3}(2D_0 t'/l_t^2)^{1/2} \quad , \qquad (5.2)$$

where α is a constant, $D_{-3}(x) = u(5/2,x)$ is the parabolic cylinder (weber) function. Figures 5.2(a) and 5.2(b) display several theoretical curves[22] simulated using Eqn. (5.1) and (5.2) for different values of transport mean free paths and absorption lengths, respectively.

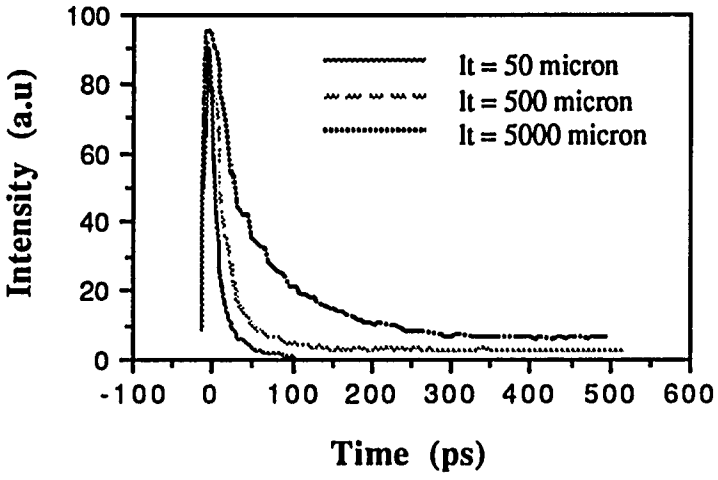

Fig. 5.2(a) Temporal Profiles of backscattered pulses computed from eqn. (5.1) with convolution of 8ps Impulse response function for various values of l_t = 50, 500,5000, 50000 μm.

It is clear from these set of simulated curves that the peak region of these temporal profiles and the FWHM are greatly dependent on the transport mean free paths (l_t)while the tails show a strong dependence on the absorption lengths (l_a).

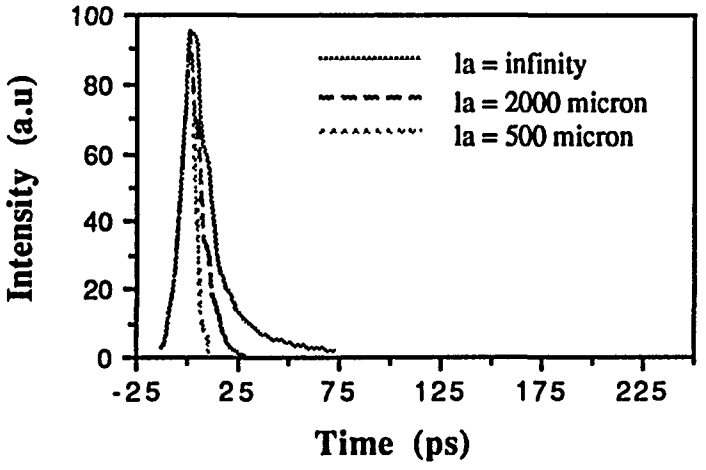

Fig. 5.2(b) Temporal Profiles of backscattered pulses computed from eqn.(5.1) with convolution of 8ps impulse response function for various values of $la = \infty$, 2000 and 500 μm given that l_t = 200 μm.

5.2.2 Two-fiber Input Output Configuration

In this case the source and the detector are at two separate locations as shown in Fig. 5.3. For such a case of semi-infinite scattering medium photon migration has been studied in greater detail using the diffusion approximation[23-24].

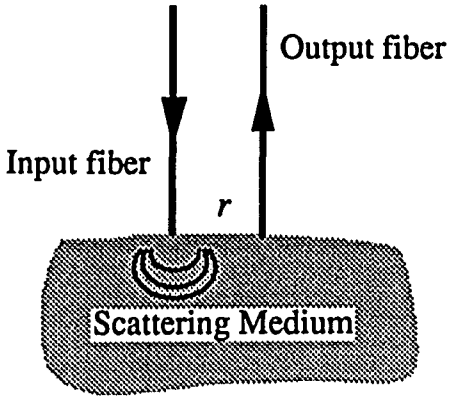

Fig. 5.3 Backscattered light with different input-output positions.

The expression for the temporal profile of a backscattered pulse for this configuration in

Fig. 5.3 is given as:

$$I = \frac{1}{(4\pi Dt)^{3/2}} exp - (\frac{r^2}{4Dt} + \frac{vt}{l_a}).exp - (\frac{z_0^2}{Dt}).\frac{z_0}{t} \quad , \qquad (5.3)$$

where r is the radial distance between the collection point and the point of incidence, $D \approx \frac{vl_t}{3}$ is the diffusion constant, and $z_0 = 0.71l_t$ is the extrapolation length.

Figure 5.4(a) displays two theoretically simulated temporal profiles of backscattered pulses for transport mean free paths of 0.5 mm (solid) and 2.0 mm (dotted) with an absorption length of 250 mm, and a radial distance of 7.5 mm. The profile representing the shorter transport mean free path case (solid curve) is broadened associated with a shift in the peak. This is because smaller the transport mean free path larger is the scattering and that broadens the temporal profile with a large number of

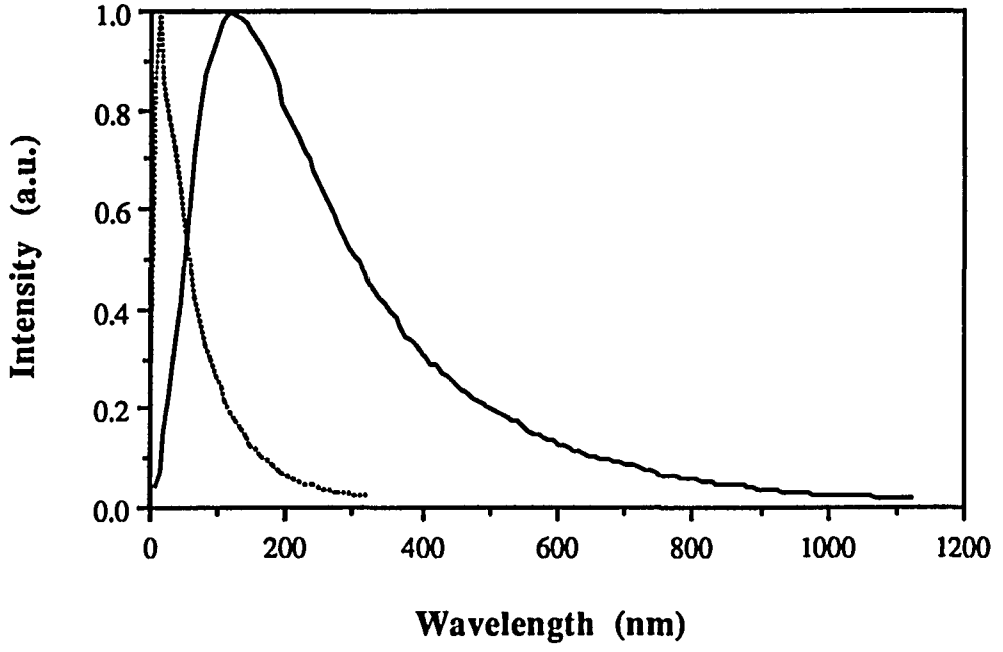

Fig. 5.4(a) Temporal profiles of two backscattered pulses with transport mean free paths of 0.5 mm (solid) and 2.0 mm, and an absorption length of 250 mm at a radial distance of 7.5mm.

photons arriving late. There is a reduction in the absolute intensity in the higher scattering case which is not seen in the figure as the curves are normalized.

Figure 5.4(b) displays two simulated time-resolved backscattered intensity curves for two different absorption lengths of 100 mm (solid) and 250 mm (dotted) with a transport mean free path of 0.5 mm, and a radial distance of 7.5 mm. The change in the curve profile is mainly in the tail region and its dependence on absorption length is not very strong as long as the scattering is much more dominant which is the case in tissues.

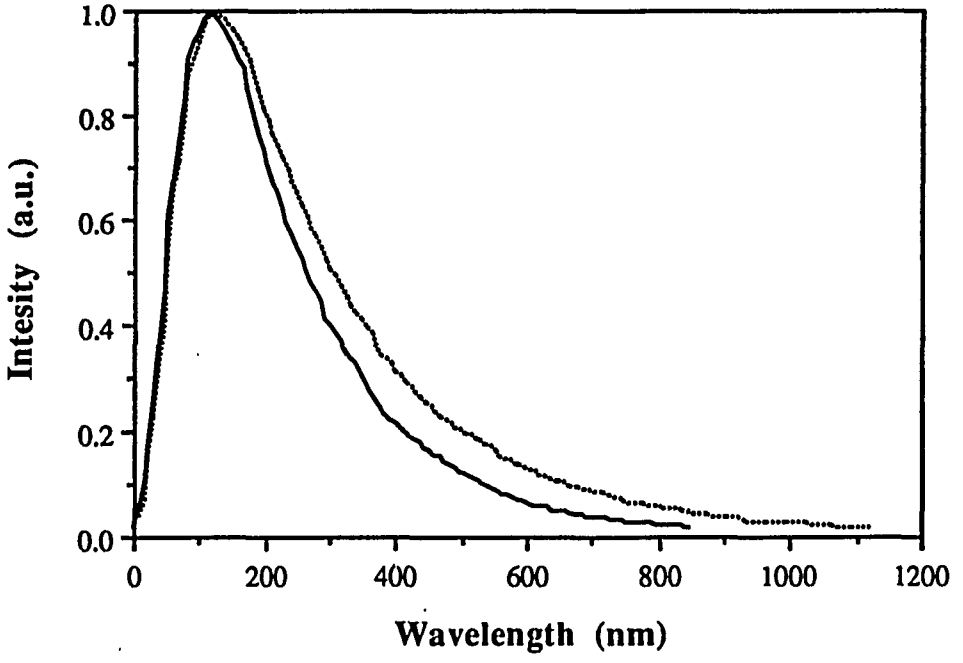

Fig. 5.4(b) Temporal profiles of two backscattered pulses with absorption lengths of 100 mm (solid) and 250 mm, and a transport mean free path of 0.5 mm at a radial distance of 7.5mm.

5.3 Experimental Methods

Time-resolved backscattered pulse measurement with the single point incidence-collection configuration was performed on several breast tissue samples and milk samples using a femto-second laser and a streak camera. The schematic diagram of the

experimental setup is displayed in Fig. 5.5, where 100 fs ultrashort laser pulses were incident on various samples.

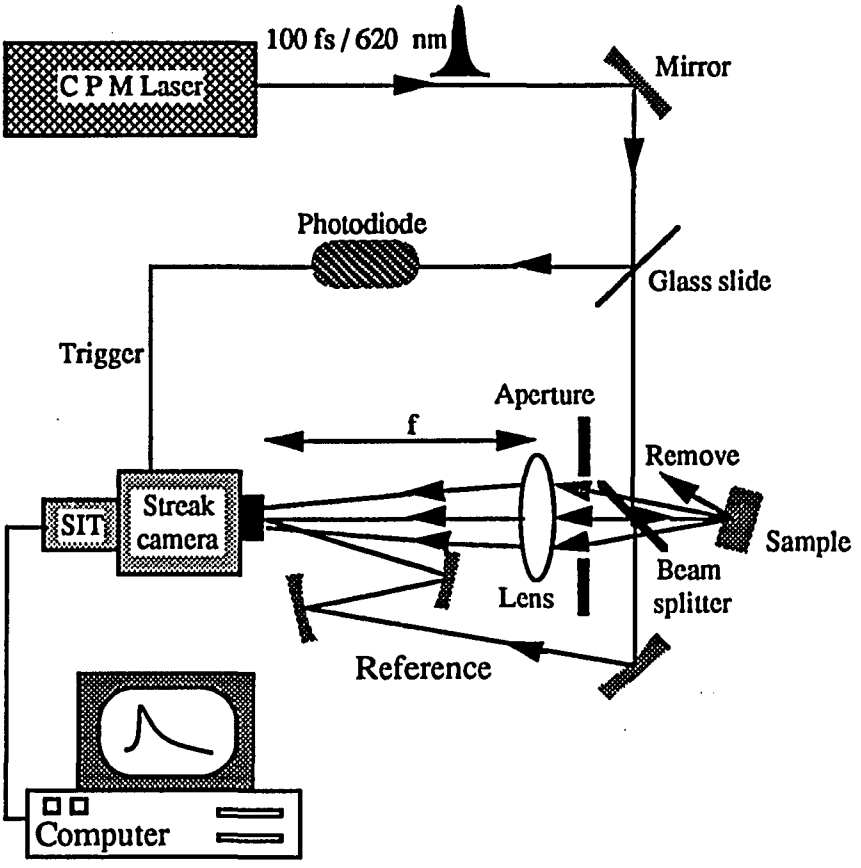

Fig. 5.5 The experimental setup for the time-resolved back-scattering measurements using 100 fs laser pulses.

These laser pulses were generated by a colliding pulse mode-locked dye laser (CPM) which normally produces 50-100 fs pulses. The pulse repetition rate was 82 MHz at 625 nm with a spectral bandwidth of 15 nm. The beam diameter and the beam power were 3 mm and 10 mW, respectively. The sample was placed with its normal at a small angle with respect to the incident beam such that the specular reflection was rejected from the detection system. A part of the beam was used to trigger the streak camera using a photodiode. Another part of the beam through a beam splitter was used

as a reference beam. The temporal distribution of the multiple scattered light from the tissues around the backward direction within 1° was measured by a synchroscan streak camera as shown in the above figure for the single point source-detection configuration. For the two fiber configuration the beam splitter and the lens were taken out. The input beam was coupled to a 100 μm fiber for delivery. The backscattered light was collected at various radial distances using a second 100 μm fiber.

Various breast tissue samples were collected fresh from Beth Israel Medical Center, North Division, New York, immediately after surgery without any addition of preservatives like formalin. Backscattered pulse measurements were performed on these samples the same day or the next day and the samples were kept in a refrigerator.

To observe the dependence of tissue absorption characteristics on wavelength backscattered pulses from a malignant breast tissue at 480 nm, 590 nm, and 700 nm were measured using a super-continuum light source. This light source was obtained by amplifying the laser pulses from the CPM laser by a copper vapor laser (CVL) to 1 μJ per pulse at a 6.5 KHz pulse repetition rate. These amplified pulses were focused onto an ethylene glycol jet to generate a super continuum light source. Three different wavelengths - 480, 590 and 700 nm - were chosen from this super continuum source using the corresponding narrow band filters.

5.4 Results

5.4.1 Single Point Source-detection

Four malignant tumors (ductal carcinoma) and two benign tumor samples from human breast were collected fresh after surgery and were placed in quartz cells and tering measurements were performed on them. Two typical temporal profiles of backscattered pulses from malignant and benign breast tumor samples are displayed in Fig. 5.6. The solid curve is for the benign tissue while the dotted one is for the

malignant sample. The first peak is due to the reference pulse.

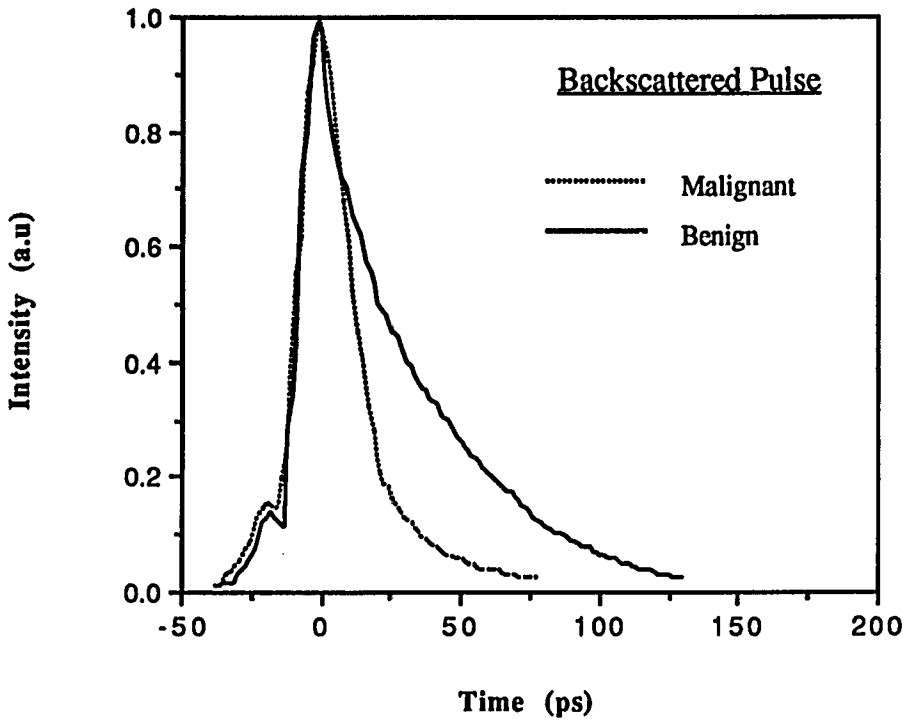

Fig. 5.6 Time-resolved backscattered intensity curves from human malignant and benign breast tissues at 625 nm. The first peak is due to the reference pulse.

The backscattered pulses from the cancerous tissues were found to be significantly narrower than the pulses from the benign samples. The full width at half maximum (FWHM) for the four malignant samples were found to be 16.9, 20.7, 17.3, 17.3 ps, and for the two benign samples were 31.1 and 31.1 ps. The average values were 18 ± 1.5 and 31.1 ps respectively.

This difference in pulse widths for various types of tissues can be highly helpful for medical diagnosis. The difference in pulse widths may be a result of different scattering and absorption parameters arising from different amount of cellular and fibrous contents, and blood in these tissues. In general, the amount of cellular component decreases as we go from malignant to benign tumor (fibroadenoma) while the amount of fibrous component increase in the same order. A least square fitting of

these curves using eqn (5.1) yields the values of l_t for the malignant and the benign tissue as 2.2 mm and 10 mm respectively, while the values for l_a were found to be 43.5 and 20.2 mm respectively. The increase in the transport mean free path indicates that a decrease in cellular content in tissue will decrease the amount of scattering and lengthen the mean free path for benign tissue as compared to malignant tissue.

As we shall see later these values of the optical parameters measured using this experimental configuration are several times larger than those obtained using more consistent and reliable methods of transmission and two-fiber back-scattering. This inaccuracy is due to the application of the diffusion approximation where most of the backscattered photons are not randomized enough. In this experimental configuration a significant portion of the light is scattered back from the immediate neighborhood of the point of incidence where the diffusion theory is not valid.

Though this configuration does not give accurate values for the optical parameters, still it can provide a diagnostic tool based on the significant difference in the pulse profiles and the FWHM measurements. This technique has the potential to complement the uv fluorescence ratio technique discussed earlier in the diagnosis of breast cancer.

Absorption characteristics of tissues depend not only on the chemical composition but also on the wavelength of light used. To observe this dependence, backscattered pulses from a malignant breast tissue at 480 nm, 590 nm, and 700 nm were measured using a super-continuum light source. The temporal profiles of the backscattered pulses for a malignant breast tissue at these wavelengths are displayed in Fig. 5.7. The profiles with solid, dotted and dashed lines correspond to 700, 570 and 480 nm, respectively.

A substantial change in the pulse profile was observed as the incident wavelength changed from 480 to 700 nm. When we go to longer wavelengths the

FWHM of the pulse increases and a more prominent tail appears. This

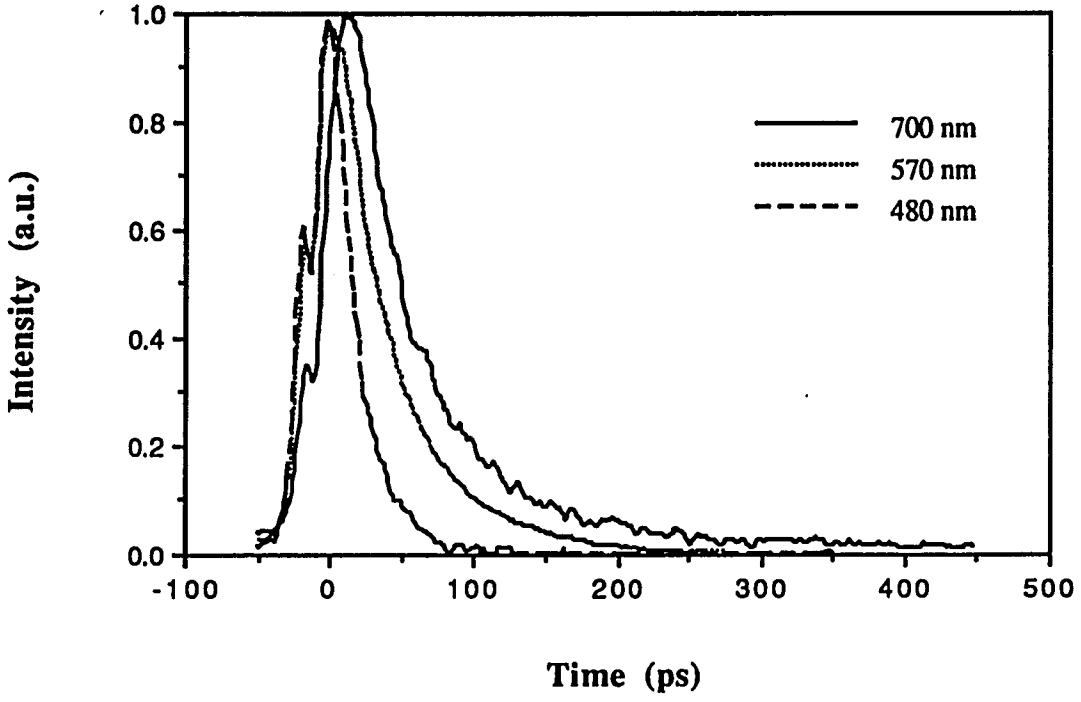

Fig. 5.7 Temporal profiles of back scattered pulses from a malignant breast tissue sample at different wavelengths

change is primarily due to a change in absorption. The narrow pulse width and shorter tail at 480 nm indicate that light is being more strongly absorbed in the tissue at this wavelength. Since the scattering cross-section does not change appreciably with wavelength in this range as discussed in the previous chapters the marked difference in the profiles is attributed to absorption which is stronger near the lower end of the visible spectrum.

5.4.2 Two Fiber Input-output Configuration

Backscattered pulse measurements in this experimental configuration were

performed using the CPM laser (λ = 625 nm) on a human fatty normal tissue from breast reduction and a milk sample. The milk sample (Delwood Co.) was prepared by diluting the whole milk to a 25% concentration using distilled water. Time-resolved transmission measurements on this sample gave the values for l_t and l_a as 0.8 ± 0.1 mm and 253 ± 80 mm, respectively.

Two-fiber pulse measurements were performed at various radial distances (r = 2.5, 5, 7.5, 12.5 mm) to test the theoretical predictions. Three time-resolved intensity profiles for these cases are displayed in Fig. 5.8. These profiles show longer tails and more temporal broadening as the radial distance is increased.

These curves were fitted to the eqn. (5.3) using a least square fitting program to obtain the values for l_t and l_a. These values are presented in Table 5.1. It is clear that the transport mean free paths and the absorption lengths for radial distances of 5 mm,

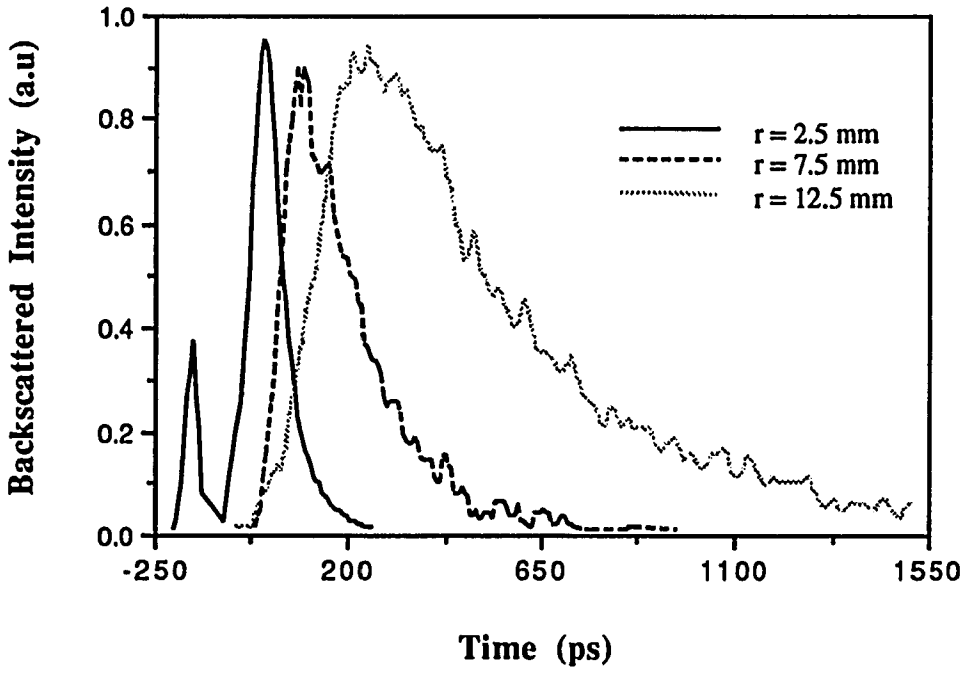

Fig. 5.8 Time-resolved back scattered pulse profiles for various radial distances between the two fibers. The first peak is due to the reference pulse.

7.5 mm and 12.5 mm are very close and match with the value obtained by the time-

resolved transmission method while the transport mean free path for the 2.5 mm case does not. This shows the limitation of using diffusion approximation at short radial distances. At the neighborhood of the source the photons are not randomized and

Fiber distance (r)	2.5 mm	5.0 mm	7.5 mm	12.5 mm
(l_t) *mm*	0.38	0.65	0.7	0.8
(l_a) *mm*	350	350	253	350

Table 5.1 The transport mean free paths and the absorption lengths at 625 nm wavelength for 25% whole milk (Delwood) measured using two fibers. r is the distance between the input and the output fibers.

the diffusion approximation breaks down when the radial distance is less than about 7 times the transport mean free path ($r/l_t > 7$).

5.5 A Comparison of Time-resolved Back and Forward Scattering

We have shown that time-resolved light scattering provides various ways to obtain quantitative information regarding the optical parameters of a random medium. One can choose, depending on the situation, between time-resolved transmission and the two backscattering methods to obtain this basic information. To investigate the suitability of these methods, all three experiments were performed on several samples to compare the transport mean free paths (l_t) and the absorption lengths (l_a). Figures 9,10 and 11 display temporal profiles of a transmitted pulse, and backscattered pulses with two-fiber and single point source-detection configurations respectively for a 3 cm thick human fatty breast tissue. The figures also show the best fit curves using the least square fit method.

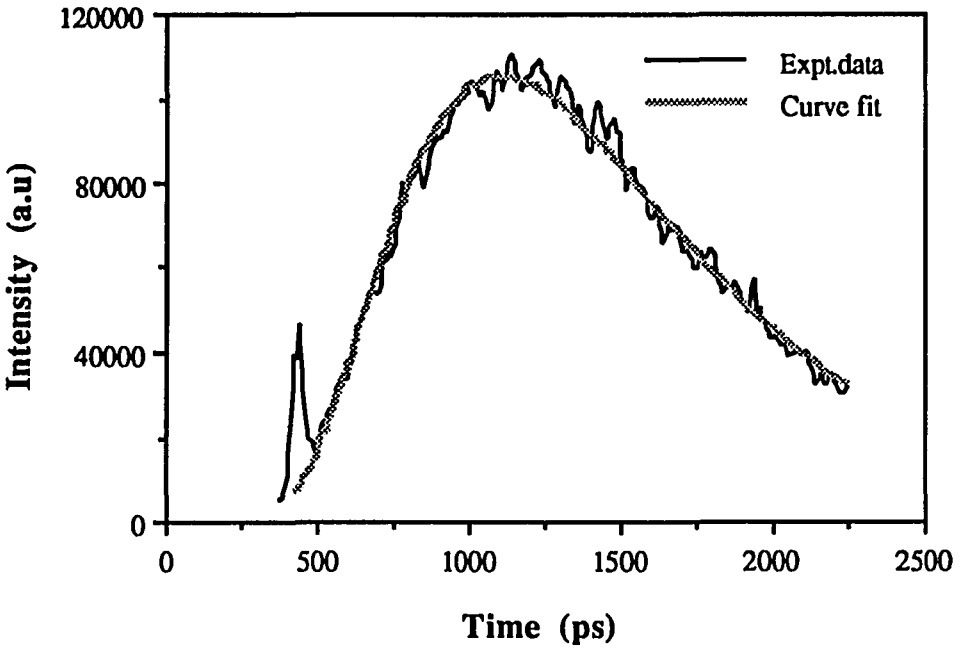

Fig. 5.9 The temporal profile of a transmitted signal through a 3 cm thick human fatty breast tissue with its best fit curve giving l_t = *0.7 mm and* l_a = *208 mm* at 620nm.

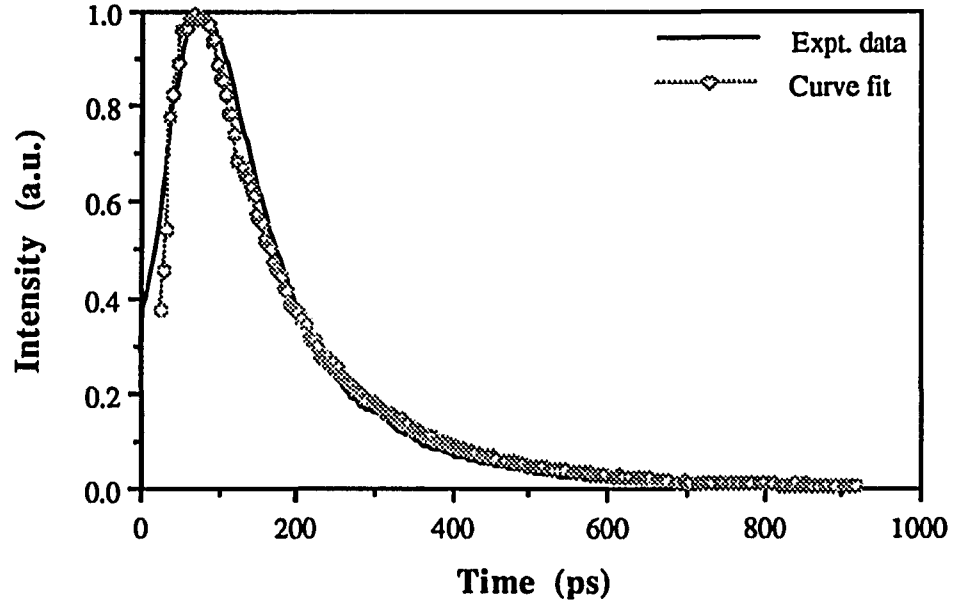

Fig 5. 10 Backscattered pulse with the two fiber configuration from a human fatty breast tissue at 620 nm fitted (open circles) according to the eqn. 5.3 with l_t = *0.7 mm and* l_a = *242 mm.*

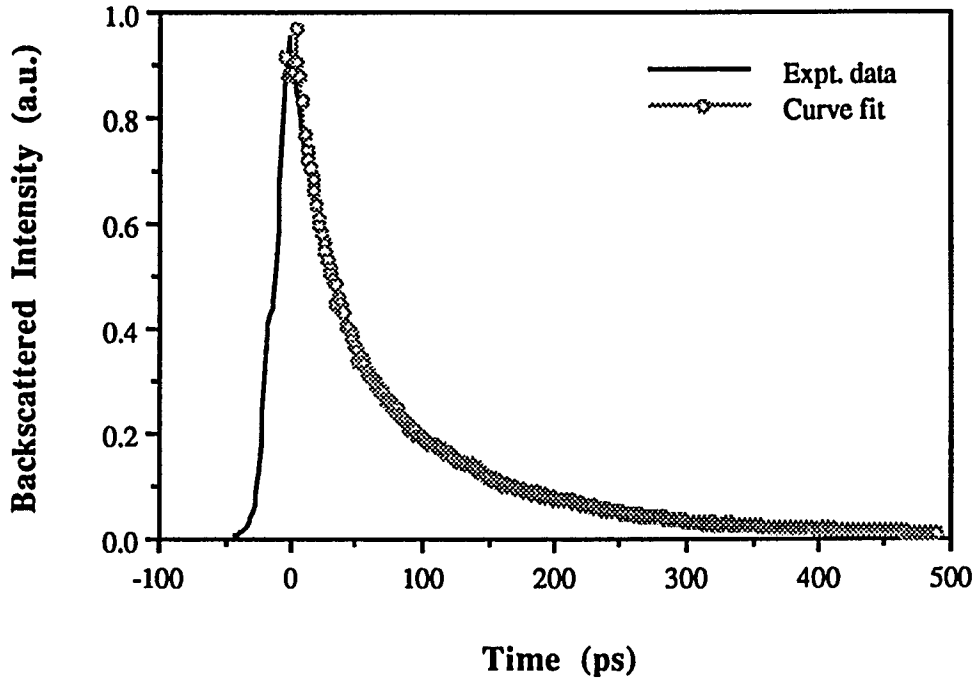

Fig 5. 11 Backscattered pulse with the single point source-detection configuration from a human fatty breast tissue at 620 nm fitted according to the eqn. 5.1 with $l_t = 6.0\ mm$ and $l_a = 80\ mm$.

The values of the optical parameters obtained by these measurements are listed in Table 5.2.

Tissue Type	*Transmission*		*Two-fiber B.Sc.*		*Single Point B.Sc.*	
	(l_t) *mm*	(l_a) *mm*	(l_t) *mm*	(l_a) *mm*	(l_t) *mm*	(l_a) *mm*
Human fatty	0.7	208	0.7	242	6.0	80
Human benign	2.5	30			10.0	22
Human Malig.					2.2	44
Chicken breast	2.5	52				
Chicken fat	0.6	139				
Milk (25%)	0.8	253	0.8	350		

Table 5.2 Transport mean free paths and absorption lengths measured using back and forward scattering of light.

One sample measured using all the three techniques was a human fatty normal tissue from a breast reduction case (Fig.s 9-11). One can see from the values listed in the Table 5.2 that the measurements match quite accurately for the transmission and the two-fiber back scattering cases while the value obtained from the single point source-detection technique is much larger and inaccurate. Similarly the transport mean free paths for a 25% milk solution obtained from transmission and two-fiber backscattering agree as long as the radial distance is not less than about 7 times the transport mean free path of the medium (discussed earlier). Measurements on one benign breast tissue sample show that the transport mean free path obtained by the single point source-detection backscattering technique differs significantly from the value obtained by transmission. This suggests the unsuitability of the single point source-detection approach to measure the optical parameters. This large inaccuracy is due to the application of the diffusion approximation where most of the backscattered photons are not randomized.

In this experimental configuration a significant portion of the light is scattered back from the immediate neighborhood of the point of incidence where the diffusion theory is not valid. This means the theory describing the backscattered light in this configuration must be modified to give a better fit to the experimental curves. Time-resolved transmission and two-fiber backscattering approach are both found to be suitable as long as the thickness of the sample and the radial distance is more than about 7 times the transport mean free path of the sample in their respective cases where the diffusion approximation is valid.

5.6 Conclusion

We have shown that the scattering and the absorption parameters of a random medium can be obtained accurately from time-resolved back scattering in the two-fiber

configuration as long as the radial distance is more than about seven times the transport mean free path of the sample. The values obtained this way agree with the values obtained from previously established method of time-resolved pulse transmission. The single point source-detection technique provides a tool to diagnose breast malignancy though it fails to give accurate values of the optical parameters of tissues with the present theoretical model.

5.7 References

1. W. G. Egan and T. W. Hilgeman, *Optical Properties of Inhomogeneous Materials*, Academic, New York, 1979

2. K. Shimizu, A. Ishimaru, L. Reynolds and A. P. Bruckner, "Backscattering of a Picosecond Pulse from Densely Distributed Scatterers," *Appl. Opt.*, 18, p3484, 1979

3. R. A. J. Groenhuis, J. J. Ten Bosch, and H. A. Ferwerda,"Scattering and absorption of turbid materials determined from reflection measurements," *Appl. Opt.* Vol. 22, No. 16, p. 2463, 1983

4. P. Parsa, S. L. Jacques, and N. S. Nishioka,"Optical properties of rat liver between 350 and 2200 nm," *Appl. Opt.*, Vol. 28, No. 12, p. 2325, 1989

5. R. L. Barbour, H. L. Graber, R. Aronson, and J. Lubowsky," Determination of Macroscopic properties of Multilayer Random Media by Remote Sensing," *SPIE* Vol. 1431, p. 52, 1991

6. R. L. Barbour, H. L. Graber, J. Lubowsky, R. Aronson, B. B. Das, K. M. Yoo, and R. R. Alfano, "Imaging of diffusing media by a progressive iterative backprojection method using time-domain data," SPIE, Vol. 1641, p.21, 1992

7. R. L. Barbour, H. L. Graber, R. Aronson, and J. Lubowsky," Imaging of subsurface regions of random media by remote sensing," *SPIE*, Vol. 1431, 1991

8. J. Chang, Y. Wang, R. Aronson, H. L. Graber, R. L. Barbour, B. B. Das, J. Dolne, K. M. Yoo, and R. R. Alfano, "Time-resolved imaging in dense scattering media," SPIE Vol. 1887, in press.

9. B. C. Wilson and M. S. Patterson,"The Physics of Photodynamic Therapy," *Phys. in Med. Biol.*, Vol. 31, No. 327, 1986

10. M. S. Patterson, B. Chance and B. C. Wilson, "Time Resolved Reflectance and Transmittance for the Noninvasive Measurement of Tissue Optical Properties," *Appl. Opt.*, 28, p2331-2336, 1989

11. S. L. Jacques, "Time Resolved Propagation of Ultrashort Laser Pulses within Turbid Tissues," *Appl. Opt.*, 28, p2223-2229, 1989

12. K. M. Yoo, F. Liu and R. R. Alfano, "Angle-and Time-Resolved Studies of Backscattering of Light from Biological Tissues," Proceedings of *SPIE:* Time-Resolved Laser Spectroscopy in Biochemistry II Convention-1990, 1990

13. K. M. Yoo and R. R. Alfano, "Time-Resolved Depolarization of Light Scattering in Random Media," *Phys. Lett. A*, 142, p531, 1989

14. K. M. Yoo and R. R. Alfano, "Determination of Attennuation Lengths Arising from Scattering and Absorption from the Temporal Profile of the Backscattered Pulse," *Opt. Lett.*, 15, p276, 1990

15. K. M. Yoo, K. Arya, G. C. Tang, J. L. Birman and R. R. Alfano, "Coherent Backscattering of a Picosecond Pulse from a Disordered Medium : Analysis of Pulse Shape in the Time Domain," *Phys. Rev. A*, 39, p3728-3731, 1989

16. R. A. Ahmed, K. M. Yoo, R. M. Klapper and R. R. Alfano, "Time Resolved Backscattering of Pulse to Monitor Different Stages of Eye Cataract," *Appl. Opt.*, 29, p896, 199

17. R. Vreeker, M. P. Van Albada, R. Sprik and A. Lagendijk, "Femtosecond Time-Resolved Measurement of Weak Localization of Light," *Phys. Lett.*, 132, p516-519, 1988

18. H. Taitelbaum, S. Havlin, and G. H. Weiss,"Approximate theory of photon migration in two-layered medium," *Appl. Opt.*, 28, p. 2245-2249, 1989

19. S. Takatani and M. D. Graham,"Theoretical analysis of diffuse reflectance from a two-layer tissue model," *IEEE Transactions* on Biomedical Engineering, 26, p. 656, 1979

20. A. Ishimaru,"Diffusion of a pulse in densely distributed scatterers," *J. Opt. Soc. of Am.* Vol. 68, p. 1045, 1978

21. K. Furutsu,"On the diffusion equation derived from the space-time transport equation," *J. Opt. Soc. of Am.* Vol. 70, p. 360, 1980

22. K. M. Yoo, Ph. D. Thesis, The City Univ. of New York, 1990

23. M. Lax, V. Nayaramamurti and R. C. Fulton in Laser *Optics of Condense Matters,* eds. J. L. Birman, H. Z. Cummins, A. A. Kaplyanskii, Plenum, New York, 229 (1987)

24. G. H. Watson, S. L. McCall, P. A. Fleury and K. B. Lyons, *Phys. Rev. B*, 41, 10947, 1990

CHAPTER 6

Ultrafast Time-gated Imaging In Thick Tissues

6.1 Introduction

Imaging a translucent (turbid) object hidden in a highly scattering random medium using light is one of the most challenging problems in science and engineering. Conventional transillumination techniques have shown indication of large objects, where a cw light beam is incident on a medium and the shadow of a hidden object is observed. In 1929 transillumination was first used in an attempt to image growths in a breast[1]. Recent work has shown[2-5] strong random multiple scattering of light in tissues washes out the shadow and renders this technique ineffective for imaging small tumors. The advent of ultrafast pulse lasers and novel time-resolved detection techniques on picosecond and femtosecond time scales has made it possible to selectively eliminate the multiple scattered light that limits the steady-state transillumination for imaging. Most recently, time-resolved transillumination techniques have been used to image opaque[6-11] and partially absorbing[12-18] objects hidden in various random media. In this chapter our work[18] on imaging one type of tissue inside another is described showing the potential of ultrafast time-gated detection in building an optical mammographic system.

When ultrafast laser pulses are incident on a slab of scattering medium the transmitted pulses consist of a ballistic (coherent) component[19, 20], a diffuse component and a snake component[6] (Fig. 6.1). The ballistic component consists of photons that traverse the medium in the straight line path. These photons can be used for shadow imaging with a spatial resolution limited by diffraction.

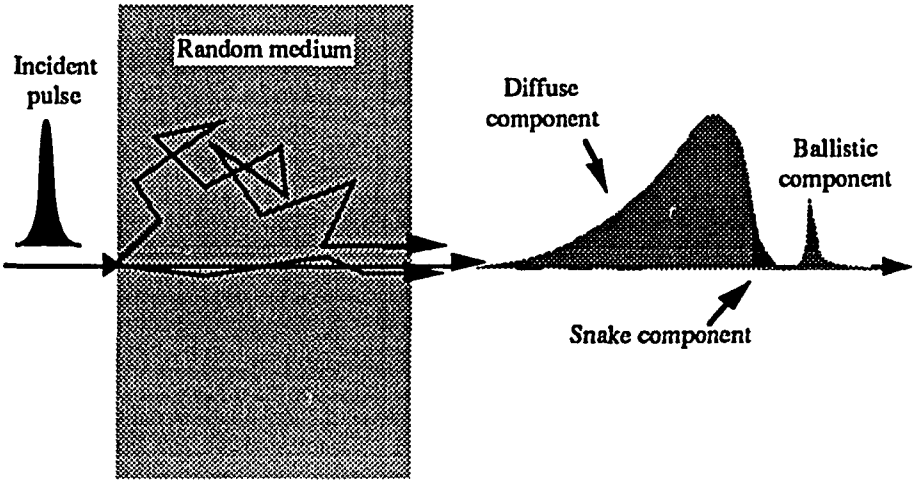

Fig. 6.1 An ultrashort pulse spreads into a ballistic and a diffuse component after propagating through a highly scattering medium. The early portion of the diffuse pulse is known as the snake component.

The intensity of the ballistic component is attenuated exponentially with the thickness of the sample as

$$I_b = I_0 e^{-(l_s^{-1} + l_a^{-1})L} \tag{6.1}$$

where I_b, I_0, l_s, l_a and L are the ballistic component, the incident intensity, the scattering length, the absorption length and the thickness of the scattering medium, respectively. For example, for a 5 cm thick chicken breast tissue sample with l_s= 0.25 mm and l_a= 52 mm the eqn. (6.1) give

$$I_b = I_0 e^{-4.02L} = I_0 e^{-201}$$

This attenuation puts a severe limitation on its practical application, especially for medical imaging in thick tissues. The diffuse component, on the other hand, consists of photons that have been scattered randomly in all directions and have traversed different path lengths. As a result, the diffuse component is temporally broadened and arrives

after the ballistic component. The spatial spreading of these diffuse photons washes out the shadow formed by the ballistic component. The diffuse pulse consists of light undergoing multiple scattering or a random walk in the medium and it contributes noise to the shadow. The temporal profile of a diffuse pulse can be approximated by the diffusion theory when the thickness of the sample is many times larger compared to the transport mean free path of the sample. For a narrow beam of ultrashort laser pulses incident at a point on a slab of scattering medium, the temporal profile of the transmitted pulses at a point on the other side of the slab is given by:

$$I(t) = \frac{D}{\pi w^2} \sum_{m=1}^{\infty} m(\pi w / d)^2 \sin(m\pi w / d) e^{-(Dt(m\pi/d)^2)} e^{-vt/l_a} \qquad (6.2)$$

where $D \approx \frac{vl_t}{3}$ is the diffusion constant, $d=w+1.42l_t$, v is the speed of light in the medium, l_t and l_a are the transport mean free path and the absorption length, respectively. The snake component, consisting of the early arriving photons that have undergone only a few scatterings along quasi-straight line paths (zigzag paths slightly off the straight line path) through the turbid medium, forms the early portion of the diffuse pulse. Since the late arriving photons of the diffuse component traverse along various different paths, the information they carry cannot easily be traced back to any particular path. But, the snake photons, on the other hand, travel slightly off the straight path and, hence, carry information on the optical properties of the medium and any foreign object lying along this path line. Using time-resolved detection techniques, these snake photons can be separated from the diffuse component and can be used to construct the image of the foreign object with different optical properties. These methods have potential use to image bones, tumors, teeth and other types of diseased tissues that differ from its surrounding medium in optical properties (scattering and absorption coefficients).

We have demonstrated for the first time that a 2.5 mm thin fat tissue embedded in a 40 mm thick chicken breast tissue can be located using state-of-the-art ultrafast time-resolved transillumination techniques. This work shows the potential of current ultrafast optical technologies for imaging breast tumors without x-ray radiation.

6.2 Experimental Methods

The schematic diagram of the time-resolved transillumination setup is shown in Fig. 6.2. A colliding pulse modelocked dye laser was used to produce ultrashort laser

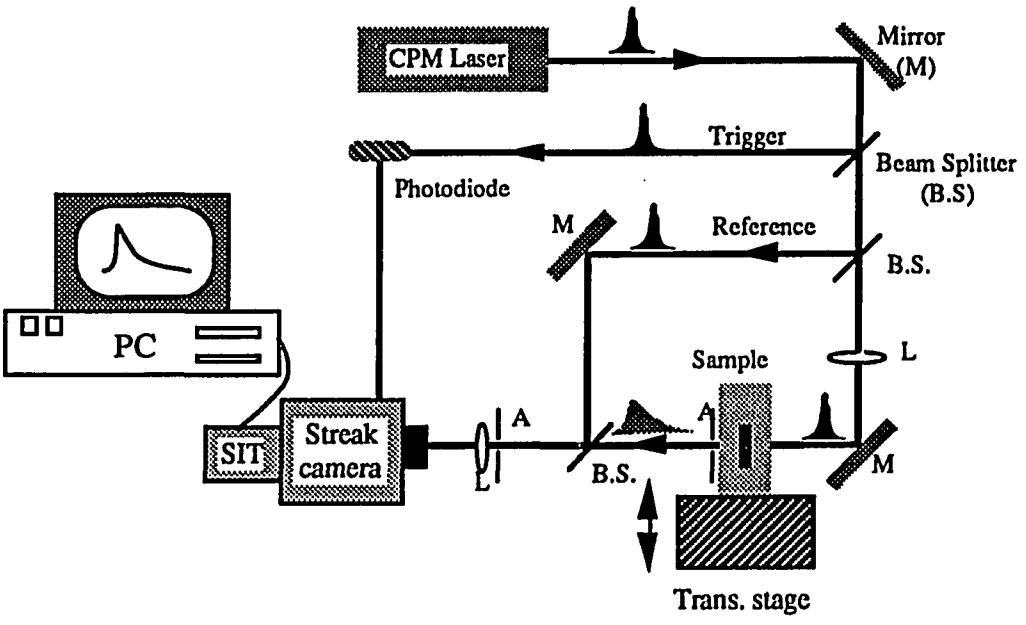

Fig. 6.2 Experimental setup for the detection of snake photons to image translucent objects hidden inside highly scattering random media.

pulses of about 100 fsec at 620 nm. The pulse repetition rate and the power output of this laser beam were 82 MHz and 5 mW, respectively. A part of the incident beam was used to trigger the streak camera using a photodiode. A reference beam was used to obtain the zero time - the time the pulses hit the sample. The beam was focused by a long focal length lens (f = 50 mm) into a small 1 mm diameter spot on the sample. Two

samples of different dimensions were prepared by embedding a thin strip of chicken fat in the middle of a thick, smooth chicken breast tissue. The samples were prepared by sandwiching the thin strip of fat between the two soft pieces of chicken breast tissues. These samples were pressed between two parallel glass plates to keep them uniformly thick. The first sample had a 2 mm thick, 5 mm wide and 40 mm high fat strip embedded in the middle of a 26 mm thick, 70 mm wide and 40 mm high chicken breast tissue. The error in each dimension is about ± 0.5 mm. The sample holder was mounted on a translation stage to let the laser beam scan across the fat strip as displayed in Fig. 6.3.

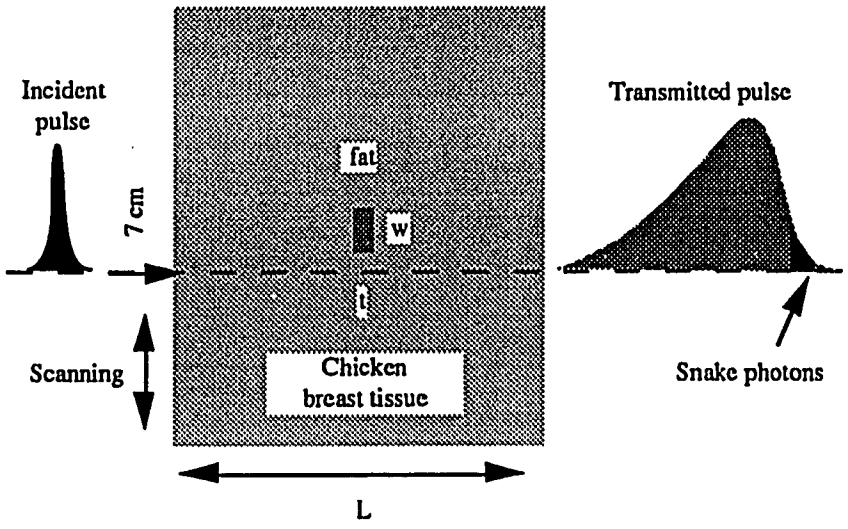

Fig. 6.3 A cross-section of the chicken breast tissue sample in the plane of the scanning with a thin fat strip embedded in it.

The sample was measured at the room temperature and the transmitted signal was detected by a streak camera. Small apertures were used to collect the transmitted photons scattered in the forward direction. These measurements were repeated for the second sample with a 2.5 mm thick, 7 mm wide and 40 mm high strip of fat inside a 40 mm thick, 70 mm wide and 40 mm high chicken breast tissue.

The transport mean free path l_t and the absorption length l_a for the fat and the chicken breast tissues were measured using the pulse transmission technique described earlier. The values for fat and chicken breast tissues are: l_t = 0.58 mm, l_a = 139.3 mm, and l_t = 2.5 mm, l_a = 51.7 mm, respectively.

6.3 Results

In order to locate the thin fat tissue inside the breast tissue, the sample was scanned laterally across the laser beam in 1 mm steps from one side of the fat tissue to the other (in 2 mm steps when scanned farther away from fat). The transmitted pulses were recorded by a synchroscan streak camera for each position. Fig. 6.4 (a) displays two temporal profiles of the transmitted pulses propagating through the 26 mm thick tissue: the dotted curve is for the case when the line of beam incidence passes through the center of the fat strip and the solid curve is when the line passes about 5 mm away from the center of the strip. Note a significant difference in the intensities of the early parts of the two transmitted signals, whereas the later portions merge with each other. This difference at the early part is due to much stronger scattering in the fat tissue compared with that in the chicken breast tissue. Since the absorption length is much larger compared to the transport mean free path in both tissues, the loss of light due to absorption is negligible compared to the loss due to scattering. This pronounced intensity difference in the early portion of the profile suggests the suitability of snake photons in obtaining the maximum contrast for imaging.

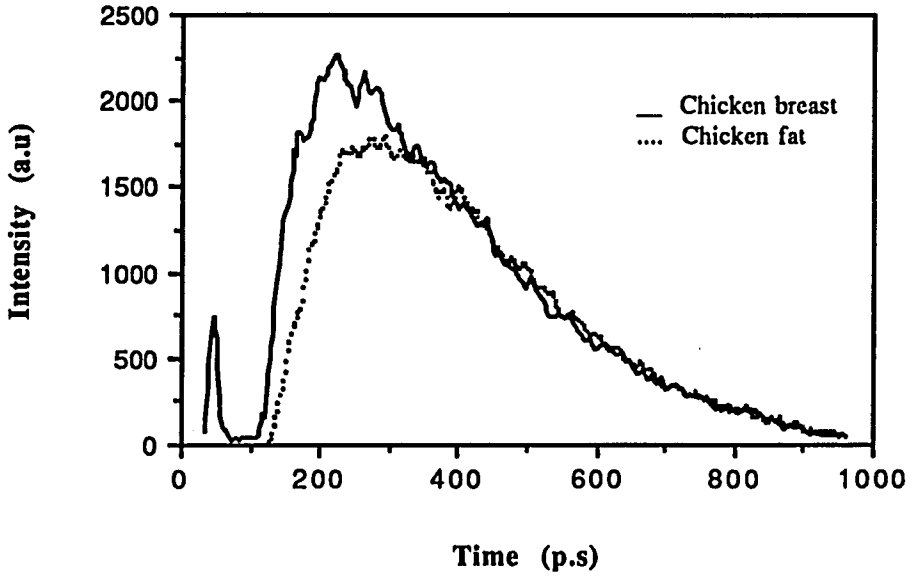

Fig. 6.4 (a) Temporal profiles of two transmitted pulses through the 2.6 cm thick sample: the dotted curve is for incidence through the center of the fat strip, while the solid curve is at a 5 mm distance away from the center.

The schematic diagram in Fig 6.4 (b) shows the advantage of using snake photons for imaging when the laser beam is incident in the line of the fat tissue (point *A*) and away from it (point *B*). The snake photons at point *A* carry information about the scattering and absorption properties of the fat tissue while the snake photons at point *B* do not. Most of the late arriving photons from both points *A* and *B*, on the other hand, do not carry information about the fat tissue. The shorter transport mean free path for fat means light is scattered more in fat than in breast tissue. When the laser beam is incident near the fat tissue a large number of the snake photons are lost due to this higher scattering in fat giving rise to the pronounced difference in the early part as shown in Fig. 6.4 (a). On the other hand, most of the diffuse photons, traveling around the small fat tissue, are not significantly affected by its presence. So, it is the snake photon that is selected to detect the location of the fat inside the breast tissue with maximum contrast.

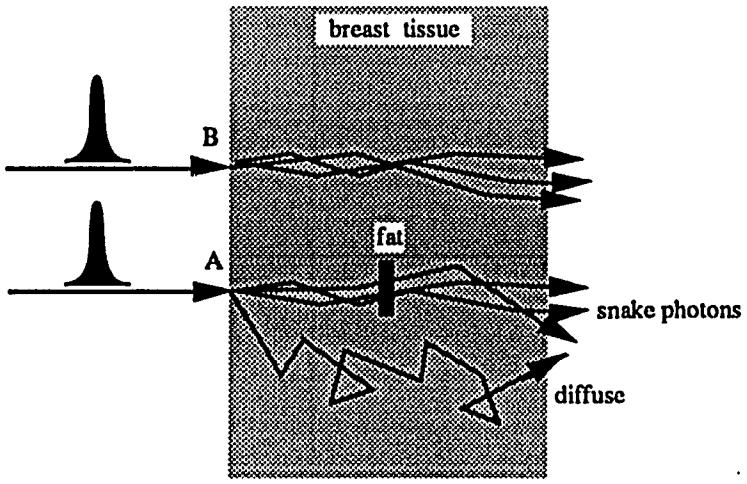

Fig. 6.4(b) Snake photons diagram: the snake photons carry information about the scattering and the absorption properties of the fat tissue when the laser beam is incident at point A, while the snake photons at point B do not carry these information.

The straight line propagation time through a 26 mm thick tissue is about 116 ps. The time-integrated intensities for four different time windows, 220-820ps, 120-967ps, 120-170ps, and 120 -130ps, were calculated from the transmitted signal for various positions of incidence on the sample. The last window captures 10 ps of snake light. The integrated intensity was calculated by summing the transmitted pulse intensity over each time window. The results are plotted in Fig. 6.5. The integrated intensity using the 220-820 ps time-gate (Fig. 6.5a), which collects most of the transmitted pulse except the snake photons, shows almost a straight line without revealing the position of the fat tissue. Fig. 6.5b displays the integrated intensity for the whole signal; and the inclusion of the snake photons, though dominated by the late arriving diffuse photons, reveals a shallow dip around the position of the fat tissue. This case is equivalent to cw transillumination. The 120-170 ps time-gate, which eliminates a significant portion of the diffuse component, displays a dip in the curve at the fat region (Fig. 6.5c). The resolution is significantly improved, with the 120-130 ps time-gate, (Fig. 6.5d) by

eliminating the late arriving photons further. By choosing mostly the snake photons (for 10 ps), not only the location of the fat tissue is correctly predicted, but also the edges of the strip are resolved. The relatively flat bottom of the curve matches well with the width of the fat strip inside the breast tissue with a millimeter resolution.

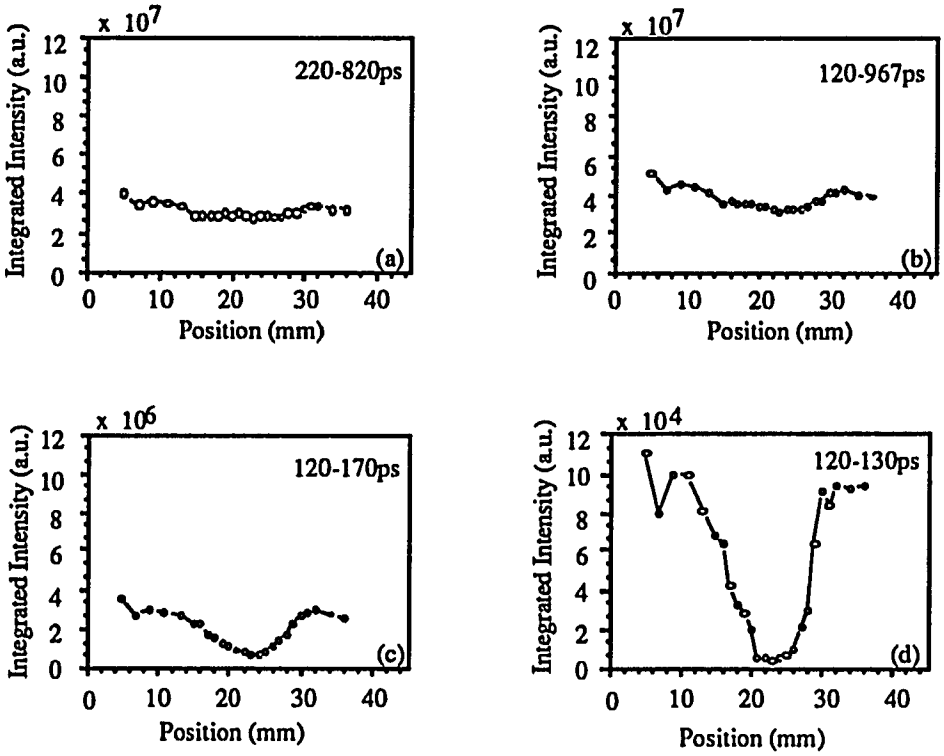

Fig. 6.5 Time integrated intensity from the transmitted signal through a 2.6 cm thick chicken breast tissue at different time gates versus different beam incidence positions. (a) 220-820ps, (b) 120-967ps, (c) 120-170ps, and (d) 120 -130ps

These measurements were repeated on the 4 cm thick sample with a fat strip inside it. The diffuse photons start to arrive at ~ 300 ps. A 20 ps time window (308 - 328 ps) was used at the early part of the diffuse pulse to collect the snake photons. The time-integrated intensity of light within this window versus the different beam incidence positions is displayed in Fig. 6.6. As in the 2.6 cm thick sample, the integrated intensity curve shows a nearly flat line at the region of the fat strip, and it rises almost as a step function once we scan past the edges of the fat strip.

This millimeter spatial resolution of our preliminary work using time-resolved optical technique is not as good as that of x-ray mammography which has been improved over decades of development. This is understandable since the use of time-resolved optical imaging techniques is just beginning.

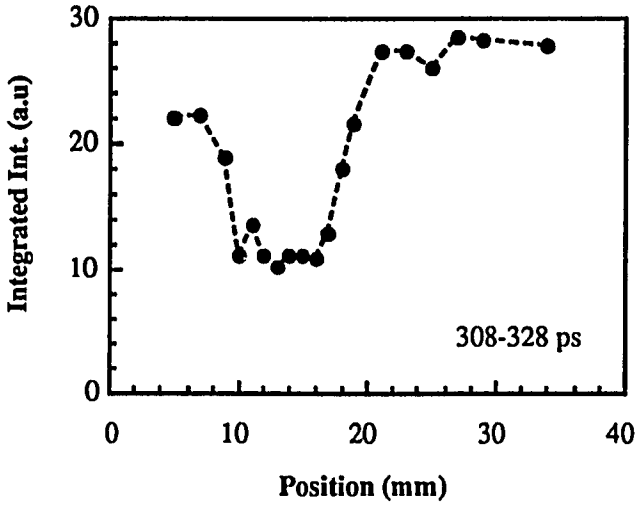

Fig. 6.6 Time integrated intensity from the transmitted signal through a 4 cm thick chicken breast tissue with a 2.5 mm thick fat strip within a 20 ps window (308-328 ps) versus different beam incidence positions.

The use of infrared laser can significantly improve the capability of time-resolved detection through thick tissue. The scattering is much less in the infrared wavelength region as compared to the visible light. Table 4.2 (Chapter 4) gives the value of the transport mean free path of chicken breast tissue as 4.9 mm at 1064 nm compared to 2.5 mm at 625 nm. An Nd-YAG laser was used to produce laser pulses at 1064 nm with a pulse width of about 5 ps. The power output was about 25 mW. A 60 mm thick 70 mm wide chicken breast tissue with a 15 mm wide, 3 mm thick fat strip located in the center was used as our sample. The sample was scanned across the laser beam and time integrated intensities at various time-gates were calculated for each pulse

profile. Fig. 6.7 displays the time integrated intensity curve for the first 100 ps versus the beam positions.

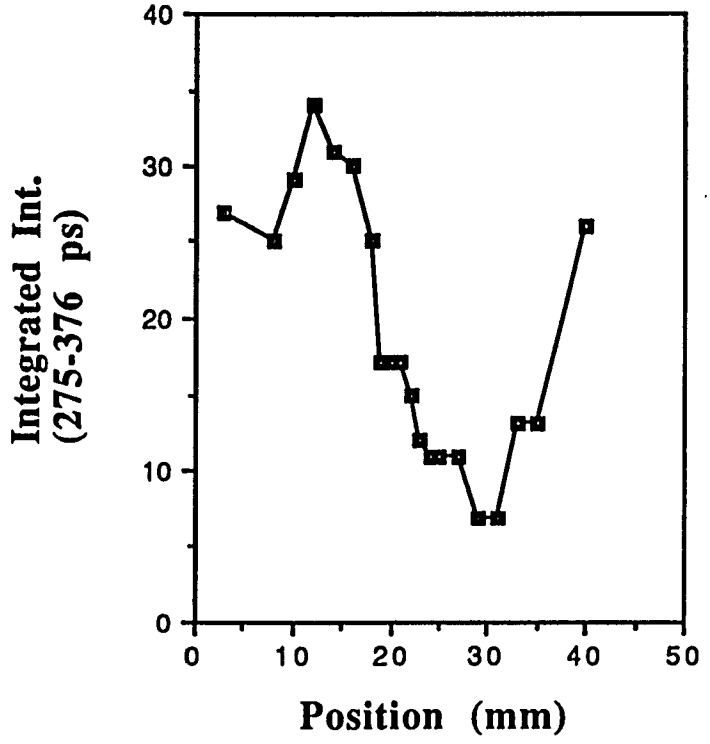

Fig. 6.7 Time-integrated intensity for first 100 ps versus beam positions for 15 mm wide fat strip in the middle of a 6 cm thick chicken breast tissue, at 1064 nm.

The bottom part of the curve shows the position of the fat strip. The slight fluctuation in the valley of the curve (in the position of the fat strip) is most likely due to the uneven thickness of the fat strip.

The lower scattering in tissue in the infrared wavelength region suggests the suitability of ultrafast infrared laser for imaging.

6.4 An Empirical Model for Snake Photon Attenuation

The curves in Fig. 6.4(a) shows an extra intensity attenuation at the early part of the temporal profile. Here we try to develop a simple model that would take into account this extra loss of light due to the hidden object. The ballistic component and the time-resolved diffuse intensity based on the diffusion approximation are given by the expressions given eqn. (6.1 & 2). It has been shown[21] before that the diffusion theory breaks down when the thickness of the sample is less than seven times the transport mean free path. This means that the diffusion theory is not a valid approximation when the photons are not randomized. The snake photons that form the early portion of the transmitted pulse cannot be described by the diffusion theory as they have undergone only a small number of scatterings.

Fig. 6.4(b) gives a pictorial explanation as to why the snake photons will be affected more by the presence of the fat strip than the late arriving photons. The more randomized the photon the more likely it would miss the fat strip, i.e., the later the photons arrive the less likely they will be attenuated by the fat. In other words, the longer the interval between the arrival time of the ballistic and the snake photon $(t-t_b)$ the less probable is the snake photon to encounter the fat strip. To take this extra attenuation of snake photons by the fat strip into account we start with the expression in eqn. (6.2)

$$I_0(t) = \frac{D}{\pi w^2} \sum_{m=1}^{\infty} m(\pi w / d)^2 \sin(m\pi w / d) e^{-(Dt(m\pi/d)^2)} e^{-vt/l_a} \quad .$$

This is the transmitted intensity in the absence of the foreign object. Now based on the discussion in the preceding paragraph we assume the probability P of a photon arriving at time t to encounter the foreign object with a thickness w' to be inversely proportional

to $(t-t_b)$:

$$P = \frac{C}{(t-t_b)} \quad , \tag{6.3}$$

where C is a constant of proportionality with dimensions of time and t_b is the arrival time of the ballistic component. The change in the intensity by an infinitesimal thickness dw' of the foreign object will be

$$dI = -P\frac{I_0}{l^*}dw' = -\frac{C}{(t-t_b)}\frac{I_0}{l^*}dw' \quad , \tag{6.4}$$

where $l^* = (\sigma_{total}^{obj} - \sigma_{total}^{med})^{-1}$ gives the extra attenuation by the object in addition to the attenuation by the surrounding medium.

By integrating the eqn. (6.4) with respect to the object thickness, we get the snake photon intensity as

$$I(t) = \frac{D}{\pi w^2}\sum_{m=1}^{\infty} m(\pi w/d)^2 \sin(m\pi w/d) e^{-(Dt(m\pi/d)^2)} e^{-vt/l_a}\theta(t-t_b)e^{-Cw'/l^*(t-t_b)} \tag{6.5}$$

where w' is the thickness of the hidden object (w is the thickness of the medium). This additional exponential term gives the extra attenuation of the snake photons and this attenuation becomes smaller and smaller as the arrival time increases. Fig. 6.8 displays two temporal profiles simulated using this equation with C equal to 0.5 ps for the two positions of A and B as shown in Fig. 6.4(b) for w'/w = 0.8 (fat thickness = 2 mm). These two curves were simulated for the 2.6 cm chicken breast sample with 2 mm fat strip embedded in the middle. The dotted curve shows the additional attenuation of the snake light. These curves show a good qualitative match with the curves in Fig. 6.4(a). Figure 6.9 (a) and (b) display two curves with w'/w = 0.01 (fat thickness 0.26 mm)

and 0.05 (fat thickness 1.3 mm) respectively. These two figures show the limitation in detecting the snake photons. In the 0.26 mm fat case the two curves overlap, while the small difference in the 1.3 mm fat case can still be detected.

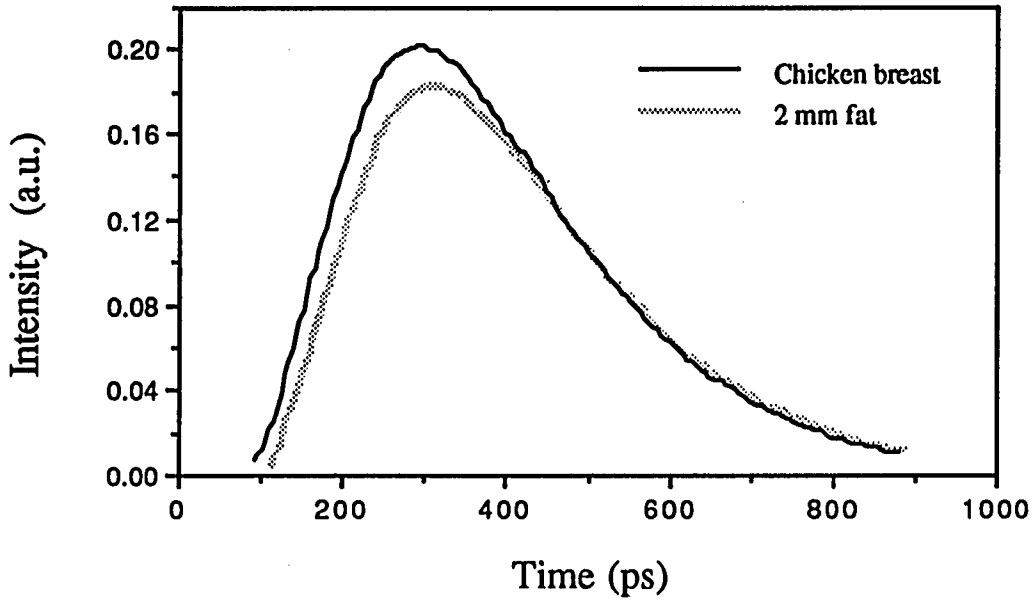

Fig. 6.8 Two temporal profiles simulated using this equation with C equal to 0.5 ps for the two positions of A and B as shown in Fig. 6.4(b) for $w'/w = 0.8$

To see how the resolution of this time-gated imaging technique deteriorates with thinner fat strips, integrated intensities ($I_{0.01}$, $I_{0.05}$ and $I_{0.08}$) for a 12 ps time gate were calculated for the above three cases of $w'/w = 0.01$, 0.05 and 0.08, and for the case without any fat strip (I_{breast}). The difference between the integrated intensities with fat and without fat was calculated for the three cases. This snake photon difference is plotted against the fat-breast thickness ratio w'/w in Figure 6.10. It shows that the snake photon intensity difference reduces sharply as we go to the 0.26 mm fat strip case. Since this snake photon intensity difference is used to locate a hidden object as in Fig. 6.6, the sharp reduction of it for $w'/w \leq 0.01$ puts a limit on our ability to detect

fat tissues thinner than 0.3 mm inside a 4 cm thick breast tissue. With more stable lasers in the IR region (e.g. Forsterite or Ti:sapphire laser), CCDs and 1 ps streak cameras this snake intensity difference can be further enhanced, and that should give better temporal and spatial resolution.

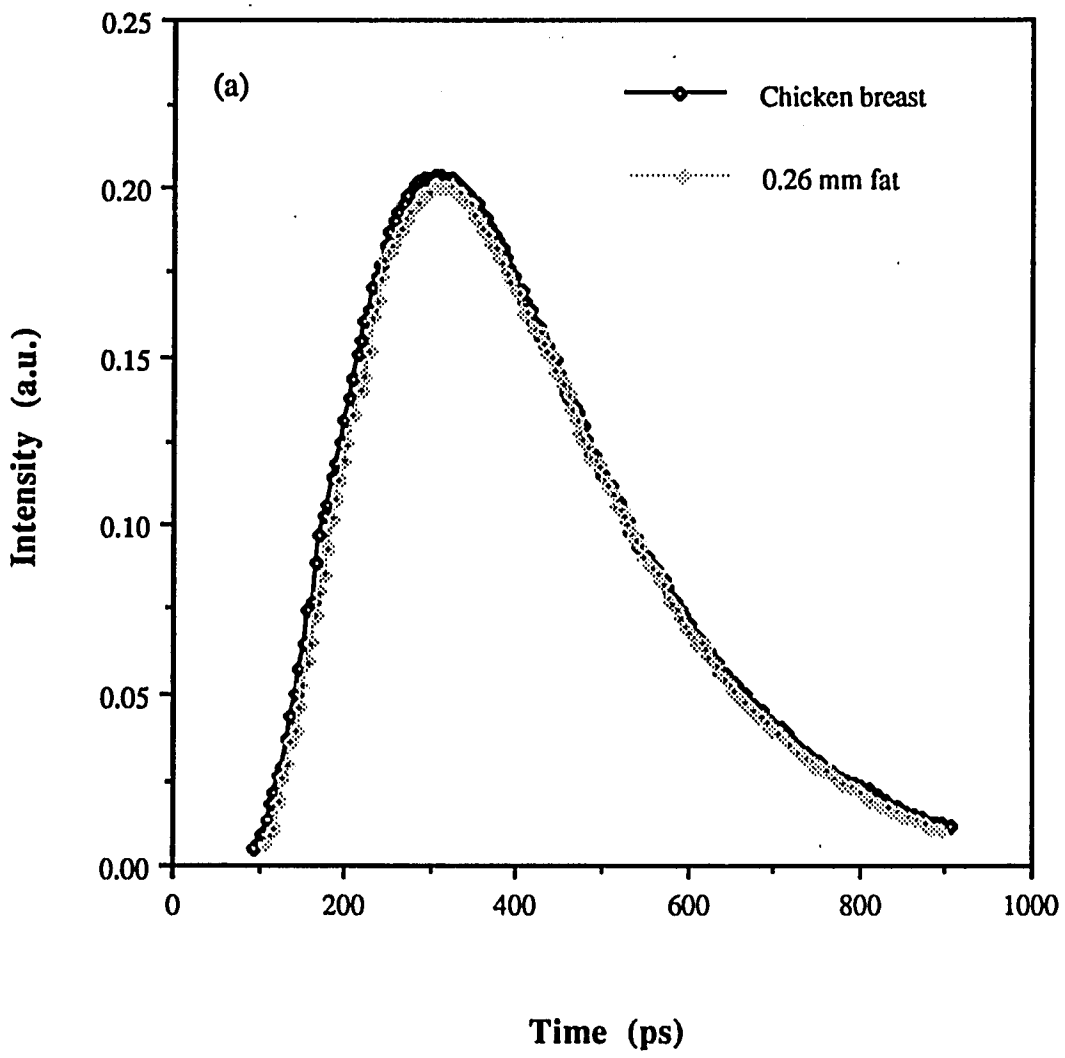

Figure 6.9 (a) The transmitted pulse profiles with $w'/w = 0.01$.

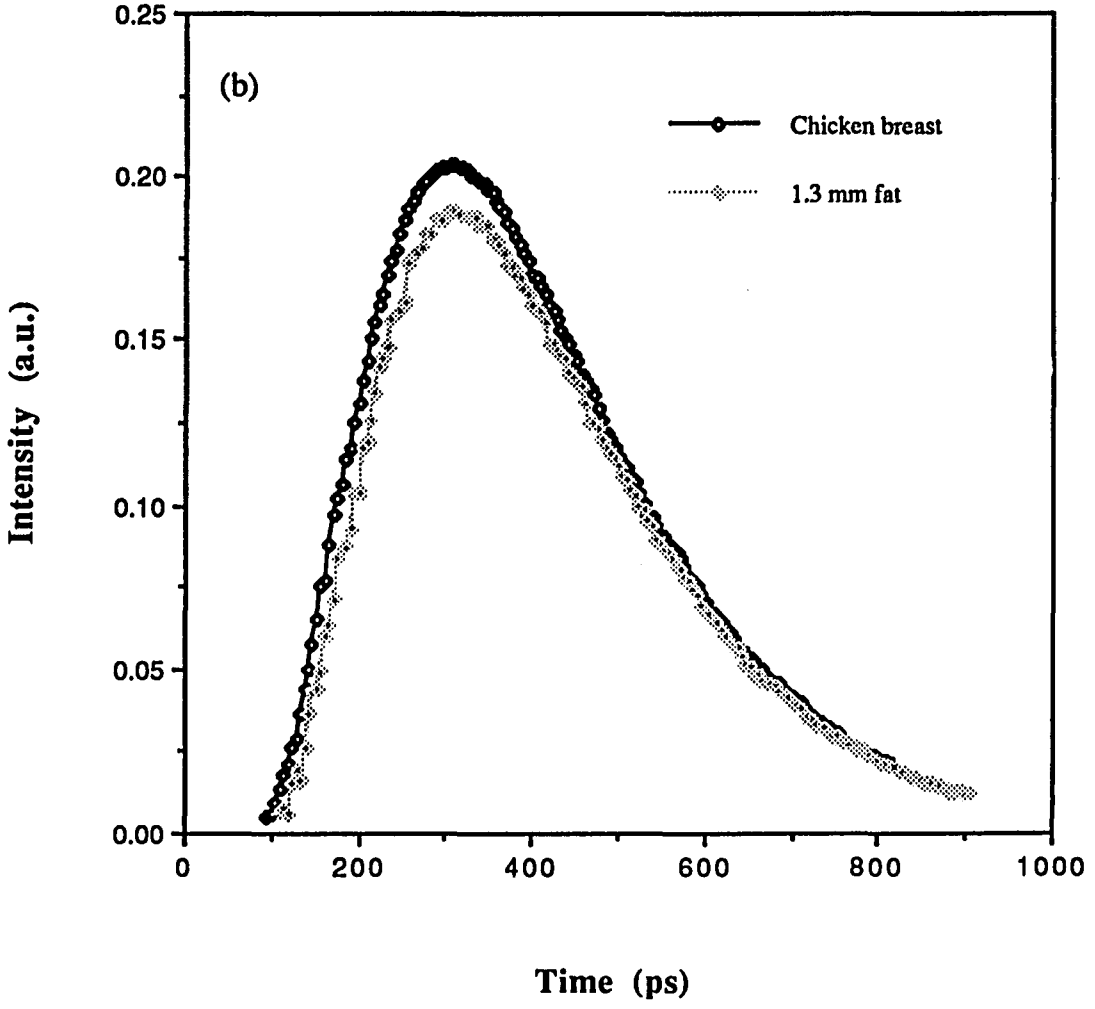

Figure 6.9 (b) The transmitted pulse profiles with w'/w = 0.05.

6.5 Conclusion

Ultrafast time-resolved optical measurements were performed to image (one-dim) a thin strip of one type of tissue inside another which is analogous to the case of a tumor in a breast. We have demonstrated that a 2.5 mm thin chicken fat strip can be detected inside a 40 mm thick chicken breast tissue using 625 nm light. We have further shown that imaging in the IR region can significantly improve the snake photon detection in thick tissues. We have also shown that the resolution of this method is limited for detecting smaller hidden objects with $w'/w \leq 0.01$. This can be improved with more stable lasers and better detection systems.

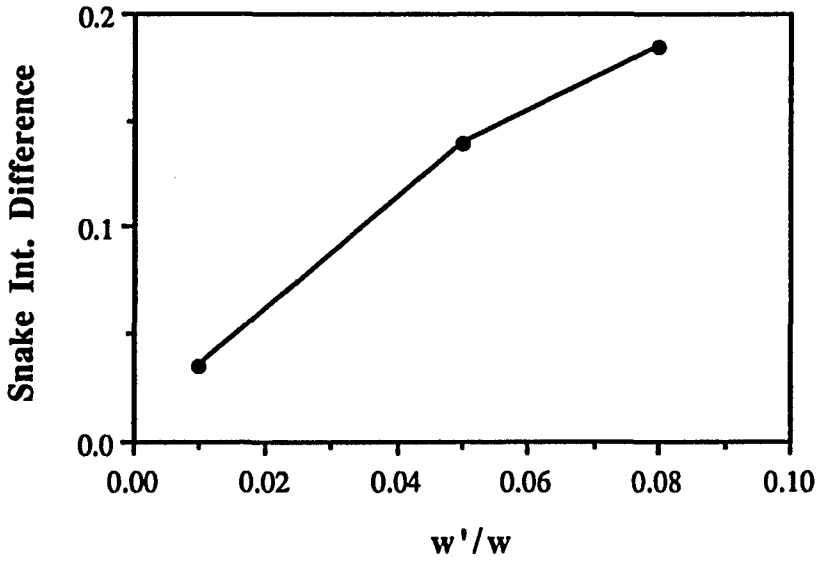

Fig. 6.10 The difference in the integrated intensity for a 12 ps time gate is plotted against the fat-breast thickness ratio (w'/w).

This work may be extended by using a two-dimensional array of fibers to obtain a two-dimensional image of the tumor. With suitable improvements in optical devices this novel method may lead in the near future to a high spatial resolution, non invasive and non ionizing technique for detecting malignant tumors in breast.

We have also developed a simple model to describe the effect of small objects embedded inside a highly scattering medium on the attenuation of snake photons.

6.6 References

1. M. Cutler, "Transillumination as an aid in the diagnosis of breast lesions," *Surg. Gynecol. Obstet*, Vol. 48, 721, 1929

2. Watmough, D. J. ; Radiology **147**, 89-92 (1983)

3. Navarro, G. A. and Profio, A. E. ; Med. Phys. **15**, 181 (1988)

4. Lafrenuere, R. ; Ashkar, F. S. ; and Ketcham, A. S. ; The American Surgeon **52**, 123 (1986)

5. Sickles, E. A. ; Recent results in Cancer Research 105, Springer-Verlag, Berlin, Heisdelberg, p 31 (1987)

6. Wang, L. ; Ho, P. P. ; Liu, C. ; Zhang, G. ; and Alfano, R. R. ; Science **253**, 769-771 (1991)

7. Chen, H. ; Chen, Y. ; Dilworth, D. ; Leith, E. ; Lopez, J. ; and Valdmanis, J. ; Opt. Lett. **16**, 487-489 (1991)

8. Leith, E. N.; Chen, C.; Chen, H.; Chen, Y.; Lopez, J.; and Sun, P. C.; Opt. Lett., **16**, 1820-1822 (1991)

9. Duncan, M. D. ; Mahon, R. ; Tankersley, L. L. ; and Reintjes, J. ; Opt. Lett. **16**, 1868-1870, (1991)

10. Yoo, K. M. ; Xing, Q. ; and Alfano, R. R. ; Opt. Lett. **16**, 1019-1021 (1991)

11. Anderson-Engels, S. ; Berg, R. ; Svanberg, S. ; and Jarlman, O. ; Opt. Lett. **15**, 1179-1181 (1990)

12. Hebden, J. C. ; Kruger, R. A. ; and Wong, K. S. ; Appl. Opt. **30**, 788-794 (1991)

13. K. M. Yoo, B. B. Das, and R. R. Alfano, "Imaging a translucent object hidden in a highly scattering medium from the early portion of the diffuse component of the transmitted ultrafast laser pulse," Opt. Lett. 17, 958 (1992)

14. K. M. Yoo, Feng Liu, B. B. Das and R. R. Alfano,"Ultrashort laser pulse propagation and imaging through biological and random media," Medical Optical Tomography, Ed. G. Muller, in press.

15 B. B. Das, K. M. Yoo and R. R. Alfano,"Ultrafast Time-gated Detection Of Translucent Objects Hidden In Biological And Highly Scattering Random Media," proceedings *SPIE* in press, 1993.

16. K. M. Yoo, B. B. Das, F. Liu, Q. Xing, and R. R. Alfano, "Femtosecond time-gating imaging of translucent objects hidden in highly scattering media," *Ultrafast Phenomena* VIII, Eds. A. Migus, F. Martin, G. A. Mourou, and A. H. Zewail, Springer-Verlag Berlin, Heidelberg, (1992)

17. K. M. Yoo, B. B. Das, Feng Liu, Qirong Xing, and R. R. Alfano, "Imaging of Translucent Objects Hidden in Highly Scattering Media Using Ultrafast Laser Technology," In the Proceedings of 5th Asia Pacific Physics Conference, Malaysia (1992)

18. B. B. Das, K. M. Yoo and R. R. Alfano, "Ultrafast Time-gated Imaging In Thick Tissues - A Step Towards Optical Mammography," Opt. Lett., Vol. 18, No. 13, p.1092-1094, 1993

19. Yoo, K. M. ; and Alfano, R. R. ; Opt. Lett. **15**, 320-322 (1990)

20. Liu, F. ; Yoo, K. M. ; and Alfano, R. R. ; Opt. Lett. **16**, 351-353 (1991)

21. Yoo, K. M. ; Liu, F. ; and Alfano, R. R. ; *Phys. Rev. Lett.* **64**, 2647 (1990)

CHAPTER 7

Summary

In this chapter I summarize my work in optical spectroscopy, light scattering and ultrafast time gated imaging in biomedical and model random media. I have shown that U-V fluorescence spectroscopy and time resolved light scattering offer novel approaches to study the optical characteristics of biomedical media.

First it was shown that visible excitation at 488 nm probing the flavin molecules was unable to distinguish malignancy from benign tissue environment. That led to a study of native tissue fluorescence in the uv region to probe highly abundant fluorophores such as tryptophan, collagen, elastin, NADH.

Excitation at 300 nm was found to be highly efficient in distinguishing human malignant breast tissue from normal and benign tissues. Taking the ratio of fluorescence intensities at 340 nm to 440 nm to eliminate the effect of absorption due to blood was a key step to achieve this separation. The fluorophores tryptophan and NADH are suggested to be the markers of malignancy.

Fluorescence in a tissue is not only affected by its reabsorption due to blood but also by the light scattering in the medium. To find the effect of scattering on the fluorescence yield, optical density (OD) measurements were performed on thin breast tissues and latex bead suspensions in water.

The OD of thin breast tissues without blood were found to be relatively constant over the visible spectrum. This observation indicates that light is effectively scattered in breast tissues by scatterers of size much larger than the wavelength of light. These scatterers in the tissues are most likely the cells that have sizes between 10 to 20 microns. The scattering cross section of a large cell or scatterer is not very sensitive to

the variations of light wavelength if the size of the particle is much larger than the light wavelength. This conclusion is confirmed from independent experimental data using model discrete random media (latex beads) of various scatterer sizes. Scatterers of sizes comparable or smaller than the light wavelength show a large variation of OD or the scattering cross section as the wavelength is varied over the optical spectrum. No variation of OD is observed when the scatterer is much larger than the wavelength of light. This simple extinction measurement provides very useful information as to the scattering and the absorption cross-sections of breast tissues.

We also come to the conclusion that the fluorescence intensity difference at 340 and 440 nm in the previously discussed cancer diagnostic method is not due to any loss by scattering but because of the difference in the intrinsic fluorescence yield in malignant and non-malignant samples.

We have measured the transport mean free paths and the absorption lengths for various tissues and model random media. We found that the scattering coefficients of chicken and human breast tissues remain relatively constant in 570 - 630 nm wavelength region while they change significantly for 1064 nm. The optical parameters of milk were found to be inversely proportional to the concentration in water. Chicken breast and fat tissues can be used as good models for human breast tissues as the optical parameters of the two tissue types are about the same. The less scattering observed at 1064 nm makes tissues more transparent in the IR region making it easier to image in thick tissues as in a real breast.

Our measurements in time-resolved backscattering show that the scattering and the absorption parameters of a random medium can be obtained accurately from time-resolved back scattering in the two-fiber configuration as long as the radial distance is more than about seven times the transport mean free path of the sample. The values obtained this way agree with the values obtained from previously known accurate

method of time-resolved pulse transmission. The single point source-detection technique provides a tool to diagnose breast malignancy though it fails to give accurate values of the optical parameters of tissues. This failure is attributed to the invalidity of the diffusion approximation in this experimental configuration.

Ultrafast time-resolved optical measurements were performed to image (one-dim) one type of tissue inside another which is analogous to the case of a tumor in a breast. We have demonstrated that a 2.5 mm thin chicken fat strip can be detected inside a 40 mm thick chicken breast tissue using 625 nm light. We have further shown that imaging in the NIR region can significantly improve the snake photon detection in thick tissues.

This work may be extended by using a two-dimensional array of fibers to obtain a two-dimensional image of the tumor. With suitable improvements in optical devices this novel method may lead in the near future to a high spatial resolution, noninvasive and nonionizing technique for detecting malignant tumors in breast.

We have also developed a mathematical model to describe the effect of small objects embedded inside a highly scattering medium on the attenuation of snake photons. The resolution of this method was tested by calculating the snake photons for a 12 ps time-gate for various values of thicknesses of the fat strip with respect to the thickness of the medium (w'/w = 0.08, 0.05 and 0.01).

CHAPTER 8

Future Experiments

The various results reported in this thesis require further investigation. More experiments in steady-state and time-resolved fluorescence should be carried out on various tissue components and model fluorophores in order to determine the exact cause of fluorescence ratio difference at 340 and 440 nm when excited at 300 nm. The change in NADH+ and NADH concentration with malignancy should be investigated in breast tissues.

Time-resolved transmission and back-scattering experiments should be conducted on various animal and human tissues to determine their optical properties which is essential to develop an optical mammographic system. It must be done at various wavelength ranges to find suitable regions for imaging. The wavelength range of immediate interest should be the NIR region (from 1 to 1.5 μm) which shows less scattering and the unset of absorption by water.

Our measurements in the single point backscattering configuration shows the inaccuracy of the theoretical model used based on the diffusion approximation. The failure of diffusion approximation to describe the behavior of the photons scattered immediately back from the neighborhood of the point of incidence requires to develop a modified theoretical model to describe the properties of these photons. This theoretical model must be verified with experimental results conducted on various samples with different scattering and absorption properties and at different wavelengths and scatterer sizes.

More experiments must be done in the infrared region to study the behavior of the snake photons to check the validity of the empirical model described before in this

wavelength region. The imaging experiments should be performed with more stable lasers like Cr:forsterite or Ti:sapphire lasers with 1 ps streak cameras and CCDs to improve the temporal as well as the spatial resolution.

Appendix I

This program calculates the mean cosine of the scatteringangle, and scattering cross-sections using Mie theory. This program was written by Dr. P. Hu.

```
#ifndef lint
#static char sccsid[] = "@(#)cosca.r 1.3.1.1 93/06/04";
#endif
#       this program computes total Mie scattering cross-section
#       and momentum-transfer cross-section.
#
complex*16 aa1,aa2,bb1,bb2,tt1,tt2,fors1,fors2,ex1
real*8aout,ra2,ra1,rfn1,rfn2,q1,q2,dex1,dex2,dex,s,s1,s2,pom,tw1,tw2,twav
#real*8ra,rfn1,q
integer ndim,ndim1,ii
print*,"ra=radius(mm),rfn1(>1),index in outside medium."
read*,ra2,rfn1,aout
print*,"starting and finishing wavelength in vacuum"
read*,tw1,tw2
#ra1=ra2/twav
tt2=(0,1)
write(22,*)"index=",rfn1
write(22,*)"outside index=",aout,"radius=",ra2
pom=0.
        do ii=1,201 {
twav=tw1+float(ii-1)*(tw2-tw1)/200.
ra1=ra2/twav*aout
ndim=int(ra1*2*3.14159+1.)
if (ndim.gt.5) {ndim=ndim+10
        }
        else {
        ndim=2*ndim+2
        }
```

```
call coout(ra1,rfn1,ndim,aa1,bb1,tt1,fors1,q1,ex1,s2)
dex1=dreal(tt1)*2./q1**2 ### total from amplitudes
s=real(ex1)*4./q1**2 ### momentum transferred
s1=s2*2./q1**2        ###total, sum directly
dex2=s/dex1 #         cos(theta) average
write(1,*)"momentum transferred=",s,s1,dex1
#dex=dex1-s
#dex=(dex1-s)*3.141592654*ra2**2
#write(1,*)dex2
#write(2,*)q1,dex1,s,dex2,dex
write(3,111)twav,q1,ndim,s,dex1,dex2
111    format(1f10.4,1x,1f10.4,1x,1i5.2,1x,3e12.5)
#write(11,*)twav,dex1
dex=dex1*ra2**2*3.14159
#dex=1./dex1
#write(22,*)twav,dex          #lambda vs. Sigma(s)
#write(11,*)twav,dex          #.. .vs. 1/Qs

                }
        stop
        end



#ifndef lint
#static char sccsid[] = "%Z%%M% %I% %E%";
#endif
#calculates the scattering intensity at different angle
#(output: j ( angle between 1-179 degree )
#       int1(j) and int2(j)
#
#       ----------------------------------------
#       ----------------------------------------
#       changed to do total scattering and momentum
```

```
#       transfered cross-section
#       ----------------------------------------
#       output:         for ref. see van de Hulst. Page 127-128.

#       exsca:          the momentum transferred cross-section(complex);
#       extin:  total scattering cross-section
#       tt:     forward scattering amplitude
#       ----------------------------------------
subroutine coout(ra,rfn1,ndim,aa,bb,tt,fors,q,exsca,extin)
complex*16 a(500),b(500),aa,bb,tt,cc,fors,exsca
real*8ra,rfn1,q,extin,fj  ###,xabs
integer ndim,j
q = 2*3.14159265358979*ra
call coef(a,b,ra,rfn1,ndim+1)
#call intensity(int1,int2,a,b,ndim)
cc=(0,1)
aa=(0.,0.)
bb=(0.,0.)
exsca=(0.,0.)
extin=0.
do j = 1,ndim {
fj=float(j)
aa=aa+a(j)*(2.*float(j)+1.)
bb=bb+b(j)*(2.*float(j)+1.)

#compute the total scattering cross-section
extin=extin+(xabs(a(j))+xabs(b(j)))*(2.*float(j)+1.)

#compute the momentum transferred cross-section
exsca=exsca+fj*(fj+2.)/(fj+1.)*(a(j)*conjg(a(j+1))+b(j)*conjg(b(j+1)))
+(2.*fj+1.)/fj/(fj+1.)*a(j)*conjg(b(j))
write(9,*)exsca,extin
#       if (ndim .lt.5) {
        write(8,*)j,a(j),b(j)
#       }
```

```
}
        tt=aa+bb
        write(1,*)"q=",q
#               write(1,*)"tt=",tt
#
#               write(1,*)"aa=",aa
#               write(1,*)"bb=",bb
#       ----------------------------
#       ----------------------------


#scattering amplitude
fors=tt/2./q
        write(1,*)"fors=",fors
return
end



subroutine intensity(int1,int2,a,b,ndim)
# This subroutine calculates the intensity of the
# scattered light for different polarization
# input :
#  ndim:  the dimension of the coefficients a and b
#   a :  the coefficient of different partial waves
#        a(ndim)
#   b :  the coefficient of different partial waves
#        b(ndim)
# return:
#  int1 :  the intensity scattered light with polarization 1,
#        int1(180) for different angle.
#  int2 :  the intensity scattered light with polarization 2
#        int2(180) for different angle.
real*8int1(180),int2(180),pix(500),taox(500),theta,dtheta,xtheta,c1,c2,cc#,#####xabs
complex*16a(500),b(500),s1,s2
```

```
integer ndim,j,jj
theta = 0
dtheta = 3.14159265358979/180
do jj = 1,179 {
        theta = theta+dtheta
        xtheta = dcos(theta) #cos(theta)
        call pitao(pix,taox,xtheta,ndim) # calculates pi(x),tao(x),see
                                         # Kerker's book
        s1 = (0,0)
        s2 = (0,0)
        do j = 1,ndim {
                c1 = float(2*j+1)
                c2 = float(j*(j+1))
                cc = c1/c2
                s1 = cc*(a(j)*pix(j)+b(j)*taox(j))+s1
                s2 = cc*(a(j)*taox(j)+b(j)*pix(j))+s2
                }
        int1(jj) = xabs(s1)
        int2(jj) = xabs(s2)
        }
return
end



subroutine pitao(pix,taox,x,ndim)
# this subroutine calculates pi(x),tao(x) for diffrent partial
# wave index l upto ndim
#input:
#  x  : cos( theta ) , real
# ndim: integer
#return:
# pix  : real pix(ndim)
# taox  : real taox(ndim)
real*8pix(500),taox(500),plg(500),plgd(500),c,x
```

```
integer ndim,n
call plgf(plg,plgd,x,ndim)# calculates the Legender polynomials
do n = 1,ndim {
        c = dsqrt(1.-x*x)
        pix(n) = plg(n)/c
        taox(n) = -plgd(n)/c
        }
return
end



subroutine plgf(plg,plgd,x,ndim)
#    this program calculates the p1(j) the associated legendre
#    function and its derivative
real*8plg(500),plgd(500),x
integer ndim,j
#    calculate first order associated legendre function
plg(1) = dsqrt(1.-x*x)
plg(2) = 3.*plg(1)*x
do j = 3,ndim+1
        plg(j) = (x*(2*j-1)*plg(j-1)-j*plg(j-2))/(j-1)
#    calculate derivative of ledendre function
#     plgd(j)=[plgd(j)]'*(sin(theta)**2)
do j = 1,ndim
        plgd(j) = -(j*plg(j+1)-(j+1)*plg(j)*x)
return
end



real function xabs(x)
#this function calculates the sqare of the absolute value for
#a double precision complex value
real*8xabs
```

```
complex*16x
xabs = dreal(x)**2+dimag(x)**2
return
end



subroutine coef(a,b,ra,rf1,ndim)
#calculates the coefficients a and b for a shelled sphere scatterer
#input:
# ra  : inner radius / wave-length
# rf1 : refraction index in the core
# ndim: dimension of the coefficients of a and b
#return:
# a   : coefficients [see Kerker's book], a(ndim)
# b   : coefficients [see Kerker's book], b(ndim)
real*8psi1a(500),psi2a(500),psi1ad(500),psi2ad(500),kapa1a(500),kapa2a(
  500),kapa1ad(500),kapa2ad(500),topi,pi,qa,ra,zm1,rf1,
  z1a,ua1,ub1
complex*16xi1a(500),xi2a(500),xi1ad(500),xi2ad(500),a(500),b(500),da1,db1

integer ndim,n
pi = 3.14159265358979
topi = 2.*pi
qa = topi*ra
zm1 = rf1
z1a = zm1*qa
call bessfunr(psi2a,kapa2a,xi2a,psi2ad,kapa2ad,xi2ad,z1a,ndim)
#functions at n*q
call bessfunr(psi1a,kapa1a,xi1a,psi1ad,kapa1ad,xi1ad,qa,ndim)
#functions at q
do n = 1,ndim {
#     calculate the coefficient a(n), kerker's book
#      formulas 5.1.29,5.1.31,5.1.33
#
```

```
          ua1 = zm1*psi2a(n)*psi1ad(n)-psi2ad(n)*psi1a(n)
          da1 = -psi2ad(n)*xi1a(n)+zm1*psi2a(n)*xi1ad(n)
          a(n)=ua1/da1
#         print*,'n,ua1,ua2,ua3,ua4,da1,da2,da3,da4'
#         print*,n,ua1,ua2,ua3,ua4,da1,da2,da3,da4,a(n)
#
#     calculate the coefficient b(n), kerker's book
#       formulas 5.1.30,5.1.32,5.1.34
#
          ub1 = -psi2a(n)*psi1ad(n)+zm1*psi2ad(n)*psi1a(n)
          db1 = zm1*psi2ad(n)*xi1a(n)-psi2a(n)*xi1ad(n)
          b(n)=ub1/db1
          }
return
end



subroutine bessfunr(psi,kapa,xi,psid,kapad,xid,x,ndim)
#input:
#  x : real
# ndim: integer
#return:
#psi   : real psi(500)
#psid  : real psid(500), derivative of psi
#kapa  : real kapa(500)
#kapad : real dapad(500), derivative of kapa
#xi    : complex xi (500)
#xid   : complex xid(500) , derivative of xi
#the difinations of the variables psi,kapa,xi can be found in
#                Kerker's book.
complex*16xi(500),xid(500),ci
real*8psi(500),kapa(500),psid(500),kapad(500),bsj(0:500),bsy(0:500),x
integer l,ndim
call bessj(bsj,x,ndim+1)
```

```
call bessy(bsy,x,ndim+1)
ci = (0,1)
do l = 1,ndim {
        psi(l) = x*bsj(l)
        kapa(l) = -x*bsy(l)
        psid(l) = x/(2*l+1)*((l+1)*bsj(l-1)-l*bsj(l+1))
        kapad(l) = -(x/(2*l+1)*((l+1)*bsy(l-1)-l*bsy(l+1)))
        xi(l) = psi(l)-ci*kapa(l)          #need to
        xid(l) = psid(l)-ci*kapad(l)       #check the sign,
                                           #       should be + ?
        }
return
end



subroutine bessj(bsj,x,ndim)
#   the subroutine bessj calculate the spherical
#       bessel function which is j[n](x) and has the relation to the
#       regular bessel function as
#     j[n](x) = sqrt(pi/(2x))j[n+1/2](x)
real*8bsj(0:500),sum,bjp,bj,bjm,bigno,bigni,bessjs,x,tox
integer iacc,n,ndim,m,i,j
parameter(iacc = 400,bigno = 1.e10,bigni = 1.e-10)
tox = 2./x
n = ndim+1
m = 2*((n+int(sqrt(float(iacc*n))))/2)
sum = 0.
bjp = 0.
bj = .0001
do j = m,1,-1 {
        bjm = (.5+j)*tox*bj-bjp
        bjp = bj
        bj = bjm
        if (j<=n)
```

```
                bsj(j) = bjp
            if (abs(bj)>bigno)
              {
              bj = bj*bigni
              bjp = bjp*bigni
              bessjs = bessjs*bigni
              sum = sum*bigni*bigni
              do i = 0,n
                    bsj(i) = bsj(i)*bigni
            }
            sum = sum+(2*j-1)*bj*bj
            }
sum = dsqrt(sum)
do j = 0,n
          bsj(j) = bsj(j)/sum
bsj(0) = dsin(x)/x
return
end


subroutine bessy(bsy,x,ndim)
#   the bessy calculate the spherical
#       bessel function which is y[n](x) and has the relation to the
#       regular bessel function as
#      y[n](x) = sqrt(pi/(2x))y[n+1/2](x)
real*8bsy(0:500),x,tox
integer ndim,n,j
tox = 2./x
n = ndim+1
bsy(0) = -dcos(x)/x
bsy(1) = -dcos(x)/(x*x)-dsin(x)/x
do j = 2,n
          bsy(j) = (j-.5)*tox*bsy(j-1)-bsy(j-2)
return
end
```

Appendix II

Program to obtain transfer mean free path and absorption length of a scattering medium by fitting transmitted pulse profiles. This program was written by Prof. Feng Liu.

```
#ifndef lint
#static char sccsid[] = "@(#)fit2.r 1.3 92/11/26";
#endif
#       Program fit2.r
#       date 11-30-91,
#       for diffusion eq. fit
#       must be linked with taurosv.f
#
#       for infinite slab, point to point source
#       ----------------------------------
#       must be linked with function subroutine
#       sublaxpl4.r, and taurosv.f
#       ----------------------------------
#
        subroutine fcn(npar, g,f,x,iflag)
        implicit double precision ( a-h, o-z)
        character * 12 anam, outfile
        character * 60 comfle,comfle1
        real*8  y(1024), z(1024), w(1024), x(6), c(1024)
        go to (10,60,60,60,120) iflag
 10     print *, "enter infile"
        read  *, anam
        open(1,file=anam)
        print *, "enter outfile"
        read *, outfile
        open(8,file=outfile)
        print *, "index, and pinhole diameter(um)"
        read*, dex,pdia
```

```
      print*, "thickness (um)"
      read*, wd
      ymax=0.
      yto=0.
      #read(1,*)comfle,comfle1
      print *, "yes"
      #read(1,*)ddjunk, ddjunk1
      do i=1,1024 {
      read (1,*,end=222)w(i), c(i)
      y(i) = c(i)
      if (y(i).gt.ymax) {ymax=y(i)
      }
#     #if (y(i).lt.0)y(i)=0.
      }
222   n=i-1
      nn=n-1
      do m=1,nn {
      yto=yto+(y(m)+y(m+1))*(w(m+1)-w(m))/2.
      }
#     write(6,*)"area=",yto
60    f=0.0
      zmax=0.
      zto=0.
      do i=1,n {
      call gg(w(i),x(1),x(2),wd,dex,pdia,z(i))
      if(z(i).gt.zmax) {zmax=z(i)
      }
      if(z(i).lt.0) z(i)=abs(z(i))
}
      do i=1,n {
      z(i)=z(i)/zmax*ymax*x(3)     #equal total intensity
      #f=f+(z(i)-y(i))*(z(i)-y(i))/sqrt(y(i)*y(i))
      f=f+(z(i)-y(i))*(z(i)-y(i))
}
      if (iflag.ne.3) return
```

```
120     print *,x(1),x(2),wd
        write(8,*)"%lt=",x(1)
        write(8,*)"%la=",x(2)
        write(8,*)"%thickness=",wd,"norm factor=",x(3)
        write(8,*)"%fcn=",f,"theory max=",zmax
        write(8,*)"%dia=",pdia,"index=",dex
        do m=1,nn {
        zto=zto+(z(m)+z(m+1))*(w(m+1)-w(m))/2.
        }
        rat=yto/zto
        write(8,*)"%total count exp.=",yto
        write(8,*)"%total count theo=", zto,"ratio=exp/theo",rat
        write(8,*)"fitda=["
        do i=1,n {
        com=(z(i)-y(i))/y(i)
        write(8,111)w(i), z(i)
#       write(18,*)w(i),com
}
111     format(1e10.5,1x,1e10.5)
        write(8,*)"];"
        close (8)
#       print *, "chi** =",xx
        end




#       Program sublaxpl4.r:  basic subroutine program to compute
#       temporal profile of point input transmitted through
#       a pin hole on the oppsite side of slab.          12/23/91
#       ---------------------------------------
#       Modified 26/1/91 to include error standard.
#       Diffusion       5/1/90 modified to fix lt, change
#       length,  absorption considered.
#       from Lax Theory
```

```
#       ----------------------------------
        subroutine gg(vv,xx1,xx2,wd,dex,pdia,uu)
        implicit double precision (a-h,o-z)
        common /fun1/pi,d,theta,theta1,dif,t
        if (vv <= 0.) { uu=0.
        }
        else {
# ------------------------------------
# paremeters
ero=1.e-6
z0=0.71*xx1  # for boundary condition
d=wd+2.*z0
pi=3.14159654
theta=wd*pi/d
theta1=2.*z0*pi/d
dif=.1*xx1/dex  # diffusion coefficient =vl/3 (um**2/fs)
ale=.3/xx2/dex          #absorption cofficent
ddia=pdia**2*.25/dif
# end parameters
# ------------------------------------
t=vv*1000.      #  t  time (fs)

call sum(ero,cjj,m)
uu=cjj*exp(-t*ale)*pi*dif/d**2*(1.-exp(-ddia/t))
        }
        end

####
#       function subroutine, func(m)
subroutine func(m, funcm)
implicit double precision (a-h,o-z)
        common /fun1/pi,d,theta,theta1,dif,t
        fm=float(m)
        ff=(pi*2.*fm/d)**2*(dif*t)
ff1=(pi*(2.*fm-1)/d)**2*dif*t
```

```
        term2=-2.*fm*sin(2.*fm*theta1)*exp(-ff) #EVEN TERMS

term1=(2.*fm-1)*sin((2.*fm-1)*theta1)*exp(-ff1) #odd term
        funcm=term1+term2   #output
        end #end of function
####
####
#       subroutine to do infinite sum to certain accuracy,
#       SUM (from m=1 to m=inf) func(m)
#       func(m) is a subroutine.
subroutine sum(err,sumf,m)
implicit double precision (a-h,o-z)
tero=1.
m=1                     #initial condition
call func(m,sumf)       #initial term
        while (tero .gt. err ) {
        nstart=m+1
        nfinish=2*m
        dsum=0.         # added part
        do i=nstart, nfinish {
        call func(i,funci)
        dsum=dsum+funci
        }
        sumf=sumf+dsum
        m=nfinish
        if (sumf .eq. 0.) {tero=1
        }
        else {
        tero=abs(dsum/sumf)
        }
        }
        end
```

Bibliography

N. J. Agnantis, N Apostolikas, I. Christodoulou, C. Petrakis, and J. Garas in *Early Detection of Breast Caner*, eds. S. Brunner, B. Langfeldt, and P. E. Anderson, Springer Verlag, New York, p. 205, 1984

R. A. Ahmed, K. M. Yoo, R. M. Klapper and R. R. Alfano, "Time Resolved Backscattering of Pulse to Monitor Different Stages of Eye Cataract," *Appl. Opt.*, 29, p896, 1990

M. S. Al-Adnani, J. A. Kirrane, J. O'D McGee," Inappropriate production of collagen and prolyl hydroxylase by human breast cancer cells in vivo, *British Journal of Cancer*, 31, 653-660 (1975)

R. R. Alfano, and M. A. Alfano,"Medical diagnostics: a new optical frontier," *Photon Spectra* 19:55-60, 1985.

R. R. Alfano, B. B. Das, J. Cleary, R. Prudente and E. Celmer, "Light Sheds Light on cancer - Distinguishing Malignant Tumors From Benign Tissues and Tumors", Bulletin of the New York Academy of Medicine, v 67, p.143-150, (1991)

R. R. Alfano, D. Tata, J. Cordero, P. Tomashefsky, F. Longo and M. A. Alfano, " Laser induced fluorescence spectroscopy from native cancerous and normal tissues," IEEE J. Quantum Electron. QE-20, 1507-1511 (1984)

R. R. Alfano, G. C. Tang, A. Pradhan, W. Lam, D. C. Choy and E. Opher,"Fluorescence spectra from cancerous and normal human breast and lung tissues," IEEE *J. Quantum Electron*, QE-23, p1806, 1987

R. R. Alfano and S. S. Yao, "Human teeth with and without caries studied by visible luminiscent spectroscopy," *J. Dent. Res.*, 60, p120-122, 1981

S. Anderson-Engels, ; Berg, R. ; Svanberg, S. ; and Jarlman, O. ; Opt. Lett. **15**, 1179-1181 (1990)

P. S. Anderson, A. Gustafson, U. Stenram, K. Svanberg and S. Svanberg, "Diagnosis of arterial artherosclerosis using laser induced fluorescence," *Lasers Med. Sci.*, 2, p261-266, 1987

R. R. Anderson, J. Hu and J. A. Parish, *Bioengineering and the skin*. R. Marks and P. A. Payne, eds. MTP Lancaster, p. 253, 1981

S. Andreola, A. Bertoni, R. Marchesini and E. Mellino,"Evaluation of optical characters of different human tissues in vitro," *Lasers Surg. Med.*, 8:142 (abstract), 1988

R. Aronson,"Extrpolation distance for diffusion of light," to be published.

C. M. Balch, S. E. Singletary and K. I. Bland, "Clinical decision making in early breast cancer," in *Annals of Surgery*, vol. 217, No. 3, p.207-225, J. B. Lippincott Co., 1993

R. L. Barbour, H. L. Graber, R. Aronson, and J. Lubowsky," Determination of Macroscopic properties of Multilayer Random Media by Remote Sensing," *SPIE* Vol. 1431, p. 52, 1991

R. L. Barbour, H. L. Graber, R. Aronson, and J. Lubowsky," Imaging of subsurface regions of random media by remote sensing," *SPIE*, Vol. 1431, 1991

R. L. Barbour, H. L. Graber, J. Lubowsky, R. Aronson, B. B. Das, K. M. Yoo, and R. R. Alfano, "Imaging of diffusing media by a progressive iterative backprojection method using time-domain data," SPIE, Vol. 1641, p.21, 1992

J. L. Bennington," Major problems in pathology," in *Problems in Breast Pathology*, Vol. II in the series, W. B. Saunders Co Ltd., London, p393 (1979)

B. Birks, *Photophysics of Aromatic Molecules*, Wiely, New York, 1970J.

S. Brunner, B. Langfeldt, and P. E. Anderson, eds., *Early Detection of Breast Caner*, Springer Verlag, New York, 1984

I. D. Campbell and R. A. Dwek, *Biological Spectroscopy*, The Benjamin/ Cummins Publishing Co., Inc. California, p.98, (1984)

G. B. Canon et al,"Immunologic relationship between breast carcinoma and benign breast disease as detected by the Leukocyte Migration Inhibition Assay," *J Natl Cancer Inst* 61, p 1181-1186, 1978

L. L. Carter and E. D. Cashwell, *Particle Transport Solution with the Monte Carlo Method* (Technical Information Center, Office of Public Affairs, US Energy Research and Development Administration) 1975

A. Cascino, C. Cangiano, F. Cefi, T. Mineot, M. Mulieri, M. Muscaritoti and F. R. Fanelli, Increased plasma free tryptophan levels in human cancer: a tumor relsted effect?" *Anticancer Res*, 11(3) : 1313, 1991,

S. Chandrasekhar, *Radiative Transfer*, Oxford University Press, London, 1950

J. Chang, Y. Wang, R. Aronson, H. L. Graber, R. L. Barbour, B. B. Das, J. Dolne, K. M. Yoo, and R. R. Alfano, "Time-resolved imaging in dense scattering media," SPIE Vol. 1887, in press.

H. Chen, Y. Chen, D. Dilworth, E. Leith, J. Lopez, and J. Valdmanis, Opt. Lett. **16**, 487-489 (1991)

M. Cutler, "Transillumination as an aid in the diagnosis of breast lesions," *Surg. Gynecol. Obstet*, Vol. 48, 721, 1929

B. B. Das, K. M. Yoo and R. R. Alfano, "Ultrafast Time-gated Imaging In Thick Tissues - A Step Towards Optical Mammography," Opt. Lett., Vol. 18, No. 13, p.1092-1094, 1993

B. B. Das, K. M. Yoo and R. R. Alfano,"Ultrafast Time-gated Detection Of

Translucent Objects Hidden In Biological And Highly Scattering Random Media," *SPIE* proceedings in press, 1993.

B. B. Das, W. Sha Glassman, R. R. Alfano, J. Cleary, R. Prudente, E. Celmer and S. Lubicz, " UV fluorescence spectroscopic technique in the diagnosis of breast, ovarian, uterus, and cervix cancer", SPIE proceedings v 427 Laser-Tissue Interaction II, p 368-373 (1991)

L. I. Deckelbaum, J. K. Lam, H. S. Cabin, K. S. Clubb and M. B. Long, "Discrimination of normal and artherosclerotic aorta by laser induced fluorscence," *Lasers surg. Med.*, 7, p330-335, 1987

W. Demtroder, *"Laser Spectroscopy"*, 2nd Ed., Springer Verlag, 1973

J. J. Duderstadt and L. J. Hamilton, *Nuclear Reactor Analysis*, Wiley, New York, 1976, p. 103-44

M. D. Duncan, ; Mahon, R. ; Tankersley, L. L. ; and Reintjes, J. ; Opt. Lett. **16**, 1868-1870, (1991)

W. G. Egan and T. W. Hilgeman, *Optical Properties of Inhomogeneous Materials*, Academic, New York, 1979

S. Ertefai and A. E. Profio," Spectral Transmittance and Contrast in Breast Diaphanography," *Med. Phys.* **12**(4), 393, 1985

I. S. Fentiman, *Detection and Treatment of Early Breast Cancer*, J. B. Lippincott Company, Philadelphia, p. 39-57, 1990

S. T. Flock, B. C. Wilson and M. S. Patterson, "Total attenuation coefficients and scattering phase functions of tissues and phantom materials at 633 nm," *Med. Phys.* 14(5) 1987

T. Foerster,"Fluorenz Organischer Verbindungen," Goettingen: Vandenhoek & Ruprecht, p.35-42, 273 (1951)

K. Furutsu,"On the diffusion equation derived from the space-time transport equation," *J. Opt. Soc. of Am.* Vol. 70, p. 360, 1980

H. S. Gallager,"Corrent concepts in breast cancer and tumor immunology," in *Newer Understanding of Pathology of Breast Cancer*, p27, New York: Medical Examinatoin (1974)

M. J. C. van Germert and H. J. P. Hulsbergen, *Arch. Dermatol. Res*, **270**, 429, 1981

R. T. Girolamo,"Imaging systems other than mammography," in *Breast Cancer : Diagnosis and Treatment*, eds. I. M. Ariel and J. B. Cleary, McGraw-Hill Book Company, 1987

R. Graaff, J. G. Arnoudse, F. F. M. de Mul and H. W. Jentink,"Light Propagation for anisotropically scattering scattering media based on a rigorous solution of the transport equation," *Appl. Opt.*, 28, p2273-2279, 1989

R. A. J. Groenhuis, J. J. Ten Bosch, and H. A. Ferwerda,"Scattering and absorption of turbid materials determined from reflection measurements," *Appl. Opt.* Vol. 22, No. 16, p. 2463, 1983

J. C. Hebden, R. A. Kruger, and K. S. Wong, Appl. Opt. **30**, 788-794 (1991)

H. C. van de Hulst, *Light Scattering by Small Particles*, Dover, New york, 1981

H. Isard, W. Becker, R. Scilo, and B. Ostrum," Breast thermography after 4 years and 10,000 studies." *Amer. J. Roentgenol* 115: 811, 1972

A. Ishimaru, *Wave propagation and scattering random media*, New York: Academic, 1978

A. Ishimaru,"Diffusion of light in turbid material," *Appl. Opt.*, 28, p2210-2215, 1989

A. Ishimaru,"Diffusion of a pulse in densely distributed scatterers," *J. Opt. Soc. of Am.* Vol. 68, p. 1045, 1978

S. L. Jacques, C. A. Alter, and S. A. Prahl, "Angular dependence of HeNe laser light scattering by human dermis," Lasers in the Life science 1, p309-333, 1987

S. L. Jacques, "Time Resolved Propagation of Ultrashort Laser Pulses within Turbid Tissues," *Appl. Opt.*, 28, p2223-2229, 1989

G. S. Johnson, and A. E. Jones, eds.,*Breast Cancer Diagnosis*, Plenum Medical Bokk Co. New York, 1980

C. R. Kapadia, F. W. Cutruzzola, K. M. O'Brein, M. L. Stetz, R. Enriquetz, and L. I. Deckelbaum,"Detection of adenomatous transformation of colonic mucosa by fiberoptic laser-induced fluorescence spectroscopy," *Gastroenterology*, 94, 216A, 1988.

C. R. Kapadia, F. W. Cutruzzola, K. M. O'Brein, M. L. Stetz, R. Enriquetz, and L. I. Deckelbaum,"Laser induced fluorescence spectroscopy of human colonic mucosa," *Gastroenterology*, 99, p150-157, 1990

J. L. Karagiannes, J. Zhang, B. Grossweiner and L. I. Grossweiner," Application of the 1-D diffusion aproximation to the optics of tissues and tissue phantoms," *Appl. Opt.*, 28, p2311-2317, 1989

C. Kittrel, R. L. Willet, C. de Los Santos Pacheo, N. B. Ratcliff, J. R. Kramer, E. G. Malk and M. S. Feld, "Diagnosis of fibrous arterial artherosclerosis using fluorescence," Appl. Opt., 24, p2280-2281, 1985

T. Kobayashi et al, "The sensitivity graded method of ultrasonotomography and clinical evaluation of its diagnostic accuracy." *Cancer* 33: 940, 1974

A. Kong, *Electromagnetic Theory*, Wiely, New York, 1986J.

R. R. Kortum, L. Tong, R. Rava et al.," Spectral studies of GI tissues: Optimizing excitation and emission wavelengths for discrimination of normal and adenomatous

tissues," *Lasers in Srg. and Med.* 9, p. 21 (abstract) 1989

R. R. Kortum, R. Rava, R. E. Petras, M. Fitzmaurice, M. SivaK and M. S. Feld," Clinical applications of fluorescence excitation and emission matrices: diagnosis of colonic adeoma," Manuscript in preparation.

R. Richards-Kartum, Masters Thesis, Dept. of Physics, M.I.T., (1987)

V. P. Kubelka and F. Munk, *Z. Tech. Phys.* **12**, 593-601

Y. Kuga and A. Ishimaru, "Retroreflectance from a Dense Distribution of Spherical Particles," J. Opt. Soc. Am. , A8, p831-845, 1984

R. Lafrenuere, F. S. Ashkar, and A. S. Ketcham, The American Surgeon **52**, 123 (1986)

M. Lax, *Symmetry Principles in Solid State and Molecular Physics*, p 198, Wiley, New York, 1974

M. Lax, V. Nayaramamurti and R. C. Fulton in *Laser Optics of Condense Matters* edited by J. L. Birman, H. Z. Cummins, A. A. Kaplyanskii, Plenum, New York, 229, 1987

E. N. Leith, C. Chen, H. Chen, Y. Chen, J. Lopez, and P. C. Sun, Opt. Lett., **16**, 1820-1822 (1991)

C. -H. Liu, B. B. Das, W. L. Sha-Glassman, G. C. Tang, H. R. Zhu, D. L. Akins, S. S. Lubicz, J. Cleary, R. Prudente, E. Celmer, A. Caron, and R. R. Alfano,"NIR Raman and fluorescence spectroscopies Diagnose cancer!" *SPIE* Vol. 1887, p.188

C. -H. Liu, B. B. Das, W. L. Sha-Glassman, G. C. Tang, K. M. Yoo, H. R. Zhu, D. L. Akins, S. S. Lubicz, J. Cleary, R. Prudente, E. Celmer, A. Caron, and R. R. Alfano,"Raman, fluorescence and time-resolved light scattering as optical diagnostic techniques to separate diseases and normal biomedical media," *J. Photochem. Photobiol., B. Biol.*, 16, p. 187-209, 1992

F. Liu, K. M. Yoo, and R. R. Alfano, Opt. Lett. **16**, 351-353 (1991)

LiuFeng , Ph. D. Thesis, The City University of New York, 1993

D. A. Long, *Raman Spectroscopy*. McGraw Hill, New York, 1977

R. Marchesini, A. Bertoni, S. Andreola, E. Melloni and A. E. Sichirollo, "Extinction and Absorption Coefficients and Scattering Phase Functions of Human Tissues *in vitro*,,"*Appl. Opt.* , 28, p2318-2324, 1989

A. Marynissen and W. M. Star in *Porphyrin Localization and Tretment of Tumors*. D. R. Doiron and C. J. Gomer, eds. New York: Liss, p. 133, 1984J. P.

M. Motamedi, S. Rastegar, G. LeCarpentier and A. J. Welch, "Light and Temperature Distribution in Laser Irradiated Tissue: The Influence of Anisotropic Scattering and Refractive Index," Appl. Opt., 28, p2230-2237, 1989

S. Nakamura, Y. Nishiwaki, S. Sujuki, S. Sakaguchi, Y. Yamashita and K. Ohta," Light attenuation in human liver and hepatic tumors after surgical resection," *Lasers in Surgery and Medicine*, 10, p12-15, 1990

G. A. Navarro and A. E. Profio, "Contrast in Diaphanography of the Breast," *Med. Phys.*, 15, p181-187, 1988

G. A. Navarro and A. E. Profio, *Med. Phys.* **15**, 181 (1988)

P. Parsa, S. L. Jacques, and N. S. Nishioka,"Optical properties of rat liver between 350 and 2200 nm," *Appl. Opt.*, Vol. 28, No. 12, p. 2325, 1989

M. S. Patterson, B. Chance and B. C. Wilson, "Time Resolved Reflectance and Transmittance for the Noninvasive Measurement of Tissue Optical Properties," *Appl. Opt.*, 28, p2331-2336, 1989

R. E. Petras, R. R. Kortrum, L. Tong, M. Fitzmaurice, M. feld and M. Sivak, "Fluorescence spectroscopy of colonic adenomas: Implications for an endoscopic laser diagnostic system," *Gastrointest. Endosc.*, 35, p181-182, (abstract), 1989

A. Pradhan, B. B. Das, K. M. Yoo and R. R. Alfano, "Time-resolved uv photoexcited fluorescence kinetics from malignant and non-malignant Human breast tissues," Lasers in Life Sciences, p 225-234, 4(4), 1992

A. Pradhan, Ph. D. thesis, The City Univ. of New York, 1991

P. Pringsheim, *Fluorescence and Phosphorescence*, Interscience, New York, 1949.

A. E. Profio, ,"Light transport in tissue," *Appl. Opt.*, 28, p2216-2222, 1989

A. E. Profio, and O. Balchum,"Fluorescence diagnosis of cancer," in *Methods in Porphyrin Photosensitization*, Ed. D. Kessel, Plenum, New York, p 843, 1985

A. E. Profio and D. R. Doiron,"Dosimetry considerations in phototherapy," Med. Phys., 8,p 190-196, 1981

G. B. Rybicki, *J. Quant. Spectrosc. Radiat. Transfer,* **11**, p. 827-49

M. Sartori, P. D. Henry, R. Roberts, R. P. Chin, and M. J. Berry," Estimation of arterial wall thickness and detection of atherosclerosis by laser induced fluorescence," *J. Am. Coll. Cardiol.*, 7: 207A (abstract) 1986

K. T. Schomacker et al,"Ultraviolet Laser Induced Fluorescence of Colonic Polyps," *Gastroenterology*, 0411, p 4-5, 1992

J. P. Schwartz, J. V. Possoneau, G. S. Johnson, I. Pastan," The effect of growth conditions on NADH+:NADH ratio in normal and transformed fibroblasts, *J. Bilo. Chem.*, 249, 4138 (1974)

W. Sha Glassman, C. H. Liu, G. C. Tang, S. Lubicz and R. R. Alfano, "Ultra Violet fluorescence spectra from non-malignant and malignant tissues of the gynecological

tract," *Lasers in the Life Sciences*, 4(1), p1-9, 1991

W. Sha-Glassman, Doctoral Thesis, The City Univ. of New york, 1993

Dezna C. Sheehan and Barbara Hrapchak, *Theory and Practice of Histotechnology*, C. V. Mosby Co., London, 1980

K. Shimizu, A. Ishimaru, L. Reynolds and A. P. Bruckner, "Backscattering of a Picosecond Pulse from Densely Distributed Scatterers," *Appl. Opt.*, 18, p3484, 1979

E. A. Sickles, Recent Results in Cancer Research 105, Springer-Verlag, Berlin, Heisdelberg, p 31 (1987)

L. O. Svaasand and R. Ellingsen, "Optical Penatration in Human Intracranal Tumors," Photochem. Photobiol., 41, p73-76, 1985

L. O. Svaasand and R. Ellingsen, "Optical Properties of Human Brain," Photochem. Photobiol., 38, p73-76, 1983

S.Taitelbaum, Havlin, and G. H. Weiss,"Approximate theory of photon migration in two-layered medium," *Appl. Opt.*, 28, p. 2245-2249, 1989H.

S. Takatani and M. D. Graham,"Theoretical analysis of diffuse reflectance from a two-layer tissue model," *IEEE Transactions* on Biomedical Engineering, 26, p. 656, 1979

G. C. Tang, A. Pradhan, W. L. Sha, J. Chen, C. H. Liu, S. J. Wahl and R. R. Alfano, "Pulsed and cw laser fluorscence spectra from cancerous normal and chemically treated normal human breast and lung tissue," *Appl. Opt.*, 28, p2337-2342, 1989

L. T. Threadgold,*The Ultrastructure of the Animal Cell*, 2nd edition, Pergamon Press. New York, (1976)

G. Tremblay, "Elastosis in tubular carcinoma of the breast," *Archives of Pathology*, 98, 302-307 (1974)

L. Tsang, J. A. Kong, and R. T. Shin, *Theory of Microwave Remote Sensing*, Wiely, New York, 1985

S. Udenfriend, *"Fluorescence Assay in Biology and Medicine"*, New York: Academic, Vol. 1, 1962, Vol. 2, 1969

S. Udenfriend, *Fluorescence Assay in Biology and Medicine,* New York: Academic, Vol. 1, 1962, Vol. 2, 1969

V. V. Varadan and V. K. Varadan, Eds., *Multiple Scattering of Waves in Random Rough Surfaces,* Penn State Univ., University Park, 1987

H. Vorherr, *Breast Cancer*, Urban & Schwarzenberg, Baltimore-London, p.343, 1980

R. Vreeker, M. P. Van Albada, R. Sprik and A. Lagendijk, "Femtosecond Time-Resolved Measurement of Weak Localization of Light," *Phys. Lett.*, 132, p516-519,

1988

L. M. Wang, P. P. Ho, C. Liu, G. Zhang and R. R. Alfano, " Ballistic 2-D imaging through scattering walls using ultrafast optical kerr gate" Science, Vol. 253, 769-771, (1991)

S. Wan, R. R. Anderson and J. A. Parish, *Photochem. Photobiol.*, **34**, 493, 1981

Y. Wang, J. Chang, R. Aronson, R. L. Barbour, H. L. Graber, and J. Lubowsky, "Imaging of scattering media by diffusion tomography: an iterative perturbation approach," SPIE Vol. 1641, p. 58, 1992

D. J. Watmough, *Radiology* **147**, 89-92 (1983)

G. H. Watson, S. L. McCall, P. A. Fleury and K. B. Lyons, *Phys. Rev. B*, 41, 10947, 1990

G. Weber, "Enunciation of components in complex systems by fluorescence spectrophotometry," *Nature* 190, 27, 1961

A. J. Welch, G. Yoon, and M. J. C. van Gemert,"Practical models for light distribution in laser irradiated tissue," *Lasers in Surgery and Medicine*, 6, p488-493, 1987

P. A. Wilksch, F. Jacha and A. J. Blake in *Porphyrin Localization and Tretment of Tumors*. D. R. Doiron and C. J. Gomer, eds. New York: Liss, p. 149, 1984

B. C. Wilson, M. S. Patterson and S. T. Flock,"Indirect versus direct techniques for the measurement of the optical properties of tissues," *Photochem. and Photobiol.* 46, p601-608, 1987

B. C. Wilson, M.S. Patterson, S. T. Flock and J. D. Moulton, "The optical absorption and scattering properties of tissues in the visible and near-infrared wavelength range," in *Light in Biology and Medicine*, vol. 1, R. H. Douglas, J. Moan, and F. Dall'Acqua, eds. Plenum, New York, 1988, p.45

B. C. Wilson, W. P. Jeeves and D. M. Lowe, "In vivo and post-mortem measurements of the attenuation spectra of light in mammalian tissue," *Photochem. and Photobiol.*, 42, p153-162

B. C. Wilson and M. S. Patterson,"The Physics of Photodynamic Therapy," *Phys. in Med. Biol.*, Vol. 31, No. 327, 1986

J. Yguerabide,"Nanosecond fluorescence spectroscopy of biological macromolecules and membranes," in *Fluorescence Techniques in Cell Biology*, Edited by A. A. Thaer and M. Sernetz, Springer Verlag, Berlin, p 311-31, 1973.

K. M. Yoo and R. R. Alfano, "Determination of Attennuation Lengths Arising from Scattering and Absorption from the Temporal Profile of the Backscattered Pulse," Opt. Lett., 15, p276, 1990

K. M. Yoo and R. R. Alfano, "Time-Resolved Depolarization of Light Scattering in Random Media," Phys. Lett. A, 142, p531, 1989

K. M. Yoo, and R. R. Alfano, *Opt. Lett.* **15**, 320-322 (1990)

K. M. Yoo, F. Liu, and R. R. Alfano, *Phys. Rev. Lett.* **64**, 2647 (1990)

K. M. Yoo, ; Xing, Q. ; and Alfano, R. R. ; Opt. Lett. **16**, 1019-1021 (1991)

K. M. Yoo, B. B. Das, and R. R. Alfano, "Imaging a translucent object hidden in a highly scattering medium from the early portion of the diffuse component of the transmitted ultrafast laser pulse," Opt. Lett. 17, 958 (1992)

K. M. Yoo, B. B. Das, F. Liu, Q. Xing, and R. R. Alfano, "Femtosecond time-gating imaging of translucent objects hidden in highly scattering media," *Ultrafast Phenomena* VIII, Eds. A. Migus, F. Martin, G. A. Mourou, and A. H. Zewail, Springer-Verlag Berlin, Heidelberg, (1992)

K. M. Yoo, B. B. Das, Feng Liu, Qirong Xing, and R. R. Alfano, "Imaging of Translucent Objects Hidden in Highly Scattering Media Using Ultrafast Laser Technology," In the Proceedings of 5th Asia Pacific Physics Conference, Malaysia (1992)

K. M. Yoo, F. Liu and R. R. Alfano, "Angle-and Time-Resolved Studies of Backscattering of Light from Biological Tissues," Proceedings of *SPIE:* Time-Resolved Laser Spectroscopy in Biochemistry II Convention-1990, 1990

K. M. Yoo, F. Liu and R. R. Alfano, "Biological Materials Probed by the Temporal and Angular Profiles of the Backscattered Ultrafast Laser Pulses," J. Opt. Soc. Am. B, 7, p1685-1693, 1990

K. M. Yoo, Feng Liu, B. B. Das and R. R. Alfano,"Ultrashort laser pulse propagation and imaging through biological and random media," Medical Optical Tomography, Ed. G. Muller, in press.

K. M. Yoo, K. Arya, G. C. Tang, J. L. Birman and R. R. Alfano, "Coherent Backscattering of a Picosecond Pulse from a Disordered Medium : Analysis of Pulse Shape in the Time Domain," *Phys. Rev. A*, 39, p3728-3731, 1989

K. M. Yoo, Ph. D. Thesis, The City University of New York, 1990

K. M. Yoo, Y. Takiguchi and R. R. Alfano, "Dynamic Effect of Weak Localization on the Light Scattering from Random Media Using Ultrafast Laser Technology," Appl. Opt., 28, p2343-2349, 1989

Y. Yuanlong, Y. Yanming, L. Fuming, L. Yufen and M. Paozhong, "Characteristic autofluorescence for cancer diagnosis and its origin," *Lasers Surg. Med.*, 7, p528, 1987